UNIVERSITY OF NAPLES FEDERICO II

DOCTORATE IN
MOLECULAR MEDICINE AND MEDICAL BIOTECHNOLOGY

XXXIII CYCLE

Valeria Pistorio

Unravelling CtsD-cell-specific role in macrophages during tissue remodelling in kidney disease
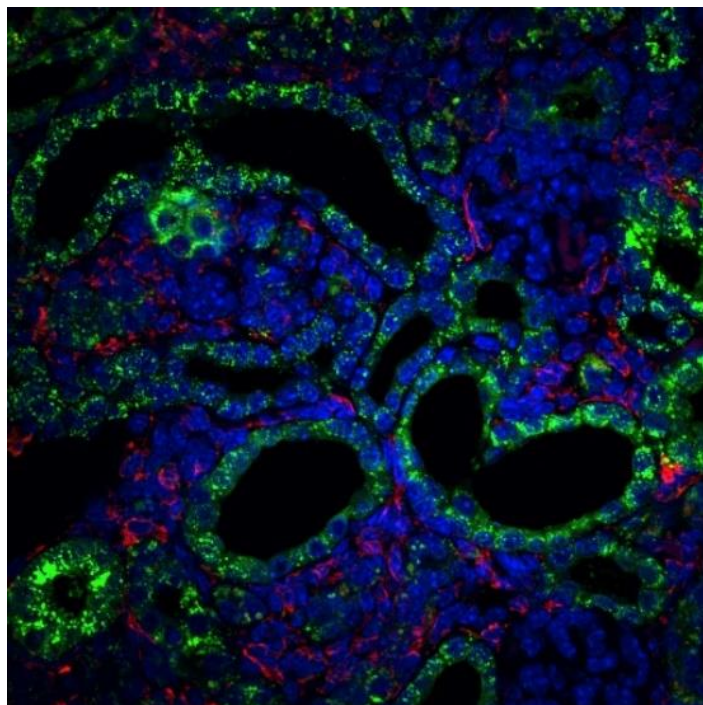
Year 2021

UNIVERSITY OF NAPLES FEDERICO II

DOCTORATE IN
MOLECULAR MEDICINE AND MEDICAL BIOTECHNOLOGY

XXXIII CYCLE

Unravelling CtsD-cell-specific role in macrophages during tissue remodelling in kidney disease

Tutor   Candidate
Prof. Luigi Michele Pavone   Valeria Pistorio

Co-Tutor
Dr. Ana Belen Moles Fernandez

Year 2021

LIST OF ABBREVIATION (stated as they appear in the text)

GBM	Glomerular Basement Membrane
FP	Foot Processes
GFR	Glomerular Filtration Rate
BUN	Blood Urea Nitrogen
ECM	Extracellular Matrix
AKI	Acute Kidney Injury
CKD	Chronic Kidney Injury
ESRD	End Stage Renal Disease
RRT	Renal Replacement Therapy
TEC	Tubular Epithelial Cells
CCR2	CC Chemokine Receptor 2
CSF-1	Colony Stimulating Factor-1
IL	Interleukin
KC	Keratinocyte Chemokine
MCP1	Monocyte Chemotactic Protein 1
MIP-2	Macrophage-Inflammatory Protein-2
MMPs	Matrix Metalloproteinases
TIMPs	Tissue Inhibitor Of Metalloproteinase
PDGF	Platelet-Derived Growth Factor
TGF- β	Transforming Growth Factor-B
TNF	Tumor Necrosis Factor
LLC	Large Latent Complex
DAMP	Damage-Associated Molecular Patterns
PAMP	Pathogen-Associated Molecular Patterns
EMT	Epithelial–Mesenchymal Transition
EndoMT	Endothelial–Mesenchymal Transition
MMT	Macrophage-Myofibroblast Transition
APC	Antigen-Presenting Cell
LPS	Lipopolysaccharide
ROS	Reactive Oxygen Species
TLR	Toll-Like Receptor
MHC	Major Histocomplatibility Complex
Ly-6C	Lymphocyte Antigen 6 Complex
NO	Nitric Oxide
UUO	Unilateral Ureteral Obstruction
Cts	Cathepsin
pCtsD	Pro-CtsD
NCL10	Neuronal Ceroid Lipofuscinosis 10
uPA	Urokinase-Type Plasminogen Activator
uPARAP	uPAR Associated Protein
LysM	Lysozyme M

PMT	Peritoneal Macrophages elicited with Thioglycolate isolation
PBS	Phosphate Buffer Saline
DMEM	Dulbecco's Modified Eagle Medium
EDTA	Ethylenediaminetetraacetic Acid
BSA	Bovine Serum Albumin
SDS	Sodium Dodecilsulphate
APS	Alkaline Phosphatase Buffer
TEMED	N,N,N',N'- Tetramethylethylenediamine
Tris	Tris[Hydroxymetyl]Aminomethane
IHC	Immunohistochemistry
PAS	Periodic Acid Schiff's
RT	Room Temperature
DAPI	4,6-Diamidino-2-Phenylindole, Dihydrochloride
LAMP2	Lysosome-Associated Membrane Protein 2
NIMP	Nogo Interacting Mitochondrial Protein
SEM	Standard Error of the Mean

Index

Abstract

Kidney disease is increasingly considered as a global public health issue. Prolonged tissue damage, accompanied by activation of proinflammatory and pro-fibrotic signaling pathways, causes an excess of extracellular matrix (ECM) deposition resulting in renal fibrosis and chronic kidney disease (CKD). Unfortunately, due to the lack of adequate specific treatments, many patients (>2 million worldwide) progress from CKD to end-stage renal disease requiring transplantation. Targeted treatments for kidney disease are not currently available or are mainly limited on managing the underlying cause of the disease. Therefore, it is essential to improve our knowledge about the cellular and molecular drivers controlling kidney disease to find new therapeutic candidates and develop new and more specific drugs for treating CKD. Previous reports about the role of cathepsin D in renal disease are controversial, pointing towards a cell-specific role for this protease in kidney disease progression. Thus, the aim of this project was to elucidate the role of CtsD during progressive kidney disease using a novel conditional knockout mouse model with the specific deletion of the CtsD in macrophages. Macrophage-CtsD sufficient ($CtsD^{\Delta Myel+/+}$) and deficient ($CtsD^{\Delta Myel-/-}$) mice were used to study *in vivo* the effects of CtsD deletion in macrophages both in early-stage and chronic kidney disease. Moreover, peritoneal macrophages isolated from macrophage-CtsD sufficient and deficient mice were used to study *in vitro* the effects of CtsD deletion on macrophage activation and polarization. Our results validate for the first time the $CtsD^{\Delta Myel-/-}$ mouse strain by demonstrating the CtsD cell-specific deletion in macrophages. Macrophage-CtsD specific deletion in an early-stage kidney disease model (unilateral ureteral obstruction, UUO, 5 days) caused a decrease of kidney inflammation and number of total macrophages as well as an impaired M2 macrophage polarization. However, these changes did not translate into an alteration of kidney damage. On the other hand, the absence of CtsD in macrophages during chronic kidney disease (UUO 10 days) resulted in an increased kidney fibrosis with no changes in tubular cell damage or inflammation. Our *in vitro* results, using isolated peritoneal macrophages, proved that the enhanced ECM accumulation and renal fibrosis, observed in the macrophage-CtsD deficient mice, were the consequence of a deficient proteolytic enzyme profile and of an impairment in lysosomal degradation of collagen. In summary, our results provide novel experimental evidence of the fundamental role played by CtsD in driving collagen recycling and controlling proteolytic enzymes during chronic renal injury. This information might be essential when considering long-term therapies based in CtsD inhibition during progressive kidney disease.

1 Background

1.1 Kidney anatomy and physiology

Kidneys are complex organs crucial in maintaining normal body functions. Their primary function is to regulate fluid and electrolytes of the body by balancing solute and water transport, excreting metabolic waste products, keeping nutrients, and regulating acid-base balance in the body.

The renal-urologic system is made up of two kidneys, two ureters, a urinary bladder, and the urethra. A normal adult kidney is bean-shaped and is located retroperitoneally between the level of the 12th thoracic and third lumbar vertebrae. The right kidney lies lower than the left because of displacement by the liver. The left kidney is slightly longer than the right and lies closer to the midline. The ureters are tubes (27 to 30 cm long and approximately 1 to 5 mm in diameter) which extend from the kidneys to the bladder. Their function is to move urine from the kidney pelvis to the bladder by peristaltic contractions. In the bladder, located behind the symphysis pubis, the urine is collected before being expelled passing through the urethra, a tube leading from the bladder to the outside of the body (Wallace 1998) (**Fig. 1a**).
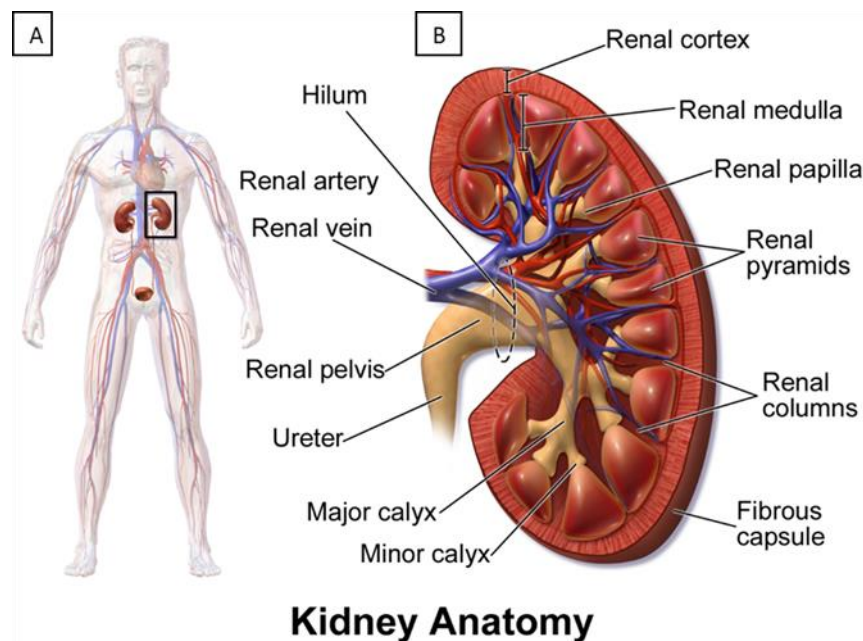
Figure 1. Kidney anatomy. Blausen.com staff (2014). "Medical gallery of Blausen Medical 2014". WikiJournal of Medicine 1. DOI:10.15347/wjm/2014.010. ISSN 2002-4436. (**a**) Renal-urologic system in human. (**b**) kidney structure.

The weight of each kidney in humans ranges from 125 g to 170 g in men and from 115 g to 155 g in women. In C57BL/6J mice (8 weeks), the weight of each kidney in males is around 0.188 g and in females ranges from 0.120 g to

0.124 g. (Jackson-Laboratory. (2007). Physiological Data Summary–C57BL/6J (000664)).

The internal structure of the kidney can be divided in three regions: the hilum, the medulla in the middle and the outer cortex (**Fig. 1b**). The hilum is the concave part of the bean-shape from which the main blood vessels, the renal artery and the renal vein, and nerves access the kidney. It is also the point of exit for the ureters. The medulla consists of multiple triangular regions with a striated appearance, called the renal pyramids, surrounded by spaces called renal columns through which the blood vessels pass. The tip of each pyramid, called renal papilla, projects into a calyx. The major calyces join to form the renal pelvis, an extension of the upper end of the ureter. The medulla contains the concentrating and diluting components of the nephrons and a system of collection ducts. These ducts funnel the urine into the pelvis, from where it moves down the ureter into the bladder. An anatomical border exists between the cortex and medulla, which is called the corticomedullary junction, corresponding to the wide base of a renal pyramid, where many macrophages reside. Loss of the corticomedullary junction is noted in cases of acute and chronic inflammatory disease, amyloidosis, some types of toxicity and end-stage kidneys. Finally, the outer cortex is the external part of the kidney which contains the filtering and reabsorptive components of the nephrons. The cortex is covered by a fibrous capsule and the whole kidney is surrounded by a cushion of fat that offers protection against injury. It provides a space for arterioles and venules, as well as the glomerular capillaries, to perfuse the nephrons of the kidney. Erythropoietin, a hormone necessary for the synthesis of new red blood cells, is also produced in the renal cortex (Chalmers 2019).

In contrast to the human kidney, the kidney of the mouse and of many other laboratory animals has a single renal pyramid and is therefore termed "unipapillate". Otherwise, rodent kidneys resemble the human kidney in their gross appearance.

1.2 The functional unit of the kidney: the nephron

The nephron is the functional unit of the kidney and regulates water and soluble substances by filtering the blood, reabsorbing what is needed, and excreting the rest as urine (**Fig. 2**). Its function is crucial for homeostasis of blood volume, blood pressure, and plasma osmolarity. It is regulated by the neuroendocrine system through hormones such as antidiuretic hormone, aldosterone, and parathyroid hormone.
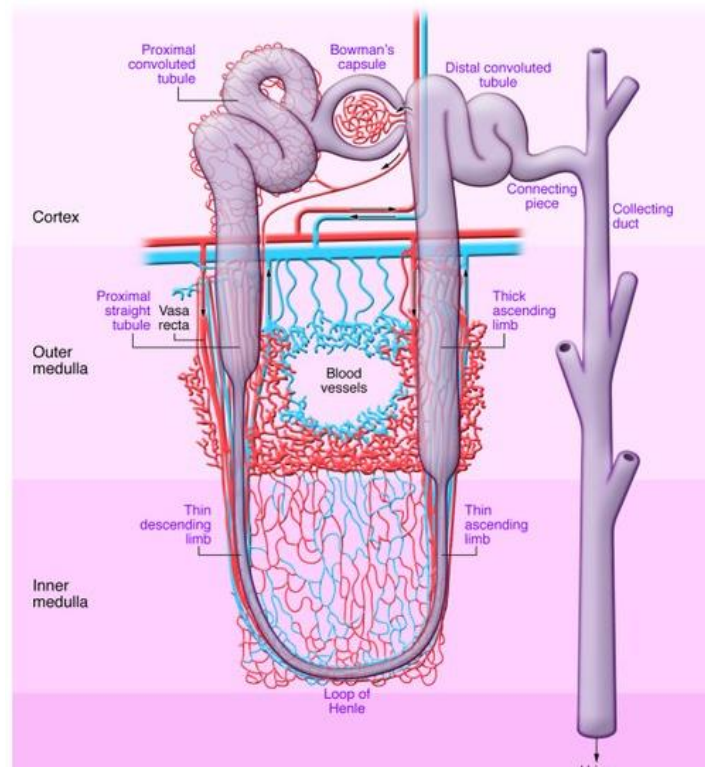
Figure 2. Anatomy of nephron with regions identified. Outer medulla vasculature is shown with capillaries in red and venous system in blue. (modified from *J Clin Invest DOI: 10.1172/JCI45161*).

Each kidney contains around one million nephrons. Approximately 85% of the nephrons are cortical nephrons, which have short loops of Henle contained in the cortex of the kidney. The other 15% of nephrons are called juxtamedullary nephrons, characterized by longer loops of Henle, which extend deep into the medulla of the kidney. The structure of the nephron is strictly related to its functions and contains five sections, each performing a distinct process (**Fig. 2**):

- the Bowman's capsule - is a cup-shaped capsule which encloses a cluster of capillaries (microscopic blood vessels) called the glomerulus. The capsule and glomerulus together constitute a renal corpuscle, also called Malpighian body. The renal corpuscle is the site in which is generated the glomerular filtrate, made up of water, ions and small molecules.
- the proximal convoluted tubule - is the site of bulk-phase reabsorption of sodium, chloride, potassium, water, glucose, amino acids, bicarbonate, calcium and phosphate. It is also the site of secretion of ammonium and creatinine.
- the loop of Henle - where the concentration and dilution of urine mainly occur, through reabsorption of water, sodium and chloride. The loops of

Henle, together with the collecting ducts which also pass through the medulla, give the pyramids of the medulla a striated appearance.

- the distal convoluted tubule - is the site of "fine-tuning" reabsorption and more secretion.
- the collecting duct - is important for the concentration of urine and for carrying urine into the renal pelvis. In the collecting duct takes place the reabsorption of sodium, chloride and water, but also the secretion of ammonium, hydrogen ions and potassium.

1.3 Glomerular filtration

Urine formation begins with the glomerular filtration of plasma. The filtrating unit of the nephron is the renal corpuscle (**Fig. 3**), also called Malpighian body. It consists of a glomerulus surrounded by the double-walled Bowman's capsule that opens into a tubule. The filtration takes place through three different layers: the endothelium, the glomerular basement membrane (GBM) and epithelial layer. The filtration starts through the endothelial layer of the capillaries, composed of fenestrated endothelial cells. These fenestrations, or slits between endothelial cells, restrict the movement of molecules according to their size (the fenestrations are approximately 60 to 80 nm wide) and to their charge, preferentially retarding anionic macromolecules (Falkson & Bordoni 2020).

Filtrate next moves through the glomerular basement membrane (GBM), composed of three layers, the lamina rara interna, the lamina densa, and the lamina rara externa. The maintenance of the GBM is assured by the mesangium, consisting of mesangial cells and the mesangial matrix that contains collagens, laminin, proteoglycans, heparin sulfate, fibronectin, entactin, and nidogen. Mesangial cells are specialized cells capable of endocytosis of macromolecules, as they remove trapped residues and aggregated proteins from the basement membrane, keeping the filter free of debris. Mesangial cells provide structural support for glomerular capillary loops. Moreover, they have contractile properties to regulate capillary flow (Davidson 2013).

Following the GBM, filtrate passes through the epithelial layer of Bowman's capsule, which is composed podocytes. Podocytes are highly specialized cells that present finger-like projections of cytoplasm referred to as "foot processes" (FP) or "pedicels", which wrap around the capillaries and leave slits between them (Reiser & Altintas 2016). Blood is filtered through these slits, known as slit diaphragms (SD), a specialized type of intercellular junction that connects neighboring podocyte foot processes. Most of nephrotic syndromes are

characterized by foot processes effacement and/or disruption of the slit diaphragm (Smoyer & Mundel 1998).
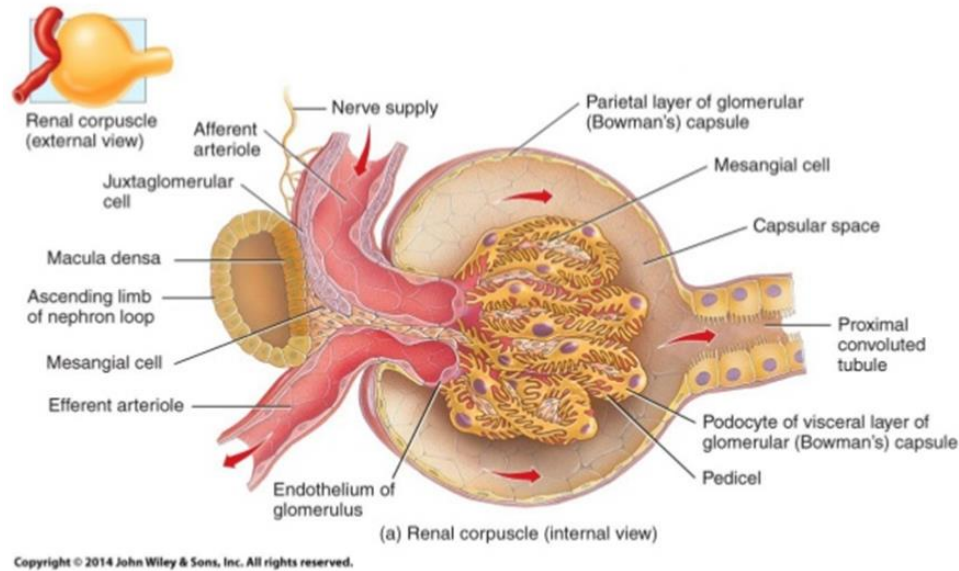
Figure 3. Renal corpuscle structure. John Wiley & Sons, Inc (2014).

These three layers (endothelium, GBM and epithelial layer) are fused together and act as a barrier to the filtration of large molecular weight molecules such as proteins. Thus, blood enters the glomerulus from a series of branches of the renal artery, ending in the afferent arteriole, then it leaves the glomerulus through the efferent arteriole rather than a vein. In the cortical nephrons, the efferent arteriole from the glomerulus divides up into capillaries, which cover the surfaces of the convoluted tubules. The capillaries finally empty into the venous system. In the deeper juxtamedullary nephrons, the efferent arteriole from the glomerulus divides to form loops which lie parallel to the loops of Henle and so run down into the medulla. These vessels are called the vasa recta and are involved in the process of concentration of the urine. Blood then leaves the kidney through a series of larger converging veins, ending in the renal vein which returns the blood to the vena cava.

1.4 The Glomerular Filtration Rate (GFR)

The GFR is one of the most important indicators of renal function. Loss or damage to nephrons leads to a corresponding decrease in GFR. In a healthy person the glomerular filtrate formed per minute (GFR) is approximately 125 mL min^{-1}. The serum creatinine and blood urea nitrogen (BUN) concentrations are also helpful to evaluate the GFR. Creatinine, a low-molecular-weight (113

Daltons) stable metabolite of protein occurring in the blood, is the end product of muscle metabolism. It is constantly produced and excreted in the urine at the same rate. The creatinine clearance test compares serum and urine creatinine levels to measure the amount removed by the kidney. An alternative method for detecting protein excretion is the evaluation of urinary albumin-to-creatinine ratio (ACR) to correct for variations in urinary concentration due to hydration. The concentration of urea nitrogen in the blood (BUN) reflects glomerular filtration and urine concentrating capacity. Urea is reabsorbed by the blood through the permeable tubules; therefore, the BUN rises in states of dehydration and renal failure when passage of fluid through the tubules slows. A normal serum creatinine level is 0.7 to 1.5 mg/100 mL, while a normal BUN level is between 10 to 20 mg/100 mL. Both creatinine and urea nitrogen are nitrogenous end products of protein metabolism normally excreted in the urine. In renal insufficiency, the GFR decreases as the plasma levels of creatinine and BUN rise (Levey 1988).

1.5 Urine formation – reabsorption and secretion

The second step in urine formation after filtration is the selective reabsorption of filtered substances. Reabsorption is the transport of molecules from this ultra-filtrate into the blood. Three classes of substances are filtered at the glomerulus: electrolytes, non-electrolytes, and water. Some of the main electrolytes are sodium, calcium, potassium, magnesium, phosphate, bicarbonate, and chloride. Non-electrolytes include glucose, amino acids, urea, uric acid, and creatinine. Tubular reabsorption is achieved by active and passive transport mechanisms. Active transport (sodium, potassium, calcium, phosphate, and uric acid) requires energy to move substances against a concentration of an electrochemical gradient. A passive transport (urea, water, chloride, some bicarbonates, and some phosphates) does not require energy to move the substance being reabsorbed or secreted down an electrochemical gradient. Most reabsorption occurs in the proximal tubule, in order to keep needed substances, but not to reabsorb metabolic waste products. The remaining filtrate passes to the loop of Henle, the distal tubule, and the collecting ducts, so that less than 1% of the filtered load is excreted into the urine. Finally, tubular secretion moves substances by active transport or passive diffusion out of the peritubular blood into the tubular lumen, from the blood into the urine. Substances secreted by the tubules include phosphate, hydrogen, ammonia, uric acid, exogenous substances, and other wastes.

1.6 Renal functions

The main functions of the kidney are to purge the body of the end-products of metabolism and to regulate the body water volume, body fluid osmolality, electrolyte, acid-base balance and blood pressure. In a healthy person, the volume of urine produced per day can vary from as little as 300 mL, if no water is ingested or there is excessive water loss, up to a maximum of 23 L in case of excessive fluid ingestion. However, the average urine output per day is approximately 1500 mL. The kidneys' ability to vary the volume of daily urine output over such a wide range is essential to maintain a constant body fluid volume in the face of adverse factors such as excessive heat, which causes sweating; colonic infections causing diarrhea, or excessive thirst and water ingestion.

The mechanism responsible for maintaining a constant blood flow through the glomerulus and fluid, as the electrolyte balance, is the renin–angiotensin system (RAS). It takes place in the juxtaglomerular apparatus, a structure made up of specialized cells, called the macula densa cells, in the wall of the distal tubule, and cells in the endothelium of the arterioles which release a hormone called renin (renin-releasing cells). The mechanism is here explained: a fall in GFR results in a fall in the chloride ion concentration in the distal tubule; this stimulates the macula densa cells to induce the release of renin by the renin-secreting cells; plasma renin then converts the Angiotensinogen, released by the liver, to Angiotensin I, which is subsequently converted to Angiotensin II by the angiotensin-converting enzyme (ACE) found on the surface of vascular endothelial cells. Angiotensin II is a potent vasoconstrictive peptide that causes blood vessels to narrow, yielding an increase in blood pressure and secretion of the hormone Aldosterone from the adrenal cortex. Aldosterone stimulates the renal tubules to increase the reabsorption of sodium and water into the blood, while at the same time cause the excretion of potassium, to maintain electrolyte balance, this way increasing the volume of extracellular fluid in the body and blood pressure (Sparks 2014).

1.7 Kidney disease

Renal tissue injury triggers inflammatory and wound healing responses in order to promote regeneration and repair. After renal injury, damaged tissue releases cytokines and chemokines, which stimulate activation and infiltration of inflammatory cells to the kidney (Black 2019). Tissue repair or wound healing processes occur simultaneously with activation of myofibroblasts, collagen deposition and cell proliferation in order to promote regeneration and restore the normal tissue homeostasis. However, prolonged or repetitive damage, together

with activation of proinflammatory and pro-fibrotic signaling pathways, causes excess extracellular matrix deposition resulting in fibrosis and chronic kidney disease. Kidney disease can be divided into two categories depending on the length of the disease encompassing: acute kidney injury or chronic kidney disease.

1.7.1 Acute kidney injury (AKI)

Acute kidney injury (AKI) is characterized by a relatively sudden decrease in the production, processing, and excretion of ultrafiltrate by the kidney (decreased GFR). The Acute Kidney Injury Network (AKIN) defined AKI as "An abrupt (within 48 hours) reduction in kidney function currently assessed as an absolute increase in serum creatinine of more than or equal to 0.3 mg/dL, a percentage increase in serum creatinine of more than or equal to 50%, or a reduction in urine output (documented oliguria of less than 0.5 mL/kg per hour for more than six hours)"(Mehta 2007) . AKI reflects kidney damage from mild injury to total loss of function with severe implications for fluid homeostasis and electrolyte balance. Hospitalized patients usually present circulatory overload, hyperkalemia, metabolic acidosis, neurological complications, and increased mortality risk.

AKI may be divided into three major categories, according to the physiological location of the insult (Christ & Dainton 2015):

- Pre-renal – ineffective perfusion of the kidneys, which are structurally normal; when the renal blood supply is restricted, glomerular filtration is reduced, causing decreased perfusion of the kidneys. This event leads to ineffective filtration and disordered secretion and reabsorption.
- Renal (intrinsic) – damage of the renal parenchyma, associated with structural damage in the glomeruli and renal tubules.
- Post-renal – obstruction of the urine flow; the obstruction could be bilateral or located within the bladder or urethra.

The estimated incidence for AKI is 3-18% for all hospitalized patients and has increased in the recent years (Chawla 2011). About two-thirds of patients in intensive care units develop AKI, often as part of the multiple organ dysfunction syndrome (Chertow 2005). There is no specific current treatment for AKI and some patients require renal replacement therapy involving intermittent hemodialysis (IHD) or continuous renal replacement therapy (CRRT). Patients with AKI who require dialysis have a 50–70% mortality rate (Sakacı 2015).

Looking at the cellular mechanisms underlying AKI, several studies on animal models have shown cell-surface receptors to be implicated in both

initiation and/or propagation of epithelial injury in response to AKI. Examples of receptors involved in AKI-mediated injury include the FAS receptor and TGF-β receptor (Agarwal 2016).

In physiological condition kidney cell proliferation is limited to only a small percentage of cells, indicating that most cells are quiescent at the G0 phase. Nevertheless, in AKI there is an increase of proliferating cells in the damaged renal tubules. The mechanism of cell cycle reactivation is currently unclear, but it may involve the release of contact inhibition. When an injured renal tubular cell is dying, neighboring cells may stretch to cover the empty space, de-differentiating and activating their cell cycle (Agarwal 2016).

As shown in **Fig. 4**, renal ischemia/reperfusion injury (IRI), a common cause of AKI, results in rapid loss of cytoskeletal integrity and cell polarity. Briefly, the normally highly polar epithelial cells lose brush border mainly in the proximal tubule, and its polarity, because of a mislocalization or cytokine-induced disruption of adhesion molecules and other membrane proteins, such as the Na+K+-ATPase and β-integrins, as well as disruption of cell-cell interactions at adherent and tight junctions. With increasing time/severity of ischemia, cell death occurs by either necrosis or apoptosis. Some of the necrotic debris are released into the lumen and viable epithelial cells migrate to layer uncovered areas of the basement membrane, where they undergo division and replace lost cells. Ultimately, the cells go on to differentiate and re-establish the normal polarity of the epithelium.
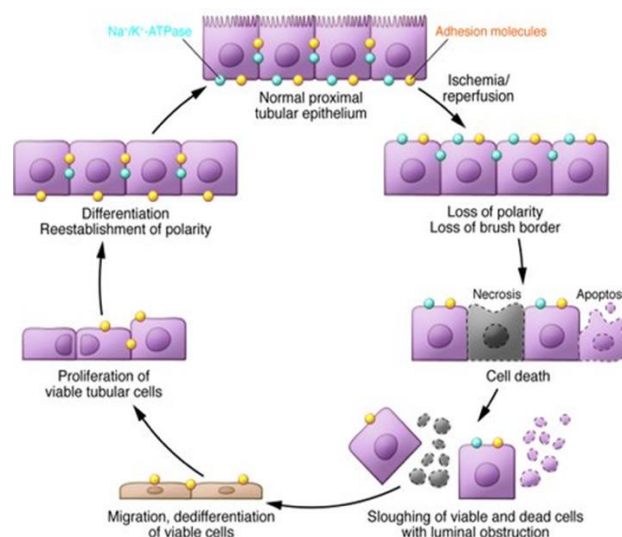
Figure 4. The current understanding of tubular injury and repair after ischemic AKI (modified from (Bonventre & Yang 2011) J Clin Invest DOI: 10.1172/JCI45161).

So, if the injury is mild, a repair process can be effective and lead to complete renal recovery. Nevertheless, severe injury are often accompanied by a maladaptive repair, which usually leads to nephron loss, fibrosis, vascular rarefaction, and chronic inflammation (Chou 2017).

1.7.2 AKI leading to chronic kidney disease (CKD)

Large population-based studies have demonstrated that patients who survive an episode of AKI are at considerable increased mortality risk and patients who recover are at much increased risk of developing chronic kidney disease (Chawla 2011). The association observed between AKI and a subsequent rapid decrease in renal function may not be the result of AKI effect, but rather due to the fact that AKI is a marker for higher-risk CKD patients to progress rapidly (Hsu & Hsu 2016). Indeed, the more recent assumption is to consider AKI and CKD as two interconnected syndromes where CKD is a risk factor for AKI and, in the meantime, AKI is a risk factor for the development and progression of CKD (Chawla 2014).

Although the kidneys are known to have a remarkable reparative capacity, when injury is extensive or prolonged, the repair in AKI may not be complete, leading to a maladaptive response that contributes to the late development of fibrosis and the progression towards CKD (Agarwal 2016). The main pathological mechanisms which concur during the AKI-to-CKD transition include endothelial dysfunction, vasoconstriction and vascular congestion, interstitial inflammation and the associated infiltration of inflammatory cells, fibrosis via myofibroblasts recruitment and matrix deposition, and tubular epithelial injury and dysregulated repair. In particular, tubular epithelial cells (TEC) have been proposed as the driving force of the AKI-to-CKD transition, acting as drivers of both inflammation and fibrosis. They produce a large variety of cytokines (e.g., IL-6, IL-1β, and TNF-α), thereby gaining a pro-inflammatory phenotype and directly influencing macrophage behavior; at the same time they are an important source of chemokines, adhesion molecules and reactive oxygen species (ROS) (Guzzi 2019).

1.7.3 CKD

According to the National Kidney Foundation Kidney Disease Quality Outcome Initiative (K-DOQI), chronic kidney disease is diagnosed when tests have persistently (for three months or more) shown a reduction in kidney function (estimated GFR less than 60 mL min^{-1} 1.73 m^{-2}), or the presence of proteinuria, with an urinary albumin: creatinine ratio persistently greater than 3 mg mmol^{-1} (CKD Evaluation and Management – KDIGO, 2012). Chronic

kidney disease is caused by a slow progression over a course of many years (generally 10–20) of pathological processes causing irreversible damage to kidney tissue. (Terrill 2002). CKD arises after many pathological insults that affects the renal function and destroys some of the nephrons, so that the other nephrons try to compensate by hyper filtration. Over a period of time, this process leads to glomerular hypertension, proteinuria, and eventually loss of renal function, as the kidneys become unable to maintain fluid and electrolyte balance and excrete waste products from the body. Besides, an increase in the glomerular capillary pressure leads to the destruction of glomerular capillary wall leading to the dysfunction of podocytes that covers the capillaries. Unlike acute kidney injury, where a full recovery of renal function can occur, in chronic kidney disease the kidneys are permanently damaged, and the disease is usually progressive.

The most common risk factors of advanced kidney disease resulting in renal replacement therapy are diabetes mellitus, glomerulonephritis, hypertension, pyelonephritis, polycystic kidney, and renal vascular disease (Bikbov 2020). Patients with genetic causes of CKD represent a few of the total number of patients with CKD.

A normochromic, normocytic anemia usually accompanies progressive CKD, and the overall prevalence of CKD-associated anemia is approximately 50% (Thomas 2008). To facilitate assessment of CKD severity, the National Kidney Foundation developed a criterium as part of its Kidney Disease Outcomes Quality Initiative (NKF K/DOQI). CKD patients are categorized into five stages based on the glomerular filtration rate (GFR) and albuminuria content (Coresh 2003):

- Stage 1: normal eGFR 90 mL/min per 1.73 m^2 and persistent albuminuria
- Stage 2: eGFR between 60 to 89 mL/min per 1.73 m^2
- Stage 3: eGFR between 30 to 59 mL/min per 1.73 m^2
- Stage 4: eGFR between 15 to 29 mL/min per 1.73 m^2
- Stage 5: eGFR less than 15 mL/min per 1.73 m^2 or end-stage renal disease

Stage 1 or 2 CKD patients progress to more advanced stages at approximately 0.5% per year. When GFR is less than 15 mL/min per 1.73m², a person has reached end stage renal disease (ESRD)(Webster 2017). End stage renal disease (ESRD) implies that deterioration of kidney function has reached a level where some form of renal replacement therapy (RRT) (in the form of dialysis or kidney transplantation), or conservative care (also called palliation or non-dialytic care), is required to sustain life (White & Cove-Smith 2015). Unfortunately, due to the lack of adequate specific treatments, many patients progress from CKD to end-stage renal disease (ESRD).

1.8 Pathophysiological events driving kidney disease

From a pathophysiological point of view, the progression of kidney disease is driven by the main following events: endothelial dysfunction, tubular epithelial injury, interstitial inflammation, and fibrosis.

1.8.1 Endothelial Dysfunction

Kidneys are metabolically highly active organs with a high oxygen demand. Early in kidney injury, interstitial capillaries become increasingly permeable, so that many plasma proteins are poured into the renal interstitium, thus triggering an inflammatory response. Once capillary rarefaction is established, tissue hypoxia, mitochondrial dysfunction, inflammation and subsequent fibrosis occur (Webster 2017). The renal pericyte is now recognized as a key contributor to vascular stability in response to kidney injury (Guzzi 2019). In addition, altered production of prostaglandins and reactive oxygen species due to injury of neighboring tubules, further impair tissue oxygen delivery, leading to a local 'no-reflow' phenomenon where the occluded microvasculature further amplifies initial injury (Ferenbach & Bonventre 2015).

1.8.2 Tubular Epithelial Injury/atrophy

As discussed above in the section "AKI leading to CKD", tubular epithelial injury is one of the driving forces of kidney disease. Different mechanisms link tubular damage with reduced glomerular filtration, thus leading to loss of renal function. First of all, tubular cell injury hampers normal tubular re-uptake of substances, which activates the tubule/glomerular feedback mechanism to reduce filtration and minimize hydro-electrolytic loss. Then, tissue debris derived from necrotic tubular cells occlude renal tubules, resulting in the formation of casts and luminal obstruction, thus hindering glomerular filtration in obstructed nephrons. Finally, tubular damage and cell death lead to activation of neighbor cells, which produce and secrete pro-inflammatory mediators, including reactive oxygen species, chemokines and cytokines (Sancho-Martínez 2015). There is a common consensus that the severity of tubulointerstitial injury correlates closely with long-term impairment of renal function (Matovinović 2009).

1.8.3 Interstitial Inflammation

Inflammation is a local response to tissue injury triggered by the immune system. The first event that occurs after any injury is the coagulation response through the anti-fibrinolytic coagulation cascade. When the endothelium is

damaged, circulating platelets are activated and the coagulation factor II (prothrombin) is proteolytically cleaved to form thrombin. Thrombin then converts soluble fibrinogen into insoluble strands of fibrin, which help in the formation of the fibrin clot to ensure quick hemostasis. Then platelets, damaged epithelial and endothelial cells release chemoattractants and cytokines in the interstitial microenvironment, such as platelet-derived growth factor (PDGF), keratinocyte chemokine (KC or CXCL1) and macrophage-inflammatory protein-2 (MIP-2 or CXCL2), which recruit neutrophils and mononuclear phagocytes to the site of injury (Black 2019). They also secrete metalloproteinases (MMPs), which disrupt the basement membrane, allowing inflammatory cells to be easily recruited to the site of injury. The circulating myeloid cells respond mainly to a gradient of Monocyte Chemotactic Protein 1 (MCP1 or CCL2), which binds to CC chemokine receptor 2 (CCR2) to promote mononuclear phagocytes adhesion and chemotaxis to the sites of injury. Both resident and infiltrating immune cells participate in inflammation, injury and repair in the acute phase of kidney injury and through a tight cross-talk with endothelial cells, epithelial cells, and pericytes, they also contribute to disease progression (Guzzi 2019). Once recruited to the site of injury, the inflammatory cells secrete pro-inflammatory cytokines with auto- and paracrine effect, in order to activate macrophages to phagocytose cellular debris and the fibrin clot, degrade the excess of extracellular matrix and restore the homeostasis. In addition, these cells also secrete a variety of toxic mediators, including reactive oxygen and nitrogen species that are harmful to the surrounding tissues. Consequently, if the inflammatory macrophages and neutrophils are not quickly eliminated, they can further spur the tissue-damaging inflammatory response that leads to scarring (Wynn & Ramalingam 2012). Macrophages exist in several different phenotypic states within the injured tissue promoting inflammation and at the same time repairing and healing the tissue, so their role in kidney disease is going to be better described in the next paragraph.

The main cytokines involved in the induction of an inflammatory response are produced predominantly by inflammatory cells, but their expression is also observed in epithelial cells and interstitial cells. Pro-inflammatory cytokines, such as tumor necrosis factor-α (TNF-α), interleukin -1β (IL-1β), interleukin-6 (IL-6), and interleukin-8 (IL-8) are associated in humans with worsened acute outcomes, chronic inflammation, and CKD. TNF-α is expressed mainly by macrophages, renal tubular cells, and mesangial cells and is known to play a pivotal role in renal inflammation and fibrosis, promoting the activation of the inflammatory and cell death signaling pathways, including those mediated by death receptor and caspase-mediated cell death and those mediated by c-

Jun/AP-122 and NF-κB (Strieter 1993). Like TNF-α, IL-1β is a potent proinflammatory mediator that worsen parenchymal cell injury. Mice that overexpress TNF-α or IL-1β in the lung develop highly progressive pulmonary fibrosis (Wynn & Ramalingam 2012). IL-1β also induces epithelial-mesenchymal transition (EMT) and myofibroblast activation through a TGF-β1–mediated mechanism, confirming that functions as a potent upstream driver of fibrosis. IL-1β and TNF-α also increase expression of IL-6, which shows autocrine growth-factor activity in fibroblasts. IL-6 is an important mediator of fibrosis in diffuse systemic sclerosis, liver fibrosis after CCl_4 exposure and fibrosis in chronic cardiac allograft rejection. Thus, many innate proinflammatory cytokines have crucial roles in the pathogenesis of fibrosis. After the initial phase of injury, early inflammation is followed by the infiltration of circulating immune cells (T- and B-cells) attracted by cytokines and damage-associated molecular patterns (DAMPs) released by injured cells. In contrast, a subset of regulatory T-cells (Treg) may act like self-tolerance inducers and suppress inflammation by enhancing immune homeostasis. Together with their positive effects, Treg depletion has been shown to aggravate ischemic AKI (Guzzi 2019).

1.8.4 Kidney fibrosis

The final pathological feature of chronic kidney diseases is renal fibrosis. Renal fibrosis is wound healing of kidney tissue after persistent injury and inflammation. Fibrosis is defined as the excessive accumulation of components of the extracellular matrix (ECM), such as collagen and fibronectin, in and around inflamed or damaged tissue, which can lead to permanent scarring, organ malfunction and, ultimately, organ death, as seen in end-stage liver disease, kidney disease, idiopathic pulmonary fibrosis (IPF) and heart failure (Bataller & Brenner 2005).

The balance between synthesis and degradation of ECM is tilted because synthesis and deposition exceed the rate at which ECM is degraded. Both insufficient extracellular or intracellular processing may lead to matrix accumulation and fibrosis. The severity of fibrosis is correlated with the progression of the disease (Webster 2017). Fibrosis is also a major pathological feature of many chronic autoimmune diseases, including scleroderma, rheumatoid arthritis, Crohn's disease, ulcerative colitis, myelofibrosis and systemic lupus erythematosus. Moreover, it influences tumor invasion and metastasis, chronic graft rejection and the pathogenesis of many progressive myopathies (Wynn & Ramalingam 2012).

The major events which characterize fibrosis in kidney are glomerulosclerosis and tubulointerstitial fibrosis.

Glomerulosclerosis is prompted by endothelial damage and dysfunction. Glomerular microinflammation is initiated by the activation of endothelial cells in response to hypertension, with inflammatory cells activating mesangial cells to proliferate. Transforming growth factor-β (TGF-β) and other growth factors (including PDGF, FGF, TNF and IFNγ) stimulate mesangial cells to dedifferentiate to mesangioblasts (immature mesangial cells). These mesangioblasts are capable of producing excessive extracellular matrix, leading to mesangial expansion, an early sign of glomerulosclerosis. Defects in podocyte structure, function, or number can expose areas of the glomerular basement membrane (GBM) and contribute to glomerulosclerosis. Then inflammatory cells are recruited from the blood flow, infiltrate the renal interstitium and interact with interstitial myofibroblasts. As fibrosis evolves, injured tubular epithelial cells lose their regenerative capacity and undergo apoptosis leading to tubular atrophy and creating non-functional sclerotic glomeruli. Risk factors for progressive glomerulosclerosis include hypertension, dyslipidemia, and smoking (Webster 2017).

The cytokine responsible of the activation of ECM producing myofibroblasts, regarded as the key mediators of fibrotic tissue remodelling, is TGF-β (Gabbiani 2003). Alongside with TGF-β, other important profibrotic factors involved in renal fibrogenesis are Angiotensin II, CTGF, PDGF, FGF-2, EGF, ET-1 and Mast cell tryptase. Angiotensin II is produced locally by activated macrophages and fibroblasts and is thought to exert its effects by directly inducing NADPH oxidase activity, stimulating TGF-β production in tubular epithelial cells and fibroblast and triggering fibroblast proliferation and differentiation into collagen-secreting myofibroblasts (Rosenkranz 2004).

TGF-β exists in three isoforms (TGF-β1, TGF-β2, and TGF-β3) and is expressed and secreted by many cell types during injury. However, TGF-β1 is the prevalent isoform, mainly produced by circulating monocytes and tissue macrophages. Acting mainly on fibroblasts, mesangial cells, and tubular cells, TGF-β is commonly regarded for its role in fibrosis; however, it exerts broad modulatory activities on numerous biological pathways, such as embryonic development, stem cell differentiation, immune cell signaling, and tissue repair. TGF-β production correlates with the progression of liver, lung, kidney, skin and cardiac fibrosis, and inhibition of the TGF-β1 signaling pathway has been shown to reduce the development of fibrosis in many experimental models.

TGF-β1 shows profibrotic effects on kidney through different mechanisms. It is involved in trans-differentiation of different cell types into

myofibroblast-like cells, but it also stimulates the production of ECM, as type I collagen, in a Smad3-dependent manner. Furthermore, TGF-β exerts matrix-preserving actions by suppressing the activity of Matrix Metalloproteinases (MMPs) and by inducing synthesis of protease inhibitors, such as Tissue Inhibitor of Metalloproteinase (TIMPs) and Plasminogen Activator Inhibitor-1 (PAI-1) (Biernacka 2011).

In macrophages, the regulation of TGF-β1 is mainly exerted on both secretion and activation of latent TGF-β1. TGF-β1 is stored inside the cell as a disulphide-bonded homodimer, non-covalently bound to a latency-associated protein (LAP) forming the Small Latent Complex (SLC), which keeps TGF-β inactive. This complex is bound to the Latent TGF-β-Binding Protein (LTBP) by disulphide bonds, forming a larger complex called Large Latent Complex (LLC). In many tissues the LLC is secreted and bound to the extracellular matrix (ECM) components, such as elastin fibrils and fibronectin-rich pericellular fibers. In this way, significant amounts of latent TGF-β are stored in the inactive form in the matrix, so that, when required, it is easily available in the tissue. Besides, due to the high affinity between TGF-β and its receptors, activation of only a small fraction of this latent TGF-β generates maximal cellular response (Biernacka 2011).

Several agents, including cathepsins, plasmin, calpain, thrombospondin, integrin-αvβ6 and matrix metalloproteinases catalyze the dissociation of the LLC in order to allow the activation of TGF-β and its binding to the receptors (Roberts 2003). Once activated, TGF-β binds its transmembrane receptors and activates the canonical ALK5/Smad3 pathway, which modulate transcription of important target genes, including procollagen I and III, thus stimulating the deposition of ECM (Biernacka 2011). Nevertheless, Smad3/TGF-β1-independent mechanisms of fibrosis have also been demonstrated in the lung and other tissues, suggesting that profibrotic mediators such as IL-4, IL-5, IL-13 and IL-21 can act separately from the TGFβ/Smad-signaling pathway to stimulate collagen deposition (Y. Liu 2011). As anticipated previously, TGF-β is pivotal in the activation of fibroblasts. After activation by TGF-β fibroblasts transform into α-SMA expressing myofibroblasts as they migrate along the fibrin lattice into the wound. The myofibroblast phenotype is characterized by formation of gap junctions and by the acquisition of a contractile apparatus due to associated contractile proteins, such as α-SMA and non-muscle myosin. TGF-β-induced α-SMA synthesis requires Smad3, but also involves FAK, JNK, TAK and PI3 kinase/Akt pathways.

Following activation, the myofibroblasts promote wound contraction, the process in which the edges of the wound migrate towards the center. Finally,

epithelial and/or endothelial cells divide and migrate over the basal layers to regenerate the damaged tissue, which completes the wound healing process; however, in pathologic conditions activated myofibroblasts become the cellular effectors of fibrosis. Myofibroblasts can be derived from multiple sources. In addition to resident mesenchymal cells, myofibroblasts can derive from epithelial cells in a process termed epithelial–mesenchymal transition (EMT), from endothelial cells through endothelial–mesenchymal transition (EndoMT)(Kalluri 2003) and finally from macrophages through macrophage–myofibroblast transition (MMT). In the kidney, all these processes are driven by TGF-β.

EMT occurs first in development, when epithelial cells differentiate into mesenchymal cells and vice versa until development is complete. Epithelial cells can dedifferentiate into mesenchymal cells secondary to injury, during which transitioning cells migrate from the basement membrane to the interstitial space and differentiate into fibroblasts. Phosphorylation of Smad3 allows it to complex with Smad4 and translocate to the nucleus to activate target pro-fibrotic genes, causing tubular cells to dedifferentiate into mesenchymal cells and driving development of renal fibrosis (Black 2019).

EndoMT is a process during which endothelial cells dedifferentiate, lose cell-specific markers, and develop into mesenchymal or myofibroblast cells. Although EndoMT was initially hypothesized to be active solely during embryonic heart development, further studies suggest the contrary. In the context of renal pathology, EndoMT has been characterized in CKD as a source of fibroblasts and myofibroblasts (Zeisberg 2008). Wang and colleagues investigated EndoMT in chronic allograft rejection and found the transition to be driven by TGF-β, Smad, and the Akt/mTOR/ p70S6K signaling (Bao 2011). EndoMT has also been examined in models of CKD, UUO, diabetic nephropathy, and Alport syndrome, in which a portion of fibroblasts were found to have endothelial origin (Zeisberg 2008). Interestingly, these models produced various amounts of EndoMT derived fibroblasts, suggesting specific stimuli may be responsible for EndoMT induction and the level of such induction (Black 2019).

MMT is a process by which macrophages differentiate into myofibroblasts. In a recent study, cell lineage tracing demonstrated that bone marrow-derived macrophages undergo differentiation into myofibroblasts during murine UUO. Interestingly, it was found that >60% of collagen-producing (α-SMA+) cells were derived from M2 (alternatively activated) macrophages. Furthermore, Wang and colleagues examined human renal allograft biopsies and demonstrated that macrophages (CD68+) actively

underwent transition into myofibroblasts (α-SMA+), similar to findings in murine UUO. Fate mapping showed that bone marrow-derived macrophages were able to differentiate into myofibroblasts, which was prevented by Smad3 deletion, highlighting the potential importance of the contribution of MMT in the development of renal fibrosis (Black 2019).

Although a large number of chemokine signaling pathways are involved in the mechanism of fibrogenesis, the CC- and CXC-chemokine receptor families have consistently exhibited important regulatory roles. Specifically, CCL3 (macrophage inflammatory protein 1α) and CC-chemokines such as CCL2 (monocyte chemoattractant protein-1), which are chemotactic for mononuclear phagocytes, were identified as profibrotic mediators. Macrophages and epithelial cells are believed to be the key sources of CCL3, and studies in the bleomycin model of pulmonary fibrosis showed that anti-CCL3 antibodies could significantly reduce the development of fibrosis (Y. Liu 2011).

1.9 Macrophages

Macrophages belong to the family of mononuclear phagocytes, a group of cell types including circulating monocytes, tissue resident macrophages and dendritic cells (DCs), which originate from common myeloid progenitor cells in the bone marrow under the influence of colony-stimulating factor 1 (CSF-1) (Geissmann 2010).

As regard to mononuclear phagocytes, monocytes are large cells, mainly agranular, with a classic unilobular nucleus, which comprise 2–10% of leukocytes in the peripheral blood, and the majority of them resides in the spleen, ready for recruitment in injured tissues. Monocyte development in the bone marrow sequentially gives rise to monoblasts, pro-monocytes and finally monocytes, which are released into the bloodstream. During inflammation, monocytes then migrate from the bloodstream into the injured tissue, where they undergo differentiation in macrophages or dendritic cells in response to microenvironmental signals to which they are exposed. Lastly, dendritic cells, which have been considered for long time as simply specialized macrophages and not as an independent lineage, present antigen to T lymphocytes with extremely high efficiency (George 2017).

Resident macrophages are less uniformly shaped and are divided into subpopulations based on their distinct functions and anatomical location (Kupffer cells in the liver, microglial cells in the central nervous system, Langerhans cells in the skin, kidney-resident macrophages in the kidney). Their main role is to provide immediate defense against foreign pathogens and organize leukocyte infiltration.

More recent studies have highlighted a different embryonic origin for kidney-resident macrophages, which actually derive from embryonic macrophage progenitors, which initially migrate from the yolk sac, and later from the fetal liver, into the developing kidney (Munro & Hughes 2017). Macrophages are an essential component of innate immunity, as they perform a wide range of critical roles in homeostasis, surveillance, immune response, and tissue injury and repair. As regard to immune response, their main function is to clear the interstitial environment by phagocyting pathogens, dying cells as well as cellular debris, aged erythrocytes, pathological matrix, and immunocomplexes. Besides, they also stimulate an adaptive immune response, by acting as antigen-presenting cells (APCs) and by recruiting other immune cells such as lymphocytes (Guiteras 2016a). Macrophages, both resident and circulating, may be activated by a wide range of stimuli. Notably, bacterial cell wall proteins such as lipopolysaccharide (LPS), flagellin, but in general Pathogen or Damage – Associated Molecular Patterns (PAMPs or DAMPs), activate macrophages by engagement of specific receptors collectively known as pattern recognition receptors (PRRs), including Toll-like receptors (TLRs) on macrophages membranes (Charles A. Janeway & Medzhitov 2003).

According to their function in inflammation, macrophages can be divided in subpopulations (Cao 2015). Two well defined phenotypes are commonly referred to as classically activated, pro-inflammatory macrophages (M1), produced by exposure to LPS or IFN-γ, and alternatively activated anti-inflammatory macrophages (M2), induced by Th2 cytokines such as IL-4 and IL-10. In the following paragraphs we are going to discuss widely their function in kidney disease. Generally, macrophage polarization is measured by changes in expression of several surface markers, genes, or proteins, which change in response to cytokines present in the microenvironment. At time during the inflammatory response macrophages can shift from the pro-inflammatory phenotype (M1) to an anti-inflammatory phenotype (M2) and vice versa. M1 macrophages produce a great amount of pro-inflammatory mediators and mediate antimicrobial defense and anti-tumor immunity; they are generally characterized by an increased expression MHCII, and CD80/86 (Bowdish 2016). Conversely, M2 macrophages have anti-inflammatory functions and are involved in parasite containment, wound healing, and fibrosis; M2 are generally characterized by an increase in CD206 and/or CD163 (the mannose and hemoglobin-haptoglobin receptors, respectively, whose expression increases endocytic uptake) (Cao 2015). Notably, M1 macrophages may convert to M2 macrophages in response to tissue factors within the tissue during the recovery phase.

M1 and M2 digest differently the terminal nitrogen linkages of Arginine (Albina 1990). Pro-inflammatory M1 macrophages preferentially produces Nitric Oxide (and Citrulline) that inhibits cell proliferation, whereas anti-inflammatory M2 macrophages produce Ornithine (and Urea) that promotes proliferation and repair (through polyamines and collagen). Other changes in macrophages typically occur together with either NO production for M1, as increased Class II expression and production of IL-12/23 and IL-8, or Ornithine production for M2, as increased TGF-β, IL-10, IFN α/β, chitinases, matrix metalloproteinases, and scavenger receptors. These different molecules stimulate very different types of immune responses. It is also noteworthy that M2 is the "default" activity in resident macrophages in normal tissues, healing wounds, or in growing tumors metabolism (Mills 2012).

Another classification system in mice uses the Ly-6C marker, a cell surface glycoprotein, to identify functionally discrete murine circulating monocyte populations: Ly-6C^{hi} (high) monocytes (analogous to CD14^{hi} CD16^{lo} human monocytes) are recruited early to inflammatory environments and thought to be pro-inflammatory, whereas Ly-6C^{lo} (low) monocytes (analogous to CD14^{lo} CD16^{hi} human monocytes) play a more surveying cell role and can restore resident tissue macrophages stock. Differential Ly-6C expression in diseased tissues has identified functionally distinct macrophage populations (Ramachandran 2012). Indeed, Ly-6C^{hi} mouse monocytes express CC-Chemokine receptor 2 (CCR2) and therefore respond to CC-chemokine ligands (CCL) including CCL2, an important chemokine expressed by most cells in response to inflammatory stimuli. By contrast, Ly-6C^{low} monocytes do not express CCR2 (Lichtnekert 2013).

1.9.1 Macrophages in kidney disease

Kidney-resident macrophages constitute the majority of the renal medullary interstitial cell population but are also found in contact with cortical, distal and proximal tubules and Bowman's capsule. They are a physical component of the juxtaglomerular complex (Hume & Gordon 1983). More recently a particular subset of renal resident macrophages has been identified, located at the abluminal side of the peritubular capillaries and capable of monitoring endothelial transport (Stamatiades 2016). These resident macrophages seem to form a distinct anatomical and functional unit with the peritubular capillary endothelial cells that have the ability to detect and scavenge circulating immune complexes pumped into the interstitium via trans-endothelial transport, possibly explaining the further recruitment of monocytes and neutrophils. This macrophage-endothelial functional unit, with a specific cross-

talk at both the cellular and molecular levels, is also likely to be involved in the response to AKI (Guzzi 2019).

Macrophages have a pivotal role in kidney inflammation and fibrosis (**Fig. 5**). Their pathogenic role has been demonstrated by depletion of kidney-resident macrophages with liposomal clodronate (LC) in different types of experimental kidney disease models (Kitamoto 2009). In agreement, in human studies the degree of glomerular or interstitial macrophage infiltration has been shown to correlate with the severity of kidney injury in patients with glomerulonephritis, suggesting their pathogenic role in kidney disease (Eardley 2008). However, mounting evidence shows that macrophages also play a reparative role during the course of disease, by actively participating in clearance of apoptotic and necrotic cells to resolve injury and in matrix remodelling to restore tissue homeostasis in acute and chronic kidney disease (Cao 2015). Indeed, the depletion of M2 macrophages in mice with established AKI results in prolongation of renal injury (Guzzi 2019).
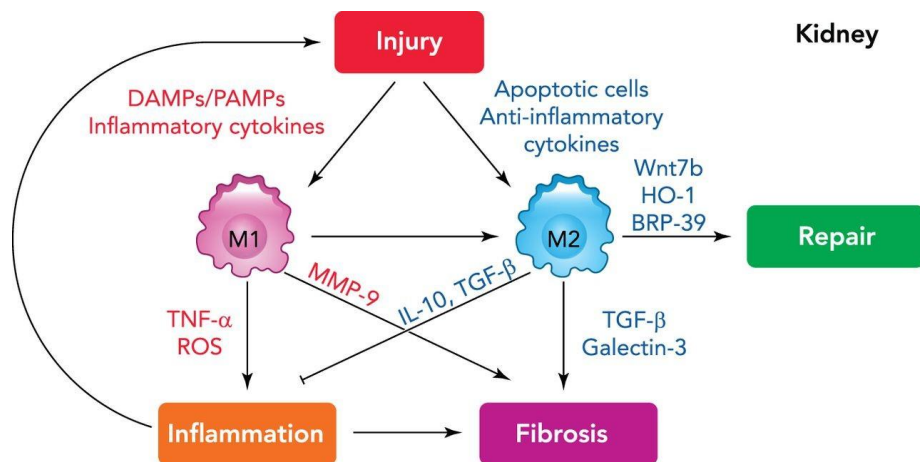
Figure 5. Diagram of monocyte recruitment after kidney injury. During the early phase of tissue injury, the kidney interstitial microenvironment is dominated by micro-organism derived PAMPs and DAMPs, as well as pro-inflammatory cytokines, which promote full activation of the pro-inflammatory M1 macrophage, leading to inflammation. In contrast, the uptake of apoptotic cells and anti-inflammatory cytokines drive macrophage polarization toward an anti-inflammatory M2 phenotype, promoting renal repair and tissue remodelling (Q. Cao 2015).

Besides the canonical classification of macrophages in M1 and M2, Anders and Ryu proposed four types of *in vivo* macrophages, defined according to their predominant roles in various phases of kidney disease, namely pro-inflammatory, anti-inflammatory, profibrotic, and fibrolytic macrophages (Anders & Ryu 2011). Distinct subsets of macrophages can co-exist in kidney tissue, and particular subsets can dominate at different stages of disease, from the initiation of kidney injury to the recovery.

1.9.2 M1 macrophages

Acute kidney injury triggers a prominent infiltrate of immune cells, firstly neutrophils, natural killer (NK) cells and T helper (Th)1/17 cells. Monocytes infiltrate the injured kidney shortly after neutrophils, being recruited by the monocyte chemoattractant protein-1 (MCP-1/ CCL2) released by resident macrophages and injured cells, so that they can differentiate into M1 macrophages and contribute to early tubular injury. IFN-γ, TNF-α, and granulocyte-macrophage colony-stimulating factor (GM-CSF-1), secreted by infiltrating Th1 cells and natural killer cells, hence, promote the activation of the pro-inflammatory tissue macrophage (M1). The full activation of M1 macrophages occurs mainly through the recognition of Damage Associated Molecular Patterns (DAMPs) via toll-like receptors (TLRs), intracellular Pattern Recognition Receptors (PRRs) and the IL-1 receptor (IL-1R) through the adaptor molecule myeloid differentiation primary response gene 88 (MyD88) (Chen 2007) (Fig. 1.5). Thus, a TLR ligand acting in an MyD88-dependent manner will induce TNF transcription, which can act together with IFN-γ, released by NK cells in response to stress and infections, in an autocrine manner to activate the M1 macrophages. The combination of these two signals results in a macrophage population with enhanced microbicidal effects as well as in increased production of pro-inflammatory cytokines, superoxide anions and oxygen and nitrogen radicals. This causes tissue inflammation and additional renal cell damage sustaining parenchymal loss and leading to renal atrophy, but also promotes cytotoxic adaptive immunity by upregulating major histocompatibility complex class II (MHC II) in conjunction with co-stimulatory molecules (CD40, CD80 and CD86) (Mantovani 2004).

M1 macrophages secrete significant amount of proinflammatory cytokines, such as IL-1β, IL-15, IL-18, TNFα, and IL-12, but also the chemokines CCL15/HCC-2, CCL20/MIP-3α, and CXCL13/BCA-1, and the angiostatic IFNγ responsive chemokines CXCL9/Mig, CXCL10/IP-10, and CXCL11/I-TAC, which coordinate NK and Th1 recruitment in type I immune responses through their activity on CXCR3 (Mantovani 2004). The proinflammatory mediators amplify inflammation and promote additional injury in a positive feedback loop (**Fig 5**). M1 macrophages also release matrix metalloproteinases (MMPs) to enable their migration through basement membranes and interstitial ECM, mainly by secretion of MMP-9, which increase tubular cell epithelial-mesenchymal transition via the β-catenin pathway (**Fig. 5**). The transcription interferon-related factor (IRF5) also seems to play a key role in M1 macrophage polarization, suggesting that inhibiting IRF5 might be useful for chronic macrophage-induced inflammation. Briefly, Toll-like receptor

(TLR) activation of the transmigrated monocyte requires IRF5 for full activation of NF-kB signaling and the secretion of proinflammatory cytokines/chemokines, reactive oxygen species, and other proinflammatory mediators that define a proinflammatory macrophage (Guiteras 2016).

In the case of AKI, after the initial inflammatory response, the microenvironment is dominated by growth factors that promote wound healing, especially in conditions of incomplete or insufficient epithelial repair. Subsequently, Th2 and Tregs are recruited into kidney and regulate immune responses, including macrophage switch towards an anti-inflammatory (M2) phenotype following uptake of apoptotic cells and stimulation by regulatory cytokines. M2 macrophages predominate at this stage and contribute to the resolution of inflammation and tissue repair (**Fig. 6a**).

As regard to CKD, due to progressive injury and persistent inflammation, M1 macrophages persistently surround sites of damaged tissue (**Fig. 6b**). Subsequently, small numbers of Th2 cells and Tregs are recruited into the kidney to regulated local immune responses. A small amount of anti-inflammatory (M2) macrophages coexists with M1 macrophages, due to a persistent inflammatory kidney microenvironment. Constant inflammatory and fibrotic factors in chronic kidney disease promote renal fibrosis (Anders & Ryu 2011).
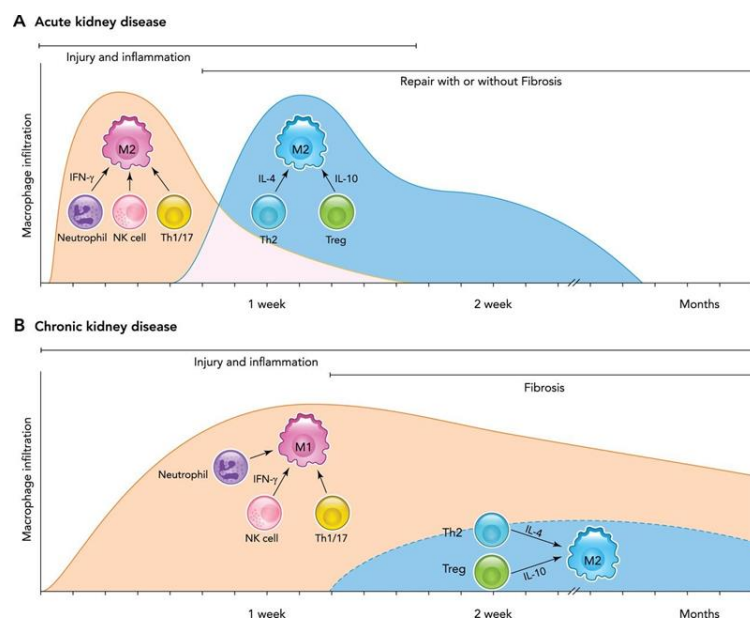
Figure 6. The phenotypic switch of macrophages during the course of acute and chronic kidney disease. (**a**) acute kidney injury. (**b**) in chronic kidney disease (Anders & Ryu 2011).

1.9.3 M2 macrophages

M2 macrophages support the resolution of the inflammation, promoting wound healing and tissue remodelling. The mechanisms underlying kidney macrophage phenotypic switch from pro-inflammatory to anti-inflammatory are not completely understood. The reduction of DAMPs and PAMPs as well as the increase of apoptotic cells represent a change in the tissue environment that might promote phenotype change of tissue macrophages.

Immunosuppressive (regulatory) T cells further promote the polarization towards anti-inflammatory macrophages (M2) via release of IL-10 and TGF-β. An integration of these different environmental signals for the deactivation of the M1 macrophages occurs at the transcriptional level via the transcription factor IRF4, which also functions as an intracellular competitor of IRF5, and thereby blocks TLR and IL-1R signaling (Anders & Ryu 2011).

The alternatively activated macrophages can be subdivided further into three subgroups: M2a macrophages induced by IL-4 and/or IL-13, M2b macrophages induced by immune complexes with LPS or IL-1β, and M2c macrophages induced by IL-10, TGF-β, or glucocorticoids (Kitamoto 2009). Macrophage subtype phenotype are summarized in **Table 1**.

M2a macrophages express high levels of mannose receptor (CD206), produce anti-inflammatory IL-10 and have immunoregulatory functions. M2a express also fibronectin 1 (FN-1) and matrix associated protein βIGH3, which promote fibrogenesis, the coagulation factor XIII and insulin like growth factor 1 (IGF-1), which provides signals for tissue repair and proliferation (Martinez 2008). These cells secrete components of the ECM and therefore their main functions seem to be associated with wound healing and tissue remodelling and repair.

Then, M2b macrophages crosstalk with B cells, efficiently sustaining antibody production, the majority of which are of the IgG1 isotype. This category is characterized by high IL-10 secretion, in addition to upregulating antigen presentation and promoting Th2 responses. Both M2a and M2b macrophages have an immunoregulatory role through downregulation of IL-12, IL-6 and TNF.

Lastly, M2c macrophages are a functionally heterogeneous group induced by IL-10, TGF-β and glucocorticoids; this subset, referred to as "deactivated" macrophages or anti-inflammatory, is known to be involved in tissue repair and remodelling, through downregulation of proinflammatory cytokines, increased anti-inflammatory cytokine production and increased debris scavenging activity.

M1	M2a	M2b	M2c
Classic type I inflammation	Alternative type II inflammation	Immunoregulatory	Immunosuppression
Ingestion of pathogens, antigen presentation, complement synthesis, stimulation of Th1 cells	Recruitment of Th2 cells, eosinophils and basophils, killing of intracellular pathogens such as helminths	Promote Th2 responses, IgG class switching by B-cells, matrix synthesis	Resolution of inflammation, matrix synthesis and remodelling
induced by IFN-γ combined with microbial stimuli (PAMPs and DAMPs)	induced by IL-4 and/or IL-13	induced by immune complexes with LPS or IL-1β	induced by IL-10, TGF-β and glucocorticoids

Table 1. Types of macrophage activation and their related phenotypes.

The uptake of apoptotic cells and anti-inflammatory cytokines drive macrophage polarization from a pro-inflammatory M1 toward an anti-inflammatory M2 phenotype, which in turn promotes renal repair through secretion of trophic factors such as Wnt7b, hem-oxygenase-1 (HO-1), and chitinase-like protein BRP-39. In addition, Galectin-3 and TGF-β produced by M2 macrophages promote kidney fibrosis directly (Cao 2015).

Therefore, renal fibrosis may not only be driven by pro-inflammatory M1 macrophages, but also by insufficient epithelial healing or by "profibrotic" M2 macrophages and fibrocytes (**Fig. 7**). In fact, persistence of the wound healing process, by constant production of several wound healing growth factors, could be pathological, resulting in irreversible fibrosis and progressive kidney tissue destruction (Lech & Anders 2013).

The mechanisms underlying the antifibrotic role of interstitial macrophages have been studied recently in unilateral ureteral obstruction (UUO), a mouse model of renal fibrosis. López-Guisa et al. demonstrated that mannose receptor 2 (Mrc2)-expressing macrophages displayed a fibrosis-attenuating role through activating a lysosomal collagen turnover pathway in UUO. They found that Mrc2, a cell surface receptor that binds to and internalizes collagen, was upregulated on macrophages and myofibroblasts in UUO, and that reduced Mrc2 expression significantly worsened kidney fibrosis in Mrc2-deficient mice with UUO (López-Guisa 2012).

In contrast to the protective effect of macrophage depletion during early phase of kidney I/R, macrophage depletion during the later recovery phase impedes tissue repair and regeneration. In fact, an inverse correlation between the number of interstitial macrophages and the degree of fibrosis has been shown recently in UUO, thereby suggesting there is a subpopulation of infiltrating macrophages with an anti-fibrotic role in the recovery phase of obstructive nephropathy. Nishida and colleagues demonstrated that interstitial macrophages display an anti-fibrotic role at day 14, but not at day 5, after UUO (Nishida 2002).
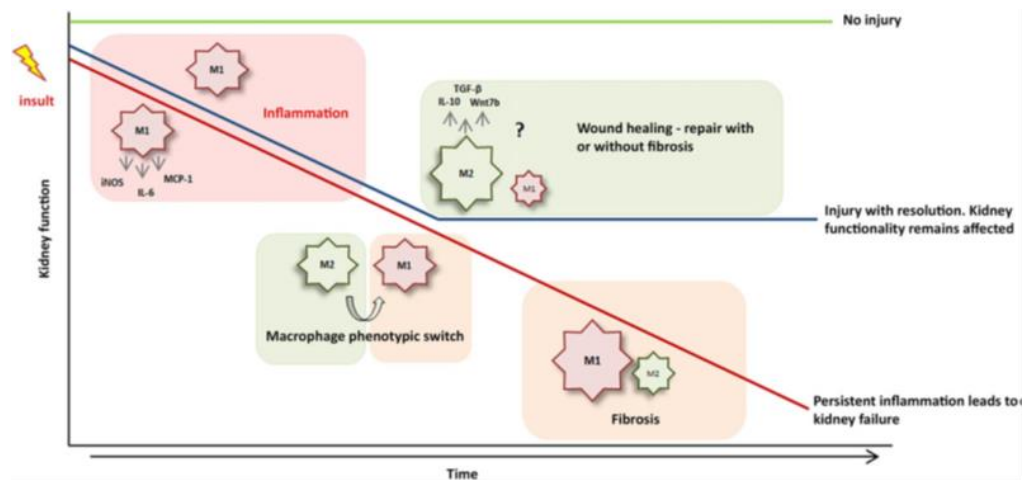
Figure 7. M1/M2 macrophage balance depending on chronic kidney disease (CKD) progression. In the early stages of kidney disease, pro-inflammatory macrophages (M1) infiltrate the injury site, promoting inflammation. If the injury is not sustained in time, renal function can recover. In this context, macrophages switch to an anti-inflammatory (M2) phenotype, leading to a wound healing phase. However, if there is no injury resolution, M1 macrophages persist at injured sites, while M2 macrophages could subsequently undergo a phenotypic switch to M1. Thus, the persistent release of profibrotic and inflammatory factors promote renal fibrosis, leading to renal failure (Guiteras 2016b).

1.10 Lysosomal Cathepsins

Cathepsins (Cts) are an extensive family of lysosomal proteases, found in many animals (Katunuma 2003). Most of the cathepsins are endopeptidases, cathepsins B and H are both endo- and exopeptidases, whereas cathepsins X and C are exopeptidases (Repnik 2012). So far, more than 20 types of Cts have been identified in animals, plants, and microorganisms. In humans, the cathepsin protease family consists of 15 known members that can be classified in 3 distinct groups, according to their active-site amino acid: serine proteases (cathepsins A and G), cysteine proteases (cathepsins B, C, H, F, K, L, O, S, V, X and W) and aspartate proteases (cathepsins D and E) (Joyce 2004). Some cathepsins are ubiquitously expressed, such as cathepsin B, L, H, and C, whereas the newly found cathepsins K, W, and X are expressed in specific cells and tissues. Cathepsins are synthesized as inactive pre-pro-enzymes having a signal peptide

and a multi- functional N-terminal pro-region. The role of the pre- peptide is to drive cathepsin precursor into the lumen of the rough endoplasmic reticulum, after which is subsequently hydrolyzed. Meanwhile the pro-region inhibits its proteolytic activity, preserving its three-dimensional structure at neutral pH and maintaining the precursor in an inactive state until cleaved. The pro-cathepsin later undergoes carbohydrate processing and asparagine-linked glycosylation in the Golgi (Guha & Padh 2008). Although all the cathepsins are targeted to the endolysosomes via the mannose-6-phosphate receptor pathway, they are not all expressed at the same levels in different tissues. Most of the members become activated in the lysosomal acidic environment where they are active and stable, however they present activity in other cell locations under certain circumstances described afterwards.

Cathepsins participate in many homeostatic and pathological processes contributing to health and disease, as summarized in **Table 2**.

Cathepsin	Class	Distribution	Function	Involvement in disease
Cathepsin B	Cysteine	Ubiquitous	Early neutrophil, T and B cell apoptosis TLRs signalling and TNF-alpha production Selectors for peptide-MHC II complexes	Inflammatory disorders Alzheimer's disease Cancer
Cathepsin C	Cysteine	Ubiquitous	Activation of granzymes A and B	Inflammatory disorders
Cathepsin D	Aspartic	Ubiquitous	Early neutrophil, T and B cell apoptosis Selectors for peptide-MHC II complexes ECM degradation	Inflammatory disorders, cancer Rheumatoid arthritis, Alzheimer's disease
Cathepsin E	Aspartic	Immune cells	Selectors for peptide-MHC II complexes	Atopic dermatitis, dermatitis
Cathepsin F	Cysteine	Ubiquitous	TLRs signalling	Cancer
Cathepsin G	Serine	Neutrophil lysosomes Human B cells (exogenous source)	IL-8, IL-1beta and TNF-alpha activation IL-6 disactivation Destruction of the autoantigen MBP (in B cells)	Inflammatory disorders
Cathepsin H	Cysteine	Ubiquitous	ECM degradation	Cancer
Cathepsin K	Cysteine	DCs, epithelial cells	TLRs signalling ECM degradation and bone remodeling	Rheumatoid arthritis
Cathepsin L	Cysteine	Ubiquitous	TLRs signalling Selectors for peptide-MHC II complexes NKT and CD4 T cells production, neuronal cell death and osteoclastic bone degradation	Thymic pathology Atherosclerosis Rheumatoid arthritis Cancer
			ECM degradation	
Cathepsin S	Cysteine	APC	TLRs signalling Selectors for peptide-MHC II complexes NKT cells production, ECM degradation	Arthritis, atherosclerosis Bronchial asthma, COPD Psoriasis, cancer
Cathepsin V	Cysteine	Ubiquitous	Selectors for peptide-MHC II complexes, NKT and CD4 T cells production	Thymic pathology, cancer
Cathepsin W	Cysteine	NK and CD8+ cytotoxic T cells	Selectors for peptide-MHC II complexes	Autoimmune atrophic gastritis
Cathepsin X	Cysteine	Ubiquitous	T cell activation	Cancer

Table 2. Table summarizing main cathepsins' functions in the immune system. Table modified from "Cathepsins and their involvement in immune responses" (Conus & Simon 2010).

Inside lysosomes, cathepsins are the main effectors of endo-lysosomal proteolysis, as they are involved in the turnover of proteins and plays various roles in maintaining the normal metabolism of the cells. However, cathepsins can also be found in the intracellular and extracellular spaces where they exert different functions (Stoka 2001) (Stoka 2016). Outside the lysosomal compartment, cathepsins are involved in degradation of the extracellular matrix or activation of fibroblast invasive growth when secreted into the extracellular

space, and execution of programmed cell death when released into the cytosol. Indeed, there are extensive evidence linking cathepsins with apoptosis, in particular cathepsins D (CtsD) and B (CtsB) (Liaudet-Coopman 2006). Furthermore, CtsK exerts collagenolytic activity, playing a pivotal role in bone resorption and lung matrix homeostasis. Besides, it has a role in the homeostasis of the dermal extracellular matrix and the dynamic equilibrium between matrix synthesis and proteolytic degradation (Rünger 2007). As regard to cathepsins role in pathological conditions, cathepsins contribute to many human pathologies such as cancer and metastasis, fibrosis, various neurodegenerative disorders, inflammatory cardiovascular diseases, and obesity amongst others.

Cathepsins are distributed ubiquitously in most cancer tissues and several studies have shown a correlation between cancer development and differential expression and localization of cathepsins. In particular, CtsD, CtsB and CtsL, have been implicated in cancer progression and metastasis (Kos 2000). In addition, cathepsins have been implicated as biomarkers for the prognosis of different types of cancer (Kos 2000). To that respect, high levels of CtsB were reported in sera of patients with breast, ovarian, uterine, liver, pancreatic, melanoma, colorectal and lung cancer. Furthermore, there is a mounting evidence that the imbalance of the regulation between cathepsins and their endogenous inhibitors, such as cystatins, has an important role in the tumor progression, metastasis, migration and extracellular turnover (Kolwijck 2010; Paraoan 2009). During cancer progression, cathepsins can be expressed at the cell surface and secreted into the extracellular space, where they can degrade components of the ECM (Joyce & Hanahan 2004). This extracellular activity allows cancer cells to invade surrounding tissues, blood, and lymph vessels and metastasize to distant sites (Tan 2013).

Cathepsins play also an important role in fibrosis. Within the cysteine proteinase family, three proteases show significant matrix-degrading activities, CtsK, CtsL, and CtsS. In particular, over-expression of CtsK reduced lung collagen deposition in bleomycin-induced pulmonary fibrosis (Srivastava 2008). Deficiency of CtsS reduces mouse myofibroblast differentiation and Smad activation and impairs post-infarct cardiac functions (H. Chen 2013). Cathepsins have also been involved in liver fibrogenesis. In particular, CtsB and CtsD exert a role in hepatic stellate cells (HSC) activation and proliferation. Downregulation of CtsB and CtsD negatively regulates the expression of phenotypic markers of myofibroblasts activation, such as α-SMA and TGF-β. These findings indicate that cysteine and aspartyl cathepsins directly modulate the early trans-differentiation into a myofibroblast-like phenotype and

perpetuation phase of HSC activation, and hence liver fibrogenesis (Moles 2009).

1.10.1 Cathepsin D

Cathepsin D (CtsD) is a soluble lysosomal aspartic endopeptidase (EC 3.4.23.5) synthesized in rough endoplasmic reticulum as pre-pro-cathepsin D. After removal of signal peptide, the 52 kDa procathepsin D (pCtsD) is targeted to intracellular vesicular structures (lysosomes, endosomes, phagosomes), where proteolytic removal of the N-terminal pro-peptide leads to the 48 kDa intermediate form. Final processing yields the two-domain mature enzyme, consisting of a heavy (34 kDa) and a light (14 kDa) chain that are non-covalently linked (Benes 2008). Its pH optimum is between pH 2.8 and 4.0. Under physiological conditions, pCtsD is found intracellularly within acidic organelles such as lysosomes but in some conditions, pCtsD/CtsD escapes normal targeting mechanism and can be extracellularly secreted. PCtsD was found in human, bovine and rat milk, serum and the presence of both pro-CtsD and mature CtsD was demonstrated in human eccrine sweat and urine (Baechle 2006). CtsD can also be found intracellularly in other locations rather than the acidic compartments. Cytosolic CtsD participates in apoptosis by activating Bax in T cells (Liaudet-Coopman 2006a) and contributing to the release of cytochrome c from the mitochondria in fibroblasts (Johansson 2003).

Briefly, lysosomal membrane permeabilization in damaged cells allows translocation of CtsD from the lysosome into the cytosol where it contributes to apoptosis. In the cytosol CtsD, cleaves Bid protein into tBid triggering the insertion of Bax protein into the mitochondrial membrane. This leads to cytochrome c release from the mitochondria into the cytosol, and the activation of pro-caspases 9 and 3 (Stoka 2001). In addition, cathepsin D, which is extremely abundant in azurophilic granules of neutrophils, can trigger neutrophils cell death by directly processing and activating caspase-8, a pathway that is blocked under inflammatory conditions (Conus 2008). Moreover, Pepstatin A (PepA), a pharmacological inhibitor of CtsD (McAdoo 1973), blocked mitochondrial cytochrome c release and caspase activation in cardiomyocytes and fibroblasts (Conus 2008). CtsD association with Alzheimer disease (AD) has been suggested. In AD, senile plaques and tangles show abundant CtsD immunoreactivity and the CtsD level increases in cerebrospinal fluid (Schwagerl 1995). Immuno-histochemical studies have indicated that CtsD, independently of its proteolytic activity, stimulates not only cancer cell proliferation, but also tumor angiogenesis (Berchem 2002).

In humans, homozygous or compound heterozygous mutation in the cathepsin D gene on chromosome 11p15 are causative of Neuronal Ceroid Lipofuscinosis 10 (NCL10) (OMIM ID: 610127). The degree of CtsD gene function loss depending on the type of mutation occurred results in a milder or more severe neuropathogenesis. Therefore, while complete loss of CtsD activity translates in an early infantile form of NCL10, with patients dying within hours to weeks after birth, patients with residual CtsD activity develop late infantile, juvenile, or adult NCL10 with milder phenotypes. The clinical course includes progressive dementia, seizures, and progressive visual failure (Steinfeld 2006). NCL type 10 histopathological characteristic is the intracellular accumulation of autofluorescent lipofuscins within neurons of the central nervous system (CNS). These lipofuscins consist of proteins, such as F1F0 ATP-synthase subunit c and/or sphingolipid activator D, as well as oxidized lipids of lysosomal/endosomal origin (Ketscher 2016). It has been shown that mutations in CtsD that significantly reduced CtsD activity and/or affect pCtsD stability, post-translational processing, and intracellular targeting, result in NCL development (Steinfeld 2006).

CtsD knock-out mouse was generated by Saftig et al. in 1995. This mouse develops normally, without any manifest phenotype at the time of birth suggesting that CtsD is not essential during embryonic development. Lysosomal bulk proteolysis is maintained. It is likely that a functional overlap in cathepsins function ensures the proper protein degradation and turnover during embryonic development even in the absence of one single cathepsin. CtsD-deficient mice, however, developed abnormalities later in life. Two weeks after birth, CtsD-deficient mice exhibited weight loss, associated with progressive atrophy of intestinal mucosa, followed by massive intestinal necrosis, thromboembolia and profound destruction of lymphoid cells in the spleen and thymus. In addition, near the terminal stage they develop seizures and progressive retinal atrophy, which leads to blindness (Saftig 1995). CtsD-deficient mice die in a state of anorexia at day 26 ± 1, but also develop a neurodegenerative lysosomal storage disease that mimics the genetic NCL type 10 condition in humans. Given the unavailability of an adult CtsD knock out model, CtsD floxed mice were generated by Reinheckel (Ketscher 2016) and Tomino (Yamamoto-Nonaka 2016) opening new avenues to better understand the cell specific role of CtsD (**Fig. 8**).
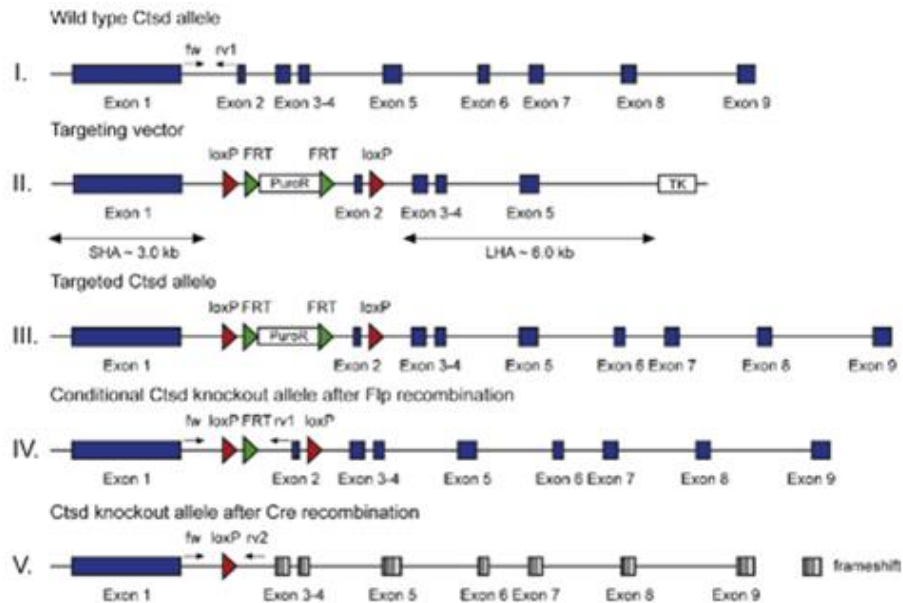
Figure 8. Generation of conditional CtsD knock-out mice by Reinheckel. Modified from figure 1(Ketscher 2016) Biochimie. 2016 Mar;122:219-26.

1.10.2 Role of cathepsins in macrophage function

Macrophages express a large amount of cathepsins, because of their pivotal role as antigen presentation cells (APC), as a result from their exposure to fragments obtained during protein turnover in endosomes and lysosomes. In fact, several cathepsins, such as Cts S, D and B, have been implicated in the degradation of proteins destined for the MHC class II processing pathway and in the proteolytic removal of invariant chain (Ii), a critical regulator of MHC class II function (Nakagawa 1999). However, macrophages can also secrete cathepsins in the extracellular space. Indeed, pCtsD and mature CtsD was found in macrophage-conditioned media and extracellularly in macrophage-rich regions of atherosclerotic lesions (Hakala 2003). Proteases of the cathepsin family are involved in the remodelling of extracellular matrix (ECM) proteins. In particular, the ability of macrophages of acidifying their environment by proton pumps and secretion of lactic acid (Tapper & Sundler 1992), ensures the macrophage pericellular environment to be sufficiently acidic for CtsD activation. Furthermore, destruction of elastin-rich tissues during inflammatory responses is associated with local accumulation of macrophages that contain high levels of elastinolytic enzymes, such as CtsB and CtsL. CtsB, CtsL and CtsD were find overexpressed in intestinal macrophages (IMAC) isolated from normal and inflamed mucosa in inflamed mucosa of patients with inflammatory bowel disease (IBD) *versus* control mucosa. Moreover, CtsD inhibition with Pepstatin A resulted in an amelioration of inflammation in inhibitor-treated mice

(Menzel 2006). The role of these three cathepsins in IBD pathophysiology is different: CtsB and CtsL are usually secreted, where they can directly degrade extracellular proteins, whereas CtsD is mainly involved in macrophage apoptosis, and once liberated from apoptotic cells, it may destroy ECM components. In healthy individuals the proteolytic action of cathepsins is restricted to controlled protein degradation in cellular processes and metabolism. However, in patients with IBD, proteolysis by cathepsins may also be triggered by bacterial invasion resulting in tissue destruction and inflammation (Menzel 2006).Thus, macrophages mobilize proteinases and participate in the pathophysiological remodelling of the ECM also in numerous tissue-destructive diseases, such as arthritis, bone resorption or metastasis (Reddy 1995). CtsB and CtsL expressing CD68-positive human mononuclear cells have been shown to play important roles in patients with rheumatoid arthritis, where they take part in joint destruction and bone erosion (Kaneko 2001).

1.10.3 Role of cathepsins in kidney disease

Cathepsins have been related to kidney disease in several reports. Cathepsins can play differential roles depending on the cell type involved in acute and chronic kidney disease. They can contribute to the inflammatory response giving their important role in macrophages but also contribute to ECM accumulation and remodelling which is the hallmark of fibrosis. Cathepsins B, D, L and S have been shown to regulate extracellular matrix homeostasis, autophagy, apoptosis, glomerular permeability, endothelial function, and inflammation in kidney (Cocchiaro 2017). CtsL–mediated proteolysis plays a critical role in the development of various forms of proteinuria. Reiser et al. demonstrated that altered filtration by podocytes, leading to proteinuria is related to CtsL overexpression and activity in podocytes (Reiser 2004). Serum CtsB concentration directly correlates with the loss of renal function in healthy individuals and the aging-related decrease of kidney function in the normal population (N. Wang 2016).

1.10.3.1 Cathepsins in Acute kidney injury (AKI)

As described in **section 1.7.1**, AKI is characterized by a relatively sudden decrease in the production, processing, and excretion of ultrafiltrate by the kidney. In agreement with previous knowledge about its contribution to apoptosis, increased expression and activation of CtsB have been observed in human proximal tubular epithelial cell line HK-2 undergoing apoptosis (Wang 2008). In a rat model of AKI, a significant decrease of CtsB was detected in the affected proximal tubules and correlated with the increased severity of the

histopathological lesions of the tubules (Švara 2010). CtsL has been identified as a strong candidate to provide a predictive value for AKI (Haase 2014), whereas CtsG has been identified as a critical component sustaining neutrophil-mediated acute tissue pathology and subsequent fibrosis after renal ischemia/reperfusion injury. Therefore, targeting CtsG may be an effective strategy to attenuate tissue injury after ischemia/reperfusion injury without depleting neutrophils (Shimoda 2007). Enhanced CtsD expression has been found in murine models of AKI, in particular its expression was highly increased in damaged tubular cells, suggesting a possible contribution of CtsD to cell death during AKI (Cocchiaro 2016). Contrarily, Suzuki et al. employed a conditional knockout CtsD$^{flox/-}$; Spink3^{Cre} mouse to investigate the function of cathepsin D in the renal proximal tubular epithelial cells, demonstrating that cathepsin D plays a cytoprotective role against ischemia/reperfusion injury in the renal proximal tubular epithelial cells. Lack of cathepsin D in renal proximal tubular cells led to the accumulation of LC3-positive signals and abnormal autophagic structures, resulting in an increase sensitivity against renal ischemia/reperfusion injury (Suzuki 2019). In addition, CtsD has been also identified as a possible novel prognostic marker for AKI, as it is differentially regulated in urine from late/non recovered vs. early/recovered AKI patients (Aregger 2014).

1.10.3.2 Cathepsins in Chronic Kidney Disease (CKD)

As described in the **section 1.8.3**, persistent inflammation promotes the progression from acute AKI to CKD. Glomerular injury and end-stage renal disease can be cause by the glomerular inflammation and cell damage caused by the activation of the NLRP3 inflammasome, a large multiprotein complex containing NOD-like receptor with pyrin domain 3 (NLRP3), triggered by the release of CtsB from the lysosomes due to their disruption. (Conley 2016). In diabetic nephropathy, a serious kidney-related complication of type 1 and 2 diabetes, the activity of CtsB but also CtsL was found decreased when the autophagy-lysosome pathway is disrupted by advanced glycation end products in HK-2 (W. J. Liu 2015). Schaefer et al. described a reduction in tubular cathepsins B, H and L in a rat model of polycystic kidney disease. According to them, the reduction in these cathepsins level was neither due to decreased gene expression nor to upregulation of specific inhibitors, but was likely to be due to enhanced apical secretion of these enzymes (Schaefer 1996). CtsL can contribute to the development of kidney disease by different mechanisms. CtsL expression increases in an experimental model of glomerulonephritis (Baricos 1991). Induction of CtsL expression in podocytes has been associated with the development of proteinuria in puromycin aminonucleoside induced-kidney

failure (Reiser 2004). Moreover, cathepsin L is necessary for podocyte FP effacement and proteinuria development in a LPS mouse model of proteinuria. In this model, cytoplasmic CtsL cleaved the GTPase dynamin resulting in podocyte failure and proteinuria. (Sever 2007). In addition, CtsL is causally involved in the pathogenesis of experimental diabetic nephropathy, by activating heparinase, a heparan sulfate endoglycosidase previously shown to be crucial for the development of diabetic nephropathy (Garsen 2016). Indeed, in CKD patients, serum CtsL activity is significantly elevated and its levels positively correlate with the severity of proteinuria, suggesting that serum cathepsin L may serve as a potential biomarker for CKD prognosis (Y. Cao 2017).

As regard to CtsD, its activity in kidney disease could be different depending on the cell type, and further studies will be required to better understand its implication in chronic kidney disease (CKD). During CKD, CtsD plays critical roles in inflammation and endothelial dysfunction (Ozkayar 2015; Fox 2016). In fact, CtsD serum levels were significantly higher and correlated with endothelial dysfunction in patients with CKD. However, no correlation was found between serum CtsD levels and traditional cardiovascular risk factors, suggesting enhanced CtsD as a selective risk factor for endothelial dysfunction in kidney in patients with chronic kidney disease (Ozkayar 2015). Yamamoto-Nonaka et al. generated a specific CD–knockout mice in podocytes, terminally differentiated cells and process bearing cells just like neurons (Yamamoto-Nonaka 2016). In this podocyte-specific knock-out mouse strain, the absence of CtsD led to an interruption of autolysosomal degradation and accumulation of proteins indicative of autophagy impairment and mitochondrial ATP synthase subunit-C accumulation in granular osmophilic deposits (GRODs), again similar to changes than those reported in CD-deficient neurons (Ketscher 2016).

Renal CtsD and CtsB expression was induced in obstructive nephropathy after unilateral ureteral obstruction (UUO), with CtsB mainly expressed in proximal tubular cells and CtsD mainly expressed in distal convoluted tubules (Fox 2016). Of note, inhibition of CtsD by Pepstatin A in murine models of progressive CKD resulted in a reduction of interstitial fibrosis (Fox 2016). CtsD inhibition, led to an upregulation in extracellular protease activity of urokinase-type plasminogen activator (uPA) due to altered lysosomal recycling; uPA processes plasminogen into plasmin, which can degrade extracellular matrix proteins resulting in a decrease in renal fibrosis.

2 Aims of the study

Previous report about the role of cathepsin D (CtsD) in renal disease are controversial, pointing towards a cell-specific role for this protease in kidney disease progression (Fox 2016, Singh 2021, Suzuki 2019, Yamamoto-Nonaka 2016). Due to the absence of a viable global knock out mouse (Saftig 1995), our knowledge about CtsD lags behind other cathepsins. Therefore, the generation of a CtsD floxed mouse (Ketscher 2016) opened new avenues for the study of the CtsD cell-specific role during pathophysiology.

Thus, the main aim of this project was to elucidate the role of CtsD in macrophages in the context of progressive kidney disease using a novel mouse strain with the conditional deletion of CtsD in macrophages. We used macrophage-CtsD sufficient (CtsD$^{\Delta Myel+/+)}$ and deficient (CtsD$^{\Delta Myel-/-}$) mice for *in vivo* studies of early-stage and chronic kidney disease and for *in vitro* studies of macrophage activation and polarization.

First, we aimed to validate the murine model by confirming the deletion of CtsD in isolated peritoneal macrophages from macrophage-CtsD deficient (CtsD$^{\Delta Myel-/-}$) mice. Then, we aimed to evaluate the effect of the macrophage-CtsD deletion in two models of kidney diseases by performing unilateral ureteric obstruction (UUO) for 5 and 10 days, respectively for an early-stage (5 days) and a chronic stage of kidney disease (10 days) (Ucero 2014). Together with an overall evaluation of the kidney functionalities, we mainly focused on the evaluation at histological and molecular levels in these mouse models of the inflammation and fibrosis, which can be considered hallmarks respectively of early-stage and chronic kidney disease. Lastly, we evaluated the effect of CtsD deletion on macrophage activation and polarization *in vitro* using isolated peritoneal macrophages, naïve or stimulated with LPS or IL4 13 in order to induce macrophage polarization toward M1 or M2 phenotype, respectively.

The expected results from this study will open the way for a better understanding of the molecular mechanisms regulated by CtsD during the development of kidney diseases with a main focus on macrophages which are often considered the main actors in the progression of many human diseases.

3 Material and Methods

3.1 LysMCre model

Macrophage-CtsD deficient and sufficient mice were generated by breeding LysMCre mice (myeloid cell) (Jackson Laboratory, B6.129P2-Lyz2$^{tm1(cre)Ifo/J}$) with CtsD floxed mice, kindly donated by Prof. Reinheckel. CtsD floxed mice generation was previously described by Ketscher in 2016. Briefly, a targeting vector containing a loxP-flanked exon 2 and a FRT-flanked puromycin selection cassette was integrated into the locus by homologous recombination. Subsequently, the selection cassette was removed by flip recombination. LysMCre mice were previously described by Clausen et al. in 1999 (Clausen 1999). The LysMcre knock-in/knockout allele has a nuclear-localized Cre recombinase inserted into the first coding ATG of the lysozyme 2 gene (*Lyz2*); both abolishing endogenous *Lyz2* gene function and placing NLS-Cre expression under the control of the endogenous *Lyz2* promoter/enhancer elements. CtsD$^{f/f}$ LysMCre$^{-/-}$ females were breed with CtsD$^{f/f}$ LysMCre$^{+/-}$ males o generate cell-specific CtsD$^{f/f}$/LysMCre$^{+/-}$ mice. 8-10 weeks female CtsD$^{f/f}$/LysMCre$^{-/-}$ and CtsD$^{f/f}$/LysMCre$^{+/+}$ littermates were used for the experiments. All the animal studies were done in accordance with the Comitè Ètic d'Experimentació Animal (CEEA-UB) and Generalitat de Cataluña Regulations and under its approval.
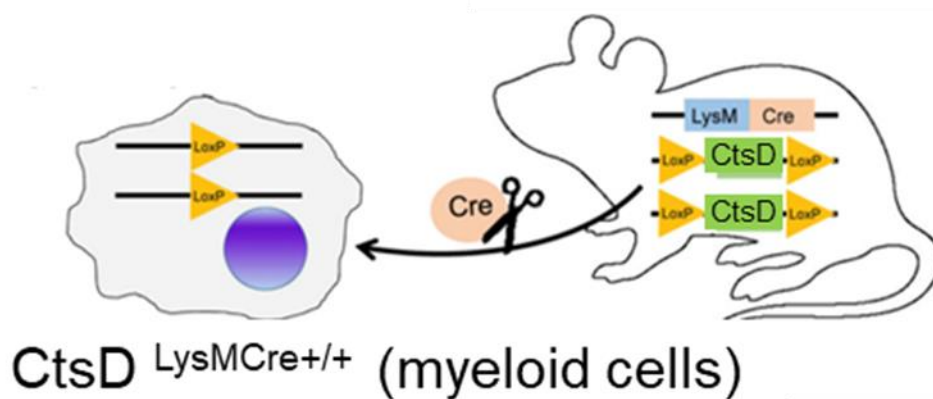
Figure 9. LysMCre model description.

3.2 Isolation of peritoneal macrophages elicited with Thioglycolate isolation (PMT)

Female mice were injected with 8.3mL/Kg 3% brewer thioglycolate (Sigma Aldrich, ref. T9032) intraperitoneal for four days before the cell

isolation, as a stimulus for eliciting inflammatory macrophages. This agent increases monocyte migration into the peritoneum, therefore increases macrophage yield. Mice were euthanized by cervical dislocation or pentobarbital overdose. An incision in the abdominal skin was performed exposing from the sternum to the pelvis. 7 mL of sterile ice-cold DPBS-/- and 3 mL of air (25G) were injected intraperitoneally, then the mouse belly was massaged for 4 minutes. 10 mL air-filled syringe (21G) (or air-filled glass Pasteur pipette) was inserted in the peritoneal cavity and the air expressed in the cavity, distending the peritoneum, then the fluid, containing the peritoneal lavage was collected. The cells were put in a 50 mL polypropylene tube and spun for 5 minutes at 500 g at 4ºC. The cells in the pellet were then resuspended by hand in 2 mL ACK buffer (150mM NH4Cl (Sigma, ref. 9718); 10mM KHCO3 (Sigma, ref. 23720); 10μM EDTA (Sigma, ref. ED4SS) in deionized water), spun 5 min at 500 g at 4ºC and resuspended in 1000 μL of ice-cold DMEM (GIBCO, ref. 41966-029) supplemented with 10% fetal bovine serum (FBS) (Sigma, ref. F7524). Around 400.000 cells per well were seeded in in 6-well plate in 2 mL DMEM supplemented with 10% fetal bovine serum (FBS). The plates were incubated at 37°C and 5% CO_2 for 2 hours, and the nonadherent cells were removed by withdrawing the culture medium and washing. The adherent cells are considered peritoneal macrophages.

3.3 DNA extraction for genotyping

Macrophage-CtsD deficient and sufficient mice were genotyped by PCR using ear clipped biopsies. Genomic DNA was extracted from ear clipped tissue from animal of 15-21 days of age with QuickExtract DNA kit (Epicentre, QE09050). 50 μL of QuickExtract solution were added to each tube containing the biopsy, vortexed for 30 sec, then incubated for 6 min at 65ºC and afterwards 2 min at 98ºC. The tubes were then vortexed again for 30 sec and centrifuged at 14.000 rpms for 2 min. 1 μL of the extracted DNA (200ng of DNA approximately) was used for each PCR reaction. To analyze the expression of the Cre recombinant fragment in peritoneal macrophages (PMT), the cells were seeded approximately for 24 hours, washed with 1X PBS and harvested by scraping in 75 μL of DNA extraction buffer, transferred into a tube. The DNA was extracted following the same DNA extraction protocol as for genotyping. PCR was performed using kit (Bioline, ref. BIO-21060) as described in table:

PCR mix	Quantities/ reaction (µL)
H₂O MilliQ	14,4
10X NH₄ reaction Buffer	2
MgCl₂	1,2
dNTPs	0,4
Primers 10uM	0,6
BioTaq	0,4
DNA	1
Up to	20

Table 3. PCR mix

The same program was used to detect the following amplification products using the primer sequences described below:

PCR program: preheat 95C 1 min - 35 cycles of Denature 95C 30sec; Annealing 60C 30sec; Extension 72C 1 min. Last cycle 72C for 10 min.

Amplification product	Primer sequences
CtsD Cre recombinase fragment	Fw:5'-CCTAACAGAACCCACTAGCC-3'
	Rv:5'-GGAGGCCAAGATATGAGGATG-3'
CtsD lox1 (genotype flox)	Fw:5'-CCTAACAGAACCCACTAGCC-3'
	Rv:5'-AGCTAAGGACATCCTATCACTACC-3'
pCMVCre (genotype Cre recombinase)	Fw:5'-ACCTGAAGATGTTCGCGATTATCT-3'
	Rv:5'-ACCGTCAGTACGTGAGATATCTT-3'

Table 4. PCR primer sequences.

3.4 Agarose electrophoresis

Electrophoresis was carried out using gels containing agarose (Sigma, ref. A9539) melted in 1x Tris Borate EDTA (TBE) (Sigma, ref. T4415). The concentration of agarose ranged between 1,5% and 2% w/v depending on the resolution of the gel required. Electrophoresis was performed in 1x TBE with a voltage between 80-150 V, for almost 20 minutes. Gels were visualized using UV light in a LAS4000 system (GE Healthcare).

3.5 Unilateral Ureter Obstruction (UUO) model of kidney disease

Left proximal ureter ligation was performed in 8-10 weeks C57BL/6 females. Mice were individually anaesthetized by 2-3% isofluorane at a flow rate of 0.5-1L O2/ hour. Mice were injected with 100 µL of 6µg buprenorphine for analgesia (Buprex 0.3mg, Indivior). A skin and muscle incision of

approximately 3cm was done in the linea alba. A Barraquer Eye Speculum was inserted in the incision and to help visualizing the left ureter. The ureter was isolated using tweezers was tied three times using 6.0 mersilk (x2 ligatures proximally and x1 distally). Between the proximal and distal ligature, a cut was performed. The linea alba was closed using round-bodied 5.0 vicryl suture and skin using cutting 5.0 vicryl suture. Mice were briefly placed on oxygen until conscious and placed in a temperature-controlled recovery cage for 30-60 minutes and placed back into standard housing 2-3 hours post-surgery. Right kidneys were not surgically manipulated and were used as negative controls for each study. After 5 or 10 days, the animals were humanely euthanized, and blood and the two kidneys were collected. A minimum of 5 animals were used in each experimental group.

3.6 Protein lysates

Proteins were extracted from a piece of kidney with 100 μL of RIPA buffer. RIPA Buffer was prepared with the following recipe: 150mM NaCl (Sigma, ref. S7453); 50mM Tris pH:7.5 (Sigma, ref. 6066); 0.1% SDS (Sigma, ref. 05030); 1% Triton X-100 (Sigma, ref. T8787); 0.5% DOC (Sigma, ref. D6750); 1 tablet of cOmplete, EDTA-free for each 50 mL of RIPA (Roche, ref. 11873580001); 10 μL of phosphatase inhibitor/mL buffer (Sigma, ref: P5726). The tissues were homogenized with a plastic pestle (Sigma, ref. Z359971), then kept on ice for 15 minutes, vortexing 4-5 times. Then the samples were sonicated for 9 minutes in a water bath, in cold water. Finally, the lysates were centrifuged at 13000rpm for 15 minutes at 4 °C, and the supernatant was collected. In case of protein extraction from cells, 24 hours approximately after seeding them, cells were washed with 1X PBS and harvested by scraping them in RIPA (75 μL) and transferred into an Eppendorf tube. Protein lysate of cells was performed as for the tissue.

3.7 Protein concentration detection (Bradford)

Total protein concentration was measured from the tissue or cell lysates prepared in **section (3.6)**. Bradford assay is a protein determination method that involves the binding of Coomassie Brilliant Blue G-250 dye to proteins that is detectable at an absorbance of 595 nm. 4 μL of samples (diluted 1/20 in MilliQ water for kidney tissue) were added to a 96 well plate in triplicates, then 196 μL of Bradford Protein Assay (Bio-Rad, ref. 500-0006) previously diluted 1/5 in distilled water were added to each well and incubated for 20 minutes at room temperature. A spectrophotometer plate reader (Bio-Rad, xMark™ microplate spectrophotometer, ref. 1681150) was used to measure the absorbance at 595

nm. Samples readings were referred to a BSA standard curve built using commercial bovine serum albumin standards (BSA, Bio-Rad, ref. 5000207) between the concentrations 0,125 and 2,0 mg/mL.

3.8 Western Blotting

Proteins (30 μg) were diluted in a loading buffer XT Sample Buffer 4x (Bio-Rad, ref. 161-0791), with 0,05% β-mercaptoethanol (Sigma, ref. M-6250), and heated to 95ºC for 10 minutes, then they were separated on SDS-PAGE 12%.

Resolving gel	7,5%	10%	12%	15%	Stacking gel	6%
Distilled water	10mL	8,4mL	7mL	5mL	Distilled water	6mL
Tris 1.5M pH8.8	5mL	5mL	5mL	5mL	Tris 0.5M pH6.8	2,5mL
SDS 10%	200μL	200μL	200μL	200μL	SDS 10%	100μL
Acrylamide 30%	5mL	6,6mL	8mL	10mL	Acrylamide 30%	1332μL
APS 10%	200μL	200μL	200μL	200μL	APS 10%	100μL
TEMED	20μL	20μL	20μL	20μL	TEMED	20μL

Acrylamide 30% (SIGMA, ref. A3699); APS 10% (SIGMA, ref. A3678); TEMED (Ultrapure bioreagent, ref. 4098-02).

Table 5. Acrylamide gels receipt.

Electrophoresis was carried out at 80V until the dye front had crossed from the stacking and into the resolving gel, then 120V until the dye reached the end of the gel. Next proteins were transferred to a Nitrocellulose membrane (Bio-Rad, ref. 1704271) with the Trans-Blot Turbo Transfer System (Bio-Rad, Trans-Blot turbo, ref. 1704150) using the Trans-Blot Buffer, obtained by mixing 200mL of buffer Trans-Blot Turbo 5x (Bio-Rad, ref. 10026938), 200mL EtOH (VWR, ref. 83813.360) and 600mL of distilled water for 1L. Membranes were blocked with blocking buffer TBS-T (Sigma, ref. T9039), containing 5% non-fat powdered Difco™ Skim Milk (BD Bioscience, 232100) for 1 hour at room temperature and incubated overnight with the required primary antibody (Table 6). After washings in TBS-T three times, membranes were then incubated in the appropriate secondary antibody conjugated to horseradish peroxidase (HRP) at room temperature for 1 hour (**Table 6**). Finally, the membranes were washed three times in TBS-T and developed using the chemiluminescent ECL Western Blotting Substrate (Thermo, ref. 31206). The images were collected with a LAS4000 (GE Healthcare).

Primary antibody	Reference	Dilution (in TBS-T)
Cts D (goat)	sc-6486, St Cruz	1/1.000
CtsB (rabbit)	sc-13985, St Cruz	1/1.000
α-SMA (mouse)	α-2547, Sigma	1/1.000
ENDO-180 (rabbit)	Ab70132, abcam	1/1.000
β-actin (HRP)	A3854, Sigma	1/20.000
Secondary antibody	**Reference**	**Dilution (in TBS-T)**
Rabbit	Sigma, ref. A0545	1/20.000
Mouse	Sigma, ref. A9044	1/40.000
Goat	Sigma, ref. A5420	1/80.000

Table 6. Primary and secondary WB antibody list.

Stripping was performed by incubating the membrane with Stripping Buffer (Thermo scientific, ref. 21059), according to the manufacturer´s instructions, when it was needed to remove the antibodies from the membrane to reblot the membrane with a different antibody pair.

3.9 Cathepsin D activity assay

Cathepsin D activity from whole kidney or PMT lysates (RIPA) was assessed with Cathepsin D Activity Fluorometric Assay Kit (APExBIO - K2154). The fluorimetric assay (λex: 355 nm; λem: 460 nm) was performed in 96-well plate black (Thermo scientific, ref. 611F96BK) using 100ng of protein per sample per assay according to manufacturer´s instructions. The plates were incubated at 37°C and measuring using a plate fluorimeter (TECAN, Infinite M nano +) at 355nm excitation and 460 emission at 0, 1 and 2 hours. Data was expressed the increment in fluorescent intensity.

3.10 RNA extraction

Total RNA was extracted from whole kidney or PMT tissue by phenol-chloroform extraction and isopropanol precipitation, according to the following protocol. For whole kidney 200 µL of Trizol (Invitrogen, ref. 15596018) were added to a small piece of frozen tissue at RT and the tissue was homogenized with a plastic RNase free pestle (Sigma, ref. Z359971). Secondly, 500 µL of Trizol were added and mixed by inversion. For PMT, 750 µL of Trizol (Invitrogen, ref. 15596018) per well of a 6 well plate were added and after 5 minutes at RT, transferred to a sterile tube. From this point onwards the protocol was common for both kidney tissue and cells. 200 µL of Chloroform (Sigma, ref. C2432) were then added to the TRIzol and the samples were mixed by inversion 10-15 times and centrifuged at 12000 rpm for 15 minutes at 4ºC.

400-500 µL of the top aqueous phase was recovered and mixed with 500 µL of 2-Propanol (Panreac, ref. A3928) three times by inversion and left 10 minutes at RT. Next the samples were centrifuged at 12000 rpm for 10 minutes at 4ºC and the supernatant was discarded. The pellet (RNA) was then washed with 1 mL of 70% EtOH (VWR, ref. 83801.360), and spun at 12000 rpm for 10 minutes at 4ºC. Finally, the pellet was airdried and reconstituted in 15-20 µL of RNase free water (Sigma, ref. W4502).

3.11 cDNA synthesis

The purified RNA was quantified by NanoDrop (Thermo, ref. NanoDrop 1000). 1 µL of RNA per sample was loaded on to the platform of the Nanodrop and the ratio of absorbance at 260 and 280nm for each sample was calculated. Ratios in the range of 1.8-2.0 were accepted as "pure" RNA. Then, 1000 ng of RNA were used for cDNA synthesis using the SensiFAST™ cDNA Synthesis Kit (BIO-65054), according to the manufacturer's instructions.

3.12 Quantitative real-time PCR (qRT-PCR)

cDNA samples were diluted up to 10 ng/µL. 2 µL diluted cDNA (20ng/reaction) were added in duplicate to a 384 well plate (4titude, ref. 4ti-1384). Then 8 µL of mastermix were added to each well, comprising of 2,6 µL DNase free water, 5 µl of 2x SYBR green The SensiFAST™ SYBR & Fluorescein Kit (BIO-96020) and 0,4 µL of the mix from forward and reverse primer (400nM – only for 18S primers 40nM). The plate was spun at 500g before running on the Bio-Rad CFX384 Touch Real-Time PCR Detection System. The standard program for each plate was: 20 seconds 95ºC; 40 cycles of 95ºC; 5 seconds denature template, 55-60ºC annealing for 10 seconds, 72ºC elongation for 20 seconds. The 40-cycle program was followed by dissociation curve of 1 minute 95ºC, 5 seconds 60ºC and 5 seconds 95ºC. Applying a threshold to the exponential phase of the amplification curve generated a cycle threshold (CT). The level of fluorescence is generated at the end of the elongation step, representing the amount of SYBR Green, bound to double stranded DNA. The 2(-Delta Delta C(T)) method was used to calculate the relative gene expression (Livak & Schmittgen 2001). Briefly, the mean CT of the gene of interest (A) was normalized to the mean housekeeping gene 18S (B), by B–A to generate the ΔCT. The ΔCT of control group (contralateral kidney CtsD$^{\Delta Myel+/+}$) is used to normalize the ΔCT of the experimental group by subtracting ΔCTx control from ΔCTy test to determine the ΔΔCT. Fold gene changes were detected using the following equation $2^{-\Delta\Delta CT}$.

3.13 Primer design

Primers sequences were obtained from PrimerBank. Selected primers were run in BLAST (http://blast.ncbi.nlm.nih.gov/Blast.cgi) to check for unspecific amplification sequences. Primers that only amplified the specific gene of study were finally selected. Primers for gene analysis were the following:

Gene (GenBank Accession Number)	Primer Sequence
CtsD (NM_009983)	Fw: 5'-CGGCACGTCCTTTGACATCC-3'
	Rv: 5'-CGATTCCAGGCTGCTTGGTG-3'
ACTA2 (NM_007392)	Fw: 5'-GGACGTACAACTGGTATTGTGC-3'
	Rv: 5'-TCGGCAGTAGTCACGAAGGA-3'
Col1A1 (NM_007742)	Fw: 5'-TAAGGGTCCCCAATGGTGAGA-3'
	Rv: 5'-GGGTCCCTCGACTCCTACAT-3'
TGFβ1 (NM_011577.2)	Fw: 5'-TGATACGCCTGAGTGGCTGT-3'
	Rv: 5'-GCAGTGAGCGCTGAATCGAA-3'
CXCL1 or KC (NM_008176.3)	Fw: 5'-CTGGGATTCACCTCAAGAACATC-3'
	Rv: 5'-CAGGGTCAAGGCAAGCCTC-3'
CCL2 or MCP1 (NM_011333.3)	Fw: 5'-AGGTCCCTGTCATGCTTCTG-3'
	Rv: 5'-TCTGGACCCATTCCTTCTTG-3'
CCL3 (NM_011337)	Fw: 5'-TTCTCTGTACCATGACACTCTGC-3'
	Rv: 5'-CGTGGAATCTTCCGGCTGTAG-3'
CCL5 (NM_013653)	Fw: 5'-TGCTGCTTTGCCTACCTCTCC-3'
	Rv: 5'-TGGCACACACTTGGCGGTTCC-3'
IL-1β (NM_008361.4)	Fw: 5'-CAACCAACAAGTGATATTCTCCATG-3'
	Rv: 5'-GATCCACACTCTCCAGCTGCA-3'
TNFα (NM_013693.3)	Fw: 5'-CAGGCGGTGCCTATGTCTCA-3'
	Rv: 5'-GGCTACAGGCTTGTCACTCG-3'
MMP-2 (NM_008610)	Fw: 5'-CCTGGACCCTGAAACCGTG-3'
	Rv: 5'-TCCCCATCATGGATTCGAGAA-3'
MMP-3 (NM_010809)	Fw: 5'-TTAAAGACAGGCACTTTTGGCG-3'
	Rv: 5'-CCCTCGTATAGCCCAGAACT-3'
MMP-7 (NM_010810)	Fw: 5'-CTTACCTCGGATCGTAGTGGA-3'
	Rv: 5'-CCCCAACTAACCCTCTTGAAGT-3'
F4/80 (NM 010130.4)	Fw: 5'-CCCCAGTGTCCTTACAGAGTG-3'
	Rv: 5'-GTGCCCAGAGTGGATGTCT-3'
CD11c (NM_021334.3)	Fw: 5'-CCAAGACATCGTGTTCCTGATT-3'
	Rv: 5'-ACAGCTTTAACAAAGTCCAGCA-3'
iNOS (NM_010927.4)	Fw: 5'-GGAGTGACGGCAAACATGACT-3'
	Rv: 5'-TCGATGCACAACTGGGTGAAC-3'
Arginase-I (NM_007482.3)	Fw: 5'-ACACTCCCCTGACAACCAGC-3'
	Rv: 5'-AGGGTCTACGTCTCGCAAGC-3'
MRC-1 (NM_008625.2)	Fw: 5'-CTCTGTTCAGCTATTGGACGC-3'
	Rv: 5'-CGGAATTTCTGGGATTCAGCTTC-3'

IL-10 (NM_010548.2)	Fw: 5'-TTACTGACTGGCATGAGGATCA-3'
	Rv: 5'- GCAGCTCTAGGAGCATGTGG-3'

Table 7. RTPCR primer sequences.

3.14 Determination of kidney damage (BUN)

Blood Urea Nitrogen (BUN) measures the amount of urea nitrogen in the blood. Urea nitrogen is excreted from the blood by the kidneys, thus high BUN levels could indicate kidney damage. The level of BUN in serum was evaluated using QuantiChrom™ Urea Assay Kit (DIUR-100) for colorimetric Urea Determination. The improved Jung method utilizes a chromogenic reagent that forms a colored complex specifically with urea. The intensity of the color, measured at 520nm, is directly proportional to the urea concentration in the sample. 5 µL water (blank), 5 µL standard (50 mg/dL) and 5 µL samples (serum), in duplicates, were transferred into wells of a clear bottom 96-well plate. Then to each well 200 µl working reagent were added, lightly mixed and incubated 20 minutes at room temperature. Lastly the Optical Density of the plate was measured at 520 nm using a spectrophotometer plate reader (Bio-Rad, xMark™ microplate spectrophotometer, 1681150).

3.15 Histology and immunochemistry analyses
3.15.1 Tissue preservation and section preparation

Tissues were quickly harvested after blood collection and placed in histology cassettes, fixed in formalin (Formalin solution, neutral buffered, 10%) (Sigma, HT501128) for 24 hours, then transferred into 70% EtOH (VWR, ref. 83801.360) and finally embedded in paraffin through an automated tissue processor (Citadel 1000, Shandon) according to the following protocol: 1h in 70% EtOH two times; 1h in 90% EtOH two times; 1h in 100% EtOH two times; 1h in xylene two times; 2h in paraffin two times. Tissue sections were then cut using a microtome (Leica, RM2155) set to 4µm. Sections were transferred to a 40°C water bath to be stretched out, then collected onto Superfrost Plus slides (Thermo Scientific, Superfrost Plus Ref. J1800AMNZ) and dried at 37°C overnight. Before each staining protocol (described below), the tissue sections were heated at 100°C in a dry heat oven in order to melt the excess of paraffin and allow the hydration of the tissue.

3.15.2 Sirius Red staining

Renal fibrosis was determined by Sirius red staining, which binds specifically to collagens I and III fibers. 4µm thick paraffin kidney slides were dewaxed in Xylene (VWR, ref. 28975.325) and rehydrated through a battery

of alcohol solutions, EtOH 100% (VWR, ref. 83813.360) and 70% (VWR, ref. 83801.360). After these steps, the sections were incubated in 0.1% Sirius Red stain for 1 hour at RT. Sirius Red was prepared diluting 20 mL of Sirius-Picric 1% (1g Sirius Red (Sigma, ref. 34149) + 100 mL of saturated picric solution (Sigma, ref. P6744) in 180 mL of saturated picric solution (Sigma, ref. P6744). Sections were then dehydrated by incubating them in a series of ethanol solutions for 5 minutes each (70%, 100%). Sections were finally incubated in Xylene twice for 5 minutes each and mounted with DPX (Merck, ref. HX98094579). Slides were dried at room temperature overnight before viewing under a light microscope. Image analysis was performed blind and in a minimum of 10 random 100X fields using a Nikon Eclipse TS100 Upright microscope. Using ImageJ Analysis software, thresholds for percentage of positive area was created and the analysis was run automatically.

3.15.3 Periodic acid Schiff's histology and scoring

In the PAS reaction, the histological specimen material is first treated with periodic acid, resulting in the oxidation of the 1,2-glycols into aldehyde groups. The addition of Schiff's reagent (fuchsin-sulfuric acid) in the second step causes the aldehydes to react to form a brilliant red color. In the end result, the PAS reaction yields a specific color reaction with unsubstituted polysaccharides, neutral mucopolysaccharides, muco- and glycoproteins, and glyco- and phospholipids. 4 µm kidney sections were deparaffinized by immersion in 100% xylene (VWR, ref. 28975.325) twice for 5 minutes and rehydrated through graded ethanol (EtOH 100%, VWR, ref. 83813.360, and ETOH 70%, VWR, ref. 83801.360) to deionized water (dH_2O). PAS staining kit (Sigma, 1.01646.0001) was used as follow, the tissue sections were incubated in 1% periodic acid (reagent 1) for 5 minutes at room temperature (RT), then washed under running tap water for 5 minutes and rinsed in dH_2O. Schiff's reagent (reagent 2) was applied to all sections for 15 minutes at RT, then slides were washed under running tap water for 5 minutes and rinsed again in dH_2O. Sections were counterstained with Harris Haematoxylin (HHS32 Sigma) for 1 second then blued under running tap water for 3 minutes. Finally, slides were dehydrated through graded ethanol washes (70% and 100%) and two final xylene washes before mounting in DPX (Merck, ref. HX98094579). Slides were dried at RT overnight before viewing under a light microscope. Tubular damage was assessed in 10-20 random 200X fields in the cortex, both for healthy kidneys and for unilateral ureteral obstruction models using a Nikon Eclipse TS100 Upright microscope. A 10 x 10 grid was superimposed onto each image and the number of grid intersections overlaying areas of cast

formation, tubular dilation, loss of brush border and epithelial flattening, used as indicators of tubular damage in the cortex, were counted and expressed as a percentage of the total area containing 81 grid intersections, for each image. All counts were performed in a blinded manner.

3.15.4 Immunohistochemical stainings

Immunohistochemical staining of αSMA, NIMP (Nogo Interacting Mitochondrial Protein) and F4/80 were performed to detect fibroblasts (scar forming cells), neutrophils and macrophages respectively in kidney tissue. Paraffin-embedded renal tissue sections 4μm in thickness were de-paraffinized by immersion in 100% xylene (VWR, ref. 28975.325) twice for 5 minutes and then rehydrated through graded ethanol EtOH 100% (VWR, ref. 83813.360), and ETOH 70% (VWR, ref. 83801.360). Endogenous peroxidase activity was blocked by immersing slides in MetOH / 2% hydrogen peroxide (MetOH: VWR, ref. 20846.292, Hydrogen peroxide 30%: Merck, ref. 1.07209.0500) for 15 minutes, then slides were washed once in PBS for 5 minutes. Next antigen for the different IHC was performed according to the following **Table 8**:

Epitope	Method	Time	Temperature
αSMA	Heat-mediated antigen retrieval using sodium Citrate Buffer	20 min	Boiling microwave
NIMP	Enzymatic antigen retrieval with Pronase 0.01%	30 min	37°C in a humified chamber
CtsD	Heat-mediated antigen retrieval using sodium Citrate Buffer	20 min	Boiling microwave
F4/80	Heat-mediated antigen retrieval using sodium Citrate Buffer	15 min	Boiling microwave

Sodium Citrate Buffer (Vector, ref. H3301), Pronase (Roche, ref. 10165921001)

Table 8. Antigen retrieval list.

In case of heat-mediated antigen retrieval 300 mL of water were added to the pot to cool down 5-10 minutes, then slides were washed in PBS and mounted into Sequenza Manual Staining system (Thermo scientific, ref. 73310017). Endogenous avidin & biotin were blocked using a Avidin/Biotin blocking kit (Vector Labs, ref. SP-2001). Briefly, slides were first incubated with avidin blocking solution for 20 minutes, washed once in PBS for 5 minutes, then incubated with biotin for 20 minutes and washed again in 1X PBS. Only for the F4/80 IHC, the sections did not need endogenous avidin & biotin blocking nor ABC amplification because we used a HRP Labelled Polymer based secondary antibody. Conversely, once mounted onto Sequenza

system, sections were permeabilized with 0.25% Triton X-100 for 10 minutes at RT and subsequentially blocked as described in **Table 9**.

Epitope	Blocking solution	Time	Company and reference
αSMA	20% Piggy serum	30 min	Bio-Rad, ref. C15SB
NIMP	20% Piggy serum	30 min	Bio-Rad, ref. C15SB
CtsD	Casein 1x	40 min	Sigma, ref. C7078
F4/80	20% Piggy serum	30 min	Bio-Rad, ref. C15SB

Note: Piggy serum was diluted in 1XPBS.

Table 9. Blocking solution list.

Then slides were incubated overnight at 4°C with the following antibodies (**Table 10**):

Epitope	Primary antibody and reference	Dilution	Company
αSMA	Mouse monoclonal anti-αSMA FITC (F3777)	1:1500	Sigma
NIMP	Rat monoclonal anti-NIMP-R14 (sc-59338)	1:200	Santa Cruz
CtsD	Goat polyclonal anti-CtsD (sc-6486)	1:100	Santa Cruz
F4/80	Rabbit monoclonal anti-F4/80 (#70076)	1:500	Cell Signalling

Note: All antibodies were diluted in 1XPBS except F4/80 that was diluted in 10% piggy serum.

Table 10. Primary IHC antibody list.

The following day, slides were washed in 1X PBS 3 times and the following antibodies were added (Table 11):

Epitope	Secondary antibody and reference	Dilution	Incubation times	Company
αSMA	Anti-Fluorescein, Biotinylated (BA-0601)	1:300	120 min	Vector lab
NIMP	Goat anti Rat IgG:Biotin (STAR131B)	1:200	90 min	Bio-Rad
CtsD	Rabbit Anti-Sheep Biotinylated (BA-6000)	1:200	120 min	Vector lab
F4/80	Envision + System-HRP Labelled Polymer Anti-rabbit (K4003)		60 min	Agilent

Note: All antibodies were diluted in 1% piggy serum/1xPBS except for F4/80.

Table 11. Secondary IHC antibody list.

Secondary antibody was washed 3 times with 1X PBS, then Vector ABC tertiary (Vector Laboratories, ref. PK-7100) was incubated for 60 minutes to enhance sensitivity of the signal, with the exception of F4/80 IHP. Next slides were washed 3 times with PBS. During the last washing, 3,3-diaminobenzidine (DAB) solution (Vector Laboratories, ref. SK-410) was prepared according to manufacturer's instructions and kept in the dark. Slides were covered with excess DAB solution and incubated for the following developing times (**Table 12**):

Epitope	Developing times
aSMA	1,5 min
NIMP	10 min
CtsD	2,5 min
F4/80	1,5 min

Table 12. Developing times list.

After DAB detection, slides were washed briefly in PBS, counterstained with Haematoxylin (Agilent, ref. S3309) for 1 second and then washed under running tap water for 5 minutes. Finally, slides were taken through a series of alcohol dehydration steps (70%, 100%, xylene), mounted in DPX (Merck, ref. HX98094579) and dried at room temperature overnight before viewing under a light microscope. Image analysis was performed blind using a Nikon Eclipse TS100 Upright microscope and as described below for each of the stainings. For αSMA image analysis was performed a minimum of 10 random 100X fields using ImageJ Analysis software, threshold for percentage of positive area was created and the analysis was run automatically. For NIMP image analysis was performed in a minimum of 10 random 200X using ImageJ Analysis software, NIMP positive cell area were manually counted, then results were expressed as average of neutrophils per field. For F4/80 image analysis was performed in a minimum of 10 random 200X fields using ImageJ Analysis software, threshold for percentage of positive area was created and the analysis was run automatically.

3.15.5 Dual IF F4/80/CtsD in kidney tissue

Paraffin-embedded 4um kidney sections were deparaffinized and rehydrated. Heat-mediated antigen retrieval was performed as described in **Table 8**. After cooling down the section for 5-10 minutes and washing them with 1X PBS, sections were permeabilized with 0.25% Triton X-100. Slides were mounted and washed in the Sequenza system before blocking them with 1% BSA for 1 hour at RT and adding the primary antibodies anti-F4/80 Ab

(Cell Signalling, ref. #70076 1:300 dilution) and anti-CtsD (St Cruz, ref. sc-6486 1:100 dilution) overnight at 4C. The following day, tissue sections were washed four times with 1x PBS and incubated 60 minutes at RT with Alexa 594 donkey anti-rabbit (Invitrogen, ref. A21207) 1:500. Sections were then washed seven times with 1x PBS and incubated with rabbit serum 20% in 1x PBS for 30 minutes. This step is important as the rabbit anti-goat FITC could be detected by the donkey anti-rabbit 594 and might result in false negatives. Rabbit anti-Goat IgG (whole molecule)–FITC antibody (Sigma, ref. F9012) was added to the slides, 1:200 for 1 hour at RT, then sections were washed five times with 1x PBS. DAPI (1:1000 Merck, D9542) was added for 10 minutes at RT. After washing five times with PBS1x the sections were mounted using Mounting Medium with DAPI – Aqueous (Abcam, ab104139). Images were acquired using a spectral Leica SPE microscope DM2500. DAPI was visualized using the 405 laser, CtsD using the 488 laser and F4/80 using the 532 laser at 630x magnification and zoom 3.1.

3.16 PMT Stimulation with LPS and IL4 IL13

PMT were isolated as described in **section (3.2)**. Around 250.000 cells per well were seeded in in 6-well plate. After 2h the cells were washed with PBS1x and the media replaced with 0%FBS DMEM +P/S. The following day cells were stimulated with LPS (LPS serotype 0128:B12 Sigma, ref. L2755) 10ng/mL or 50ng/mL or a mix of IL4 (PeproTech, ref. 200-04) and IL13 (PeproTech, ref. 200-13), 20ng/mL or 50ng/mL for 24 hours. Then cells were washed gently with PBS1x and collected in TriZol (750 μL per well). Untreated cells were used as control. Two wells of each condition were merged in order to have a better RNA isolation yield.

3.17 DQ Collagen degradation *in vitro*

500.000 PMT/well were seeded in a 6 well plates containing 4x 12mm glass coverslips (VWR, ref. ECN 631-1577) per well. After 2 hours the cells were washed with PBS1x and replace the media with 1%FBS DMEM +P/S. DQ™ Collagen type I (Invitrogen, ref. D12060) was dissolved in distilled water (1mg/mL), vortexed and sonicated in a waterbath at RT for 3 minutes. Cells were treated with or without 1ug/mL DQ™ Collagen type I for 3h or 6h at 37°C or 4°C, the last temperature used as control. Once the incubation was over, the coverslips were washed in 1x PBS and fixed in 1.5 mL of formalin for 10 min at RT. Formalin was then discarded and coverslips were washed twice in 1x PBS and stored in 1x PBS at 4°C in the dark. Confocal microscopy analysis was performed using a Leica SPE microscope number DM2500. For each individual

cell, identical exposures and image preparations were used for all photographs, making the photographs directly comparable. Overlays and image analysis were done using the Fiji software. For quantification of internalized collagen, the mean fluorescence intensity was measured in a ROI surrounding each cell. For each time point, 30–40 cells were examined.

3.18 Dual LAMP/DQ Collagen I immunofluorescence

PMT coverslips obtained from 6h incubation with DQ collagen I (section 3.17) were co-stained with LAMP2, lysosomal marker. Fixed coverslips were washed three times with 1x PBS and blocked with 3%BSA (Panreac Applichem, ref. A6588,0100) in 1x PBS for 60 minutes. Next, cells were washed three times with 1x PBS and incubated with Rat anti-LAMP2 antibody (Abcam, ref. ab13524), 1:200 in 1%BSA for 2 hours at RT. Afterwards, cells were washed three times in 1x PBS and incubated with Donkey anti-Rat IgG (H+L) Alexa 594 (Thermo, ref. A-21209) 1:500 in 1% BSA for 1 hour. Finally, cells were washed five times with 1x PBS, and counterstained with DAPI (1:1000 Merck, ref. D9542) for 10 minutes at RT. After washing five times with PBS1x the coverslips were mounted using Mounting Medium with DAPI – Aqueous (Abcam, ab104139). Images were acquired using a spectral Leica SPE microscope DM2500. DAPI was visualized using the 405 laser, DQ Collagen using the 488 laser and LAMP2 using the 532 laser at 630x magnification and zoom 3.2. Colocalization mask was obtained using Image J software.

3.19 Statistical Analysis

Results are expressed as mean + SEM unless otherwise stated in the figure legend. Most of the p values were calculated using one-way ANOVA, followed by Bonferroni's post-test. Where stated Unpaired T-test two tails was used. $*P < 0.05$, $**P < 0.01$ or $***P < 0.001$ were considered statistically significant.

4 Results

4.1. Generation of a mouse strain for CtsD cell-specific deletion in the macrophage

Although our knowledge about the pathophysiological role of CtsD is still limited due to the absence of a viable global CtsD knock-out mouse (Saftig 1995), in the 2016 a CtsD floxed mouse was generated opening new avenues to study CtsD cell-specific role (Ketscher 2016). Macrophages play important roles in kidney homeostasis and in response to the acute and chronic kidney injury (Cao 2015). In order to elucidate the effects of CtsD deletion in the macrophages during kidney diseases, a cell-specific knock-out for the CtsD gene was generated in the lab of Dr. Anna Moles Fernandez, through the Cre-Loxp technology, by using a LysMCre mouse strain for the specific deletion of genes in the domains of the myelomonocytes derivated macrophages.

LysMCre strain has been extensively applied to develop reporter mice for *in vivo* tracking or lineage tracing of macrophages and other myelomonocytic cells in normal and diseased conditions (Shi 2018). In spite of a high efficiency of LysMCre strain in manipulating endogenous macrophages, LysM can target other myeloid cells as most granulocytes, few CD11c+ dendritic cells (DCs), as well as a small percentage of non-hematopoietic cells, as long as 60–80% neutrophils in spleen (Miyake 2007). However, the lack of specific markers for monocytes/macrophages, makes the LysM-Cre mouse strain a broadly used tool to investigate the macrophage population (Shi 2018).

LysMCre mice were crossed with CtsDflox mice in order to generate a LysMCre$^{+/-}$ CtsD$^{flox/flox}$ progeny (called CtsD$^{\Delta Myel-/-}$ or macrophage-CtsD deficient).

To verify the CtsD floxed allele recombination in the macrophages from CtsD$^{\Delta Myel-/-}$ mice, isolated peritoneal macrophages were stimulated with Thioglycolate (PMT), and then seeded overnight. The day after, the cells were collected, and the DNA extracted to perform PCR using specific primers for the Cre recombinant allele. As expected, the amplification band indicating the recombination of the CtsD floxed allele, due to the Cre recombinase activity, was detected only in CtsD$^{\Delta Myel-/-}$ peritoneal macrophages but not in CtsD$^{\Delta Myel+/+}$ (**Fig. 10a**).

To evaluate the deletion of CtsD in the macrophages a western blotting was performed in cell lysates from PMT isolated macrophage-CtsD sufficient and deficient mice. CtsD protein expression was depleted in PMT lysates from CtsD$^{\Delta Myel-/-}$ as compared to wildtype CtsD$^{\Delta Myel+/+}$.

Previous studies demonstrated the interplay between different cathepsins. For instance, CtsD processing has been shown to require the function of cysteine cathepsins, such as CtsB, to generate a mature CtsD form. Conversely, CtsD has been shown to process CtsB precursor by the cleavage of the pro-cathepsin polypeptide. These results imply that CtsB and CtsD contribute to their mutual proteolytic processing in primary mouse hepatic stellate cells (Moles 2009). Cathepsins interplay can occur not only inside the lysosomes but also in the extracellular space in the tumor microenvironment (Turk 2002) where functional compensatory mechanisms have been described (Akkari 2016). Thus, to confirm that the CtsD deletion did not affect the expression of CtsB, the levels of CtsB were also analyzed and the results confirmed the specificity of the deletion and the absence of a compensatory mechanisms (**Fig. 10b**).

Lastly, CtsD activity was assessed in cell lysates from PMT isolated from macrophage-CtsD deficient and sufficient mice, by an enzymatic fluorimetric assay. This assay demonstrated a significant reduction of CtsD activity in the CtsD deficient macrophages (**Fig. 10c**).

Together these results demonstrated the validity of the macrophage cell-specific CtsD knock-out mouse strain.
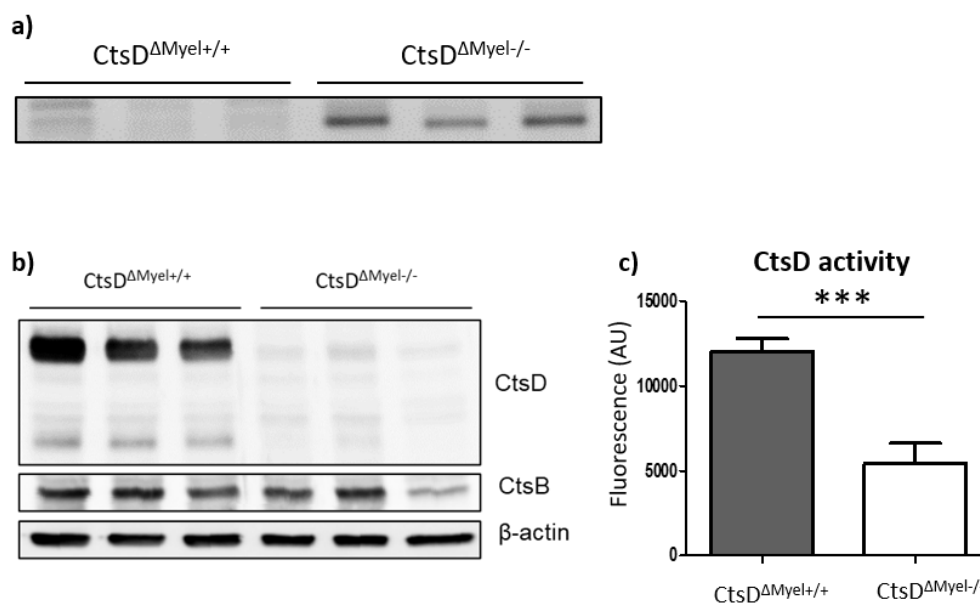
Figure 10. CtsD deletion in macrophages from CtsD$^{\Delta Myel-/-}$ mice was confirmed by PCR, WB and activity assay versus CtsD$^{\Delta Myel+/+}$ mice. (**a**) Recombinant floxed allele expression by PCR (N=5); (**b**) CtsD, CtsB and b-actin WB (N=3); (**c**) CtsD activity (N=6) in isolated PMT cell lysates from CtsD$^{\Delta Myel+/+}$ and (grey bar) and CtsD$^{\Delta Myel-/-}$ (white bar) mice. Unpaired T-test. $p<0.001$.

4.2 The absence of CtsD in macrophages did not affect basal levels of renal damage under physiological conditions

Once validated the CtsD cell-specific deletion in macrophages, we verified whether the deletion of CtsD in macrophages, in absence of external insults, could cause renal damage. Kidney function was assessed using the biomarker Blood Urea Nitrogen (BUN) in serum from the macrophage-CtsD sufficient and deficient mice under physiological conditions (**Fig. 11a**). Given that the BUN values from healthy mice are around 10 nmol/L, it is possible to conclude that the deletion of CtsD in the macrophages did not cause any alteration in kidney functions. Furthermore, the histological analysis of kidney sections from macrophage-CtsD sufficient and deficient mice using PAS staining showed preserved and normal kidney architecture (**Fig. 11b**).
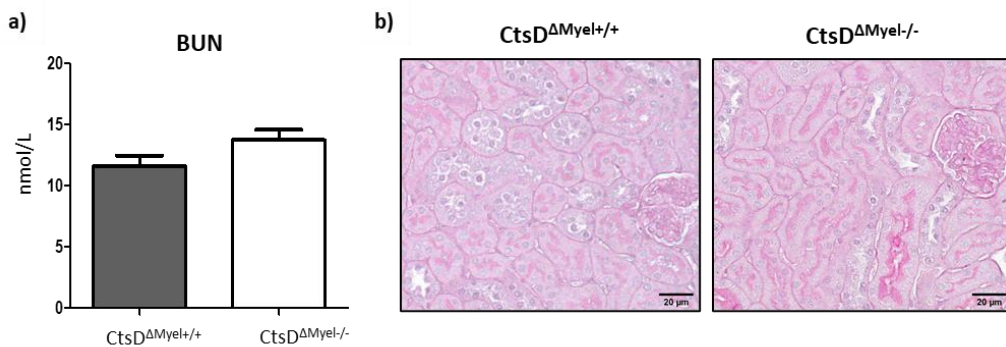
Figure 11. Renal function and architecture was not affected by CtsD deletion in macrophages. (a) Blood Urea Nitrogen (BUN) in serum from macrophage-CtsD sufficient (grey) and deficient (white) mice under physiological conditions (N=7) (**b**) Representative pictures of CtsD$^{\Delta Myel+/+}$ and CtsD$^{\Delta Myel-/-}$ kidneys. No tubular dilatation, epithelial flattening or loss of brush border were observed.

4.3 Unilateral Ureteral Obstruction (UUO) as model of progressive CKD

Once confirmed the absence of a renal damage in response to the specific deletion of CtsD in macrophages, Unilateral Ureteral Obstruction (UUO) model was performed to study the effects of CtsD deletion in macrophages during kidney disease. The UUO model is widely used to study the mechanisms underlying kidney disease progression from acute to chronic stages. The acute nature of the insult causes acute kidney injury (AKI), while the persistence of the obstruction leads to histological features of chronic kidney disease (CKD) (Ucero 2014). According to this, we performed a UUO for 5 days as a model of early-stage kidney disease, and for 10 days, to simulate CKD.

Being a unilateral disease, the UUO has the advantage of a low mortality and the availability of an internal control (the non-obstructed contralateral kidney). Conversely, the disadvantage is that is not useful to study changes in global kidney function, because of the impossibility to get any functional readout from the two kidneys separately.

4.4 Effects of CtsD deletion in macrophages during UUO-induced early-stage kidney disease (UUO 5 days)

8 to 10 weeks macrophage-CtsD sufficient and deficient mice underwent Unilateral Ureteral Obstruction (UUO). After 5 days, the animals were humanely euthanized, and the blood and the two kidneys were collected.

During early-stage kidney disease a normal repair response will restore the normal tubular epithelium. This process involves cell death, proliferation of normal viable tubular cells and the reestablishment of the cell polarity.

4.4.1 Macrophage CtsD deficient animals did not show changes in CtsD activity and gene expression after UUO-induced early-stage kidney disease (UUO 5 days)

First of all, CtsD activity was measured in kidney tissue as described before. UUO 5d kidneys showed a significant increase in CtsD activity compared with contralateral kidneys, but no significant changes were observed between the macrophage-CtsD deficient and sufficient mice (**Fig. 12**).
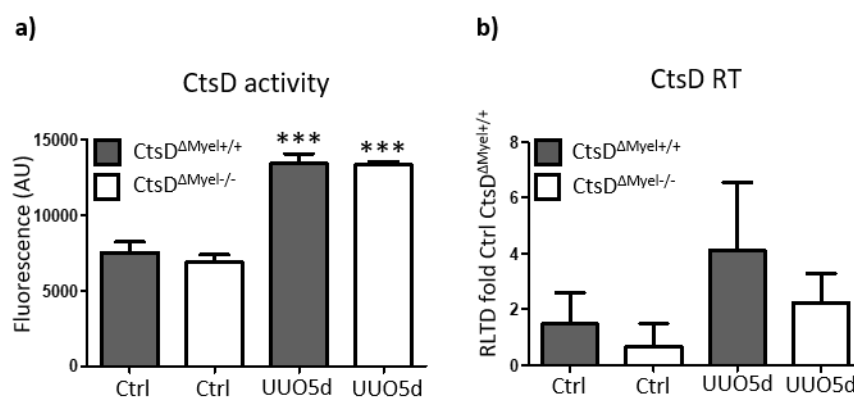
Figure 12. CtsD activity and gene expression in total kidney does not reflect changes in the macrophage cell fraction. (**a**) CtsD activity; (**b**) CtsD gene expression from total kidney in macrophage CtsD sufficient (grey) and deficient (white) 5 days after UUO (N=5). Gene expression was expressed as relative fold versus 18S Ctrl CtsD$^{\Delta Myel+/+}$. 1way ANOVA, *P $\leq$ 0.05, **P $\leq$ 0.01 or ***P $\leq$ 0.001.

In agreement CtsD mRNA expression from total kidney was increased after 5 days of UUO, but no significant changes were detected between the deficient and sufficient groups, both in the contralateral kidneys and in the injured ones. The increase in the expression of CtsD in obstructive nephropathy has been already described in the past (Cocchiaro 2016), as well as the evidence that CtsD is mainly expressed in distal tubular cells, thus the percentage of CtsD activity accounting for macrophages in the total kidney lysate is small in comparison with the activity coming from tubular epithelial cells. To confirm this, a dual immunostaining for macrophages (F4/80) and CtsD was performed in kidney sections from UUO 10 days and is shown in **section 4.5.1**. Therefore, slight changes of activity in the macrophage cell population can be challenging to be detected without the interference from the tubular epithelial cell fraction.

4.4.2 Macrophage CtsD deficient animals did not show differences in kidney damage 5 days after UUO

To determine tubular cell damage PAS staining and scoring was performed. Damaged tubules were classified according to previously described scoring system using the following criteria: tubular dilation, loss of brush border and epithelial flattening and casts formation. The tubular damage worsened 5 days after UUO, but no changes in tubular damage was observed between macrophage-CtsD sufficient (grey) and deficient (white) mice in the obstructed kidneys (**Fig. 13**).
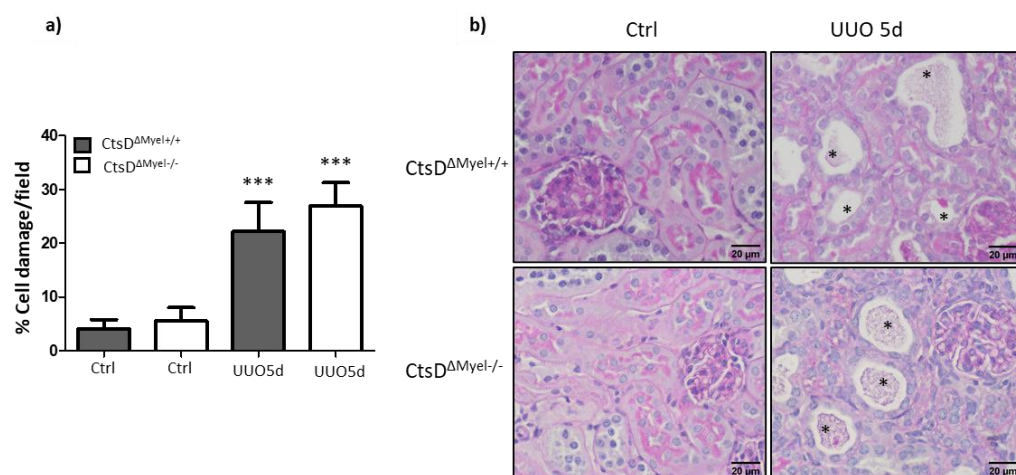
Figure 13. Lack of CtsD in macrophages does not affect renal damage 5 days after UUO. **(a)** Percentage of tubular cell damage (tubular dilation, loss of brush border and epithelial flattening and casts formation) in macrophage-CtsD sufficient (grey) and deficient (white) kidneys 5 days after UUO. Tubular damage was assessed in 10-20 random 200X fields in the cortex (N=5). **(b)** Representative pictures of PAS staining in kidney sections in UUO 10d mice, damaged tubules *. 1way ANOVA, *P ≤ 0.05, **P ≤ 0.01 or ***P ≤ 0.001.

4.4.3 Deletion of CtsD in macrophages caused decrease expression of inflammatory mediator after 5 days of UUO

During the UUO model, interstitial inflammatory cell infiltration progressively increases from 12 hours after obstruction up to 14 days. Damaged epithelial and endothelial cells are responsible for releasing of chemoattractants and cytokines, such as keratinocyte chemokine (KC or CXCL1), or monocyte chemoattractant protein 1 (MCP1 or CCL2) which promote neutrophils and mononuclear phagocytes (macrophages) adhesion and chemotaxis to the sites of injury into the interstitium (Black 2019). Both resident and infiltrating immune cells participate in inflammation, injury and repair in the acute phase of kidney injury and contribute to disease progression through a tight crosstalk with endothelial cells, epithelial cells, and pericytes. TNF-α is expressed mainly by macrophages, renal tubular cells, and mesangial cells and is known to play a major role in renal inflammation and fibrosis, activating inflammatory and cell death signaling pathways. Like TNF-α, IL1β is a potent proinflammatory mediator that amplifies parenchymal cell injury (Wynn & Ramalingam 2012). Given the important role of the macrophages in the early inflammatory response to the injury, we investigated the effect of the absence of CtsD in macrophages on the inflammatory response after 5 days of UUO. As shown by **Fig. 14**, a decrease in CXCL1(a), CCL2 (b), CCL3 (c), and CCL5 (d) and IL1β (f) gene expression was observed in obstructed kidneys (UUO) from macrophage-CtsD deficient versus sufficient mice however, it only reached statistical significance for CXCL1(a) and IL1β (f).
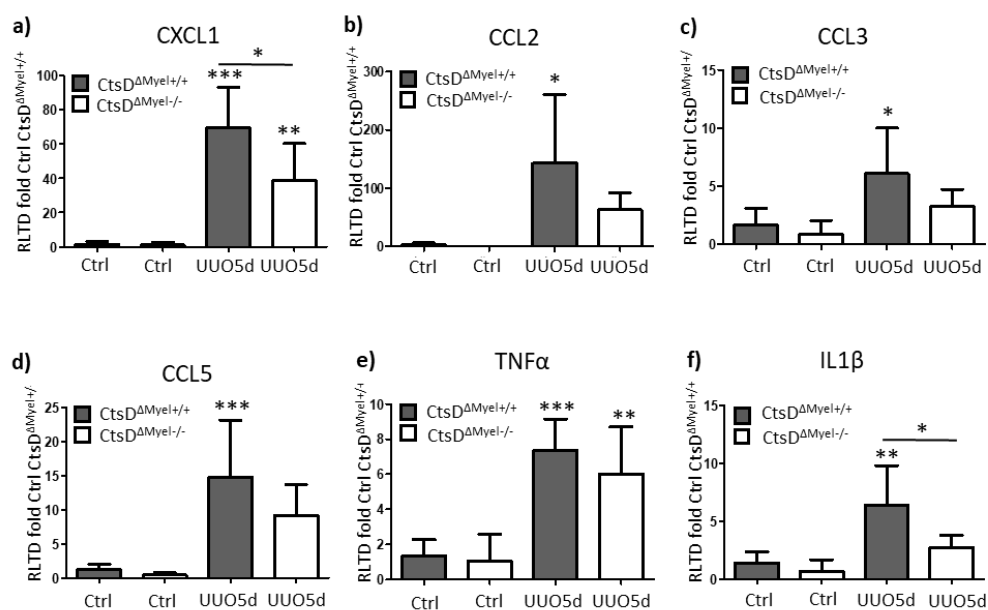
Figure 14. Macrophage-CtsD deficient kidneys present decrease inflammatory markers 5 days after UUO. (a) CXCL1, **(b)** CCL2, **(c)** CCL3, **(d)** CCL5, **(e)** TNFα and **(f)** IL1β gene expression in contralateral (Ctrl) and obstructed (UUO) kidneys 5 days after UUO in macrophage-CtsD sufficient (grey) and deficient (white) (N=5). Gene expression was expressed as relative fold versus 18S Ctrl CtsD$^{\Delta Myel+/+}$. 1 way ANOVA, *P ≤ 0.05, **P ≤ 0.01 or ***P ≤ 0.001.

No changes were observed in TNFα (e) gene expression between obstructed kidneys. Macrophage-CtsD deficient kidneys presented decreased inflammatory markers 5 days after UUO pointing towards a possible defective inflammatory response in macrophages lacking CtsD.

4.4.4 Deletion of CtsD in macrophages resulted in the reduction of the number of total macrophages in the UUO diseased kidney, mainly due to a decrease in the M2 population

Macrophages and neutrophils are involved in the innate immune response. Once demonstrated that the deletion of CtsD in macrophages decreased the expression of inflammatory mediators 5 days after UUO, we asked whether this effect could be due to an altered recruitment of macrophages during early kidney disease, or an altered polarization of macrophages involved in the inflammatory response.

According to their function in inflammation, macrophages can be divided in subpopulations (Cao 2015). Two well defined phenotypes are commonly referred to as classically activated pro-inflammatory macrophages (M1), produced by exposure to LPS or IFN-γ, and alternatively activated anti-inflammatory macrophages (M2), induced by Th2 cytokines such as IL-4 and IL-10. As expected, total macrophage levels were significantly increased 5 days after UUO as shown by increased F4/80 gene expression in total kidney (**Fig 15a**). However, this increase was far greater in macrophage-CtsD sufficient mice versus deficient ones. To analyze M1 and M2 populations within the F4/80 fraction, CD11c and Arginase-1 were selected respectively. M1 macrophages population was significantly increase in the UUO groups but not affected by CtsD specific deletion in macrophages (**Fig 15b**). On contrary, M2 macrophages were again significatively increased 5 days after UUO only in macrophage-CtsD sufficient mice but not in deficient ones (**Fig 15c**) as detected by Arginase-1 gene expression in total kidney. Thus, CtsD specific deletion in macrophages seemed to lead to a defective recruitment and polarization of macrophages in response to early-stage kidney disease.

Taken together the results obtained by analyzing the UUO 5d model, we conclude that the absence of CtsD in macrophages did not affect renal damage during early-stage kidney disease but resulted in a downregulation of

inflammatory chemokines and an alteration in the number and phenotype of macrophages.
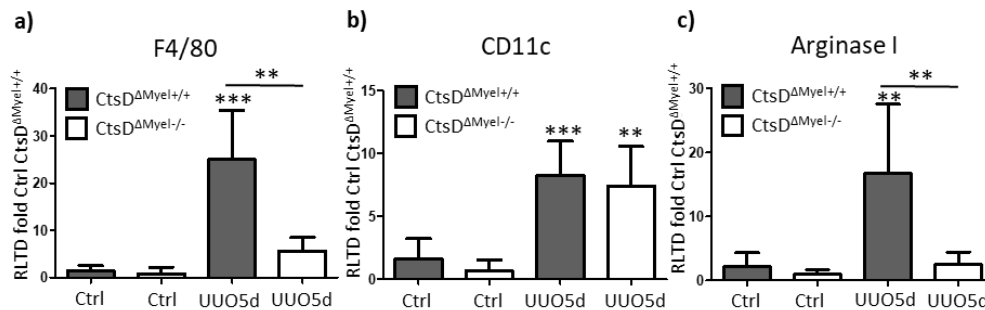
Figure 15. CtsD specific deletion in macrophages results in defective recruitment and polarization of macrophages in response to early-stage kidney disease. (**a**) F4/80 (total macrophages) (**b**) Cdc11c (M1 macrophages) and (**c**) Arginase I (M2 macrophages) gene expression in Control and 5d UUO kidneys from macrophage-CtsD sufficient (grey) and deficient (white) mice (N=5). Gene expression was expressed as relative fold versus 18S Ctrl CtsD$^{\Delta Myel+/+}$. 1 way ANOVA, *P ≤ 0.05, **P ≤ 0.01 or ***P ≤ 0.001.

4.5 Effects of CtsD deletion in macrophages during UUO-induced Chronic Kidney Disease (CKD) (UUO 10 days)

After an acute or a persistent insult, an abnormal repair response, defined as incomplete tubular repair, persistent inflammation, fibroblasts proliferation and excessive extracellular matrix deposition, will result in the progression toward CKD. Hence, 8-10 weeks macrophage-CtsD sufficient and deficient mice underwent 10 days unilateral ureteral obstruction. After that time, the animals were humanely euthanized, and the blood and two kidneys were collected.

4.5.1 Macrophage-CtsD deficient mice showed decreased CtsD activity in kidney after 10 days UUO

CtsD activity was measured in kidney tissue as described before. As for UUO 5d, an increase in the CtsD activity was observed in the obstructed kidneys versus the contralateral ones. Remarkably, this time a significant decrease in CtsD activity was observed in the obstructed kidney of the macrophage-CtsD deficient mice versus the sufficient ones (**Fig. 16**). This result indicates a more important proportion of CtsD in the total kidney coming from macrophages during chronic injury than in acute kidney injury. To confirm this, a dual immunostaining for F4/80 (marker for macrophages) and CtsD was performed in kidney sections from macrophage-CtsD sufficient and deficient mice after 10 days UUO. In agreement with previous reports, dual immunostaining pictures confirmed the high expression of CtsD in tubular epithelial cells from both

macrophage-sufficient and deficient kidneys after UUO. Dual immunostaining demonstrated high levels of F4/80 positive cells (red cells) 10 days after UUO, however, CtsD was only detected in macrophages (F4/80 red positive cells) from macrophage-CtsD sufficient kidneys and not deficient ones.
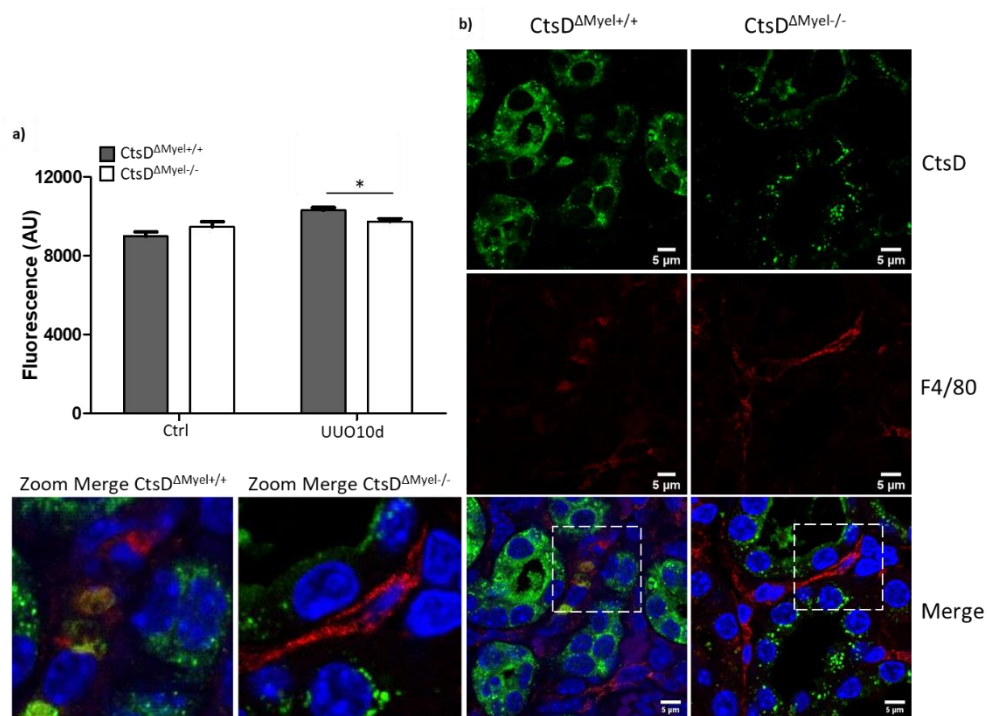
Figure 16. CtsD activity is decreased in total kidney 10 days after UUO indicating increased contribution of CtsD coming from the macrophage cell fraction to the total CtsD activity in the kidney. (a) CtsD activity in kidney lysates from UUO 10d from macrophage-CtsD sufficient (grey) and deficient (white) mice (N=7). **(b)** Representative pictures of dual immunostaining for F4/80 (red) and CtsD (green) in kidney paraffin embedded sections in UUO 10d mice and zoom image showing areas of expression in macrophages (N=3). Magnification 100X. Unpaired T-test, *P ≤ 0.05.

4.5.2 Macrophage CtsD deficient animals did not show differences in kidney damage after 10 days UUO

As for the UUO 5 days study, the tubular cell damage was determined by PAS staining and scoring. The tubular damage worsened 10 days after UUO, but no changes in tubular damage was observed between macrophage-CtsD sufficient (grey) and deficient (white) mice in the obstructed kidneys (**Fig. 17**).
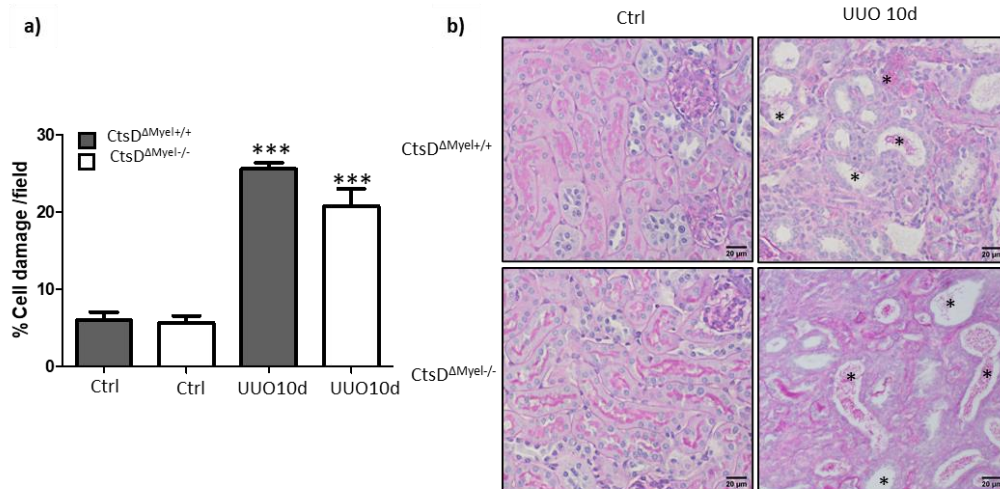
Figure 17. Lack of CtsD in macrophages does not affect renal damage 10 days after UUO. **(a)** Percentage of tubular cell damage (tubular dilation, loss of brush border and epithelial flattening and casts formation) in macrophage-CtsD sufficient (grey) and deficient (white) kidneys 10 days after UUO (N=7). **(b)** Representative pictures of PAS staining in kidney sections of UUO 10d mice, damaged tubules *. Tubular damage was assessed in 10-20 random 200X fields in the cortex. 1 way ANOVA, *P ≤ 0.05, **P ≤ 0.01 or ***P ≤ 0.001.

4.5.3 Lack of CtsD in macrophages resulted in increased renal fibrosis after UUO-induced chronic renal injury (UUO 10d)

Tubulointerstitial fibrosis is one of the main histological features of CKD. Fibrosis is characterized by the increased production and deposition of the extracellular matrix (ECM) components, including collagen type I, fibronectin, hyaluronan, and elastin, and the accumulation of activated, αSMA-positive and collagen-secreting fibroblasts, called myofibroblasts.

Therefore, fibrosis in UUO 10d kidneys was measured by morphometric analysis of Sirius Red, α-SMA IHC and WB. As expected, both macrophage-CtsD sufficient and deficient kidneys showed increased fibrosis detected by a significant increase in Sirius Red andα-SMA IHC and WB. CtsD cell-specific deletion in macrophages resulted in an enhancement of the fibrotic response as shown by an increase in Sirius red staining (**Fig. 18a-b**) and α-SMA immunohistochemistry (**Fig. 18c-d**) and WB (**Fig. 4.9e**) in macrophage-CtsD deficient mice versus sufficient ones, confirming that the absence of CtsD in macrophages amplified the fibrotic response during CKD.
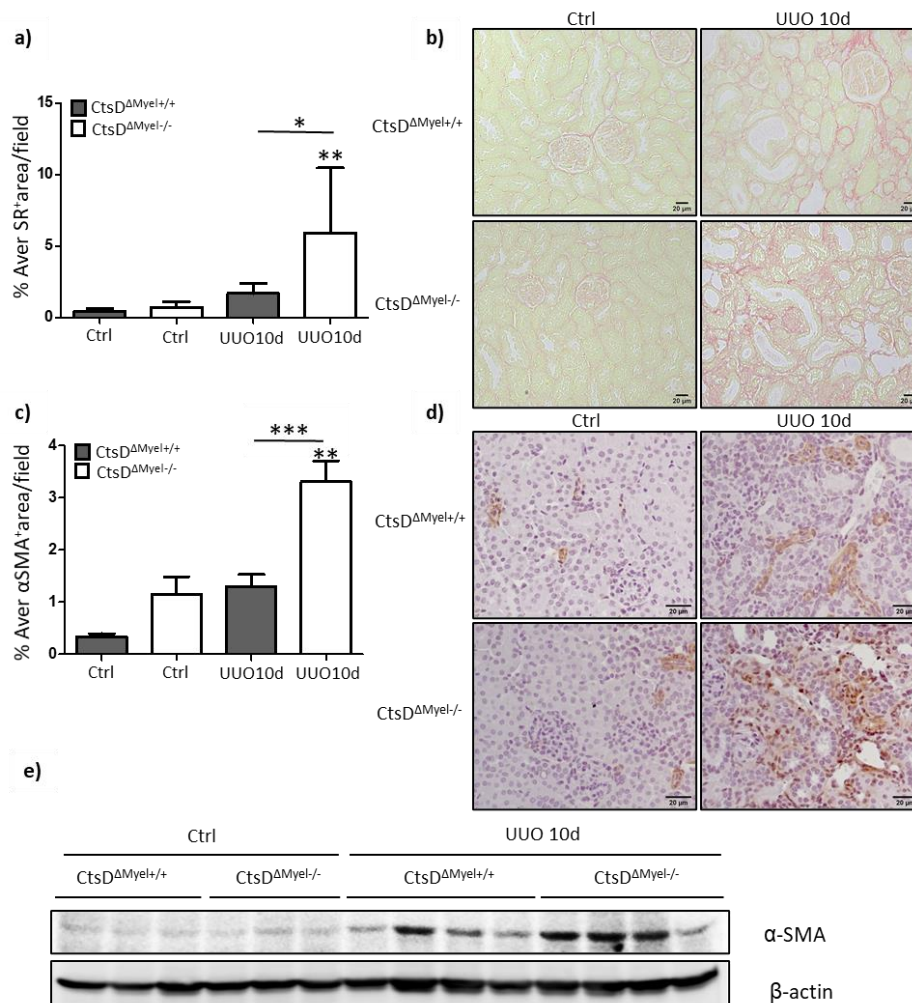
Figure 18. Absence of CtsD in macrophages amplified the fibrotic response. (a) Percentage of Sirius Red positive staining assessed in 10-20 random 100X fields in the cortex; **(b)** Representative pictures of Sirius Red staining. **(c)** Percentage of α-SMA positive areas per field, assessed in 10-20 random 200X fields in the cortex; **(d)** Representative pictures of α-SMA IHC; **(e)** α-SMA western blot on kidney lysates normalized versus β-actin of Ctrl and UUO 10d kidneys from macrophage-CtsD sufficient (grey) and deficient (white) mice (N=7). 1 way ANOVA, $*P \leq 0.05$, $**P \leq 0.01$ or $***P \leq 0.001$.

4.5.4 Macrophage-CtsD deficient animals did not show altered expression of fibrotic markers after 10 days UUO

Once established that the level of fibrosis was increased in macrophage-CtsD deficient mice 10 days after UUO we verified whether this also affected gene expression of fibrosis marker and mediators. ACTA2 (gene encoding for αSMA) (**Fig. 19a**) Col1A1 (b) and TGF-β (c) gene expression from total kidney increased 10 days after UUO, but no significant changes were detected between macrophage-CtsD deficient and sufficient mice, both in the contralateral kidneys

or in the obstructed ones. Thus, the increase in the level of fibrosis in the tissue was not a consequence of a differential increase in the expression of collagen in macrophage-CtsD deficient mice.
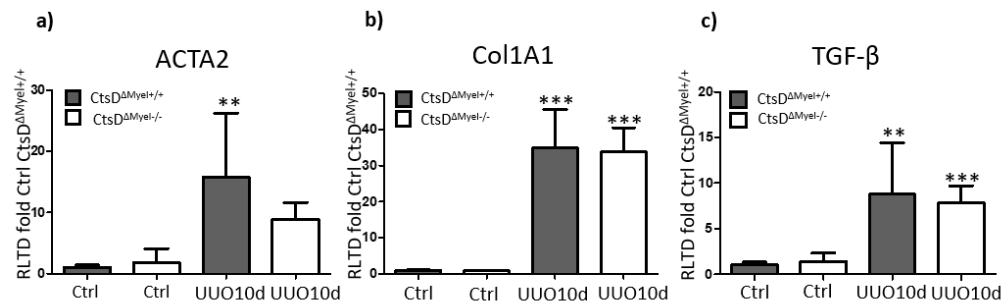
Figure 19. Macrophage-CtsD deficient mice did not present alter gene expression of fibrotic markers 10 days after UUO. (a) ACTA2, **(b)** Col1a1 and **(c)** TGFβ gene expression in contralateral (ctrl) or obstructed (UUO) kidneys 10 days after UUO from macrophage-CtsD sufficient (grey) and deficient (white) mice (N=7). Gene expression was expressed as relative fold versus 18S Ctrl CtsD$^{\Delta Myel+/+}$. 1way ANOVA, *P $\leq$ 0.05, **P $\leq$ 0.01 or ***P $\leq$ 0.001.

4.5.5 Macrophage-CtsD deficient animals showed decreased neutrophil recruitment after 10d UUO

To clarify the effect of CtsD deletion in macrophages over inflammation, we evaluated the neutrophil recruitment during CKD in our diseased models. Neutrophils are among the main players involved in the inflammatory response, therefore, the number of neutrophils recruited to the site of injury was investigated by IHC for NIMP (Nogo Interacting Mitochondrial Protein). A significant increase in the number of neutrophils (NIMP) recruited to the site of injury 10 after days of UUO in both macrophage-CtsD sufficient and deficient kidneys was observed (**Fig. 20**). However, the number of neutrophils was significantly lower in the macrophage-CtsD deficient mice in comparison with the sufficient ones.
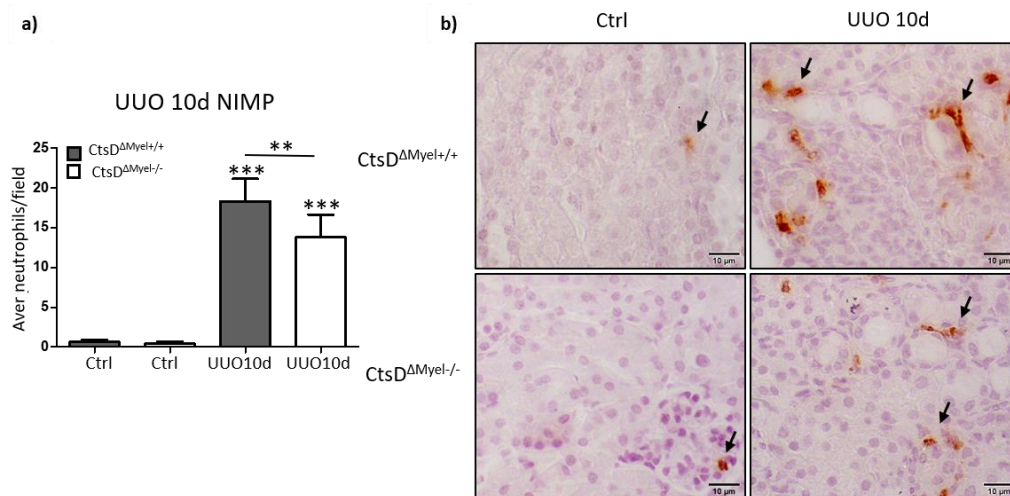
Figure 20. Lack of CtsD in macrophages results in reduced neutrophil recruitment 10 days after UUO. (a) Average of Neutrophils (NIMP) per field in Ctrl kidneys and UUO 10d kidneys from macrophage-CtsD sufficient (grey) and deficient (white) mice (N=7). Average assessed in 10-20 random 200X fields in the cortex. **(b)** Representative pictures of NIMP IHC. 1way ANOVA, *P ≤ 0.05, **P ≤ 0.01 or ***P ≤ 0.001.

4.5.6 CtsD deletion in macrophages did not influence the expression of inflammatory mediators during renal fibrosis.

Our findings showed a decrease in the number of neutrophils in the macrophage-CtsD deficient mice 10 days after UUO. Thus, we investigated the expression of some inflammatory mediators, such as CXCL-1, CCL2 and TNF-α, by RT-PCR (**Fig. 21**). The chemokine CXCL-1 plays a pivotal role in the host immune response by recruiting and activating neutrophils at the tissue site (Sawant 2016). The expression of all the investigated inflammatory mediators was significantly increased in the UUO kidneys, but CtsD specific deletion in the macrophages did not alter their expression in obstructed kidneys. It is possible that other inflammatory mediators might explain the reduced neutrophil recruitment observed in macrophage-CtsD deficient mice after 10 days UUO described in the previous paragraph. Further investigation will need to be done to clarify this, however previous studies have shown little or no influence of neutrophilic inflammation on fibrosis (Moles 2014). Hence, we focused our project on the direct role of macrophages in the inflammatory response during CKD.
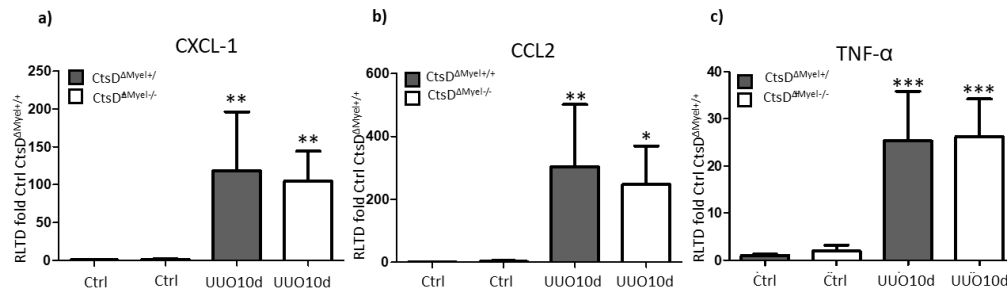
Figure 21. Macrophage-CtsD deficient animals does not present alteration of inflammatory mediators 10 days after UUO. (a) CXCL-1, **(b)** CCL2 and **(c)** TNFα gene expression in contralateral (ctrl) and obstructed (UUO) kidneys 10 days after UUO from macrophage-CtsD sufficient (grey) and deficient (white) mice (N=5). Gene expression was normalized as relative fold versus 18S Ctrl CtsD$^{\Delta Myel+/+}$. 1way ANOVA, *P ≤ 0.05, **P ≤ 0.01 or ***P ≤ 0.001.

4.5.7 Macrophage CtsD deletion did not affect the number or the populations of macrophages after 10 days UUO

In the early-stage kidney disease (UUO 5d), the specific deletion of CtsD in macrophages seemed to lead to a defective recruitment and polarization of macrophages. Macrophages have a pivotal role both in kidney inflammation and fibrosis. Indeed, mounting evidence shows that macrophages also play a reparative role during the course of the disease, by actively participating in clearance of apoptotic and necrotic cells resolving injury and remodelling matrix to restore tissue homeostasis both in acute and chronic kidney disease (Cao 2015). We evaluated the different populations of macrophages in the tissue during renal fibrosis, by detecting F4/80 as a general marker of macrophages, CD11c, as a marker of M1 macrophages, and Arginase I as a marker of M2 macrophages. All the markers were significantly increased after UUO however, no differences were detected between macrophage-CtsD sufficient and deficient mice.

To confirm that the number of the total macrophages was not affected by the depletion of CtsD in macrophages, we performed an IHC for F4/80 in kidney tissue sections. The number of macrophages was significantly increased in obstructed kidneys (**Fig. 22**), but no significant differences were observed between macrophage-CtsD deficient and sufficient mice. However, these findings suggested that the population of M2 macrophages has recovered, compared to early-stage disease (UUO 5d) (**Fig. 15**). Nevertheless, absence of CtsD in macrophages most likely resulted in defective anti-fibrotic and reparative activities, mainly attributed to the M2 population, which caused increased renal fibrosis.
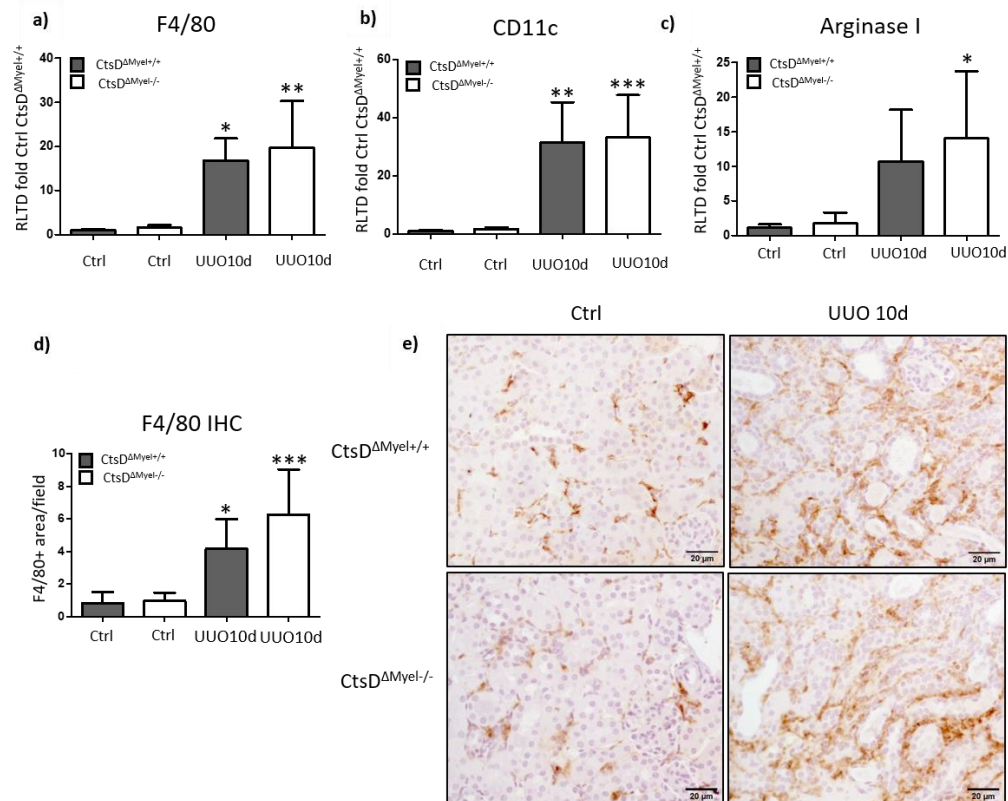
Figure 22. Macrophage CtsD deletion did not affect number or the populations of macrophages 10 days after UUO. (a) F4/80, **(b)** CD11c, **(c)** Arginase I mRNA gene expression from Control and 10d UUO kidneys from macrophage-CtsD sufficient (grey) and deficient (white) mice (N=5). Gene expression was expressed as relative fold versus 18S Ctrl CtsD$^{\Delta Myel+/+}$. **(d)** Percentage of f4/80 positive areas per field, assessed in 10-20 random 200X fields in the cortex, **(e)** Representative pictures of F4/80 IHC 1way ANOVA, *P ≤ 0.05, **P ≤ 0.01 or ***P ≤ 0.001.

4.5.8 Collagen endocytosis was not affected by absence of CtsD in macrophages

Although an increase in fibrosis was detected during CKD, no alteration in the collagen synthesis, number of macrophages or inflammation were found. Thus, we hypothesized that the excess of ECM accumulation could potentially be a consequence of the impairment in collagen turnover. The best characterized pathway of collagen turnover is the proteolytic breakdown occurring in the extracellular space. However, collagen could be also internalized through binding to collagen-specific receptors on the cell surface and delivered to lysosomes for degradation. Notably cathepsins can also participate in the proteolytic cascades implicated in collagen turnover (Cocchiaro 2016). The receptor involved in collagen uptake is the uPARAP/Endo180 (uPAR Associated Protein), belonging to the mannose receptor family (Melander 2015). In healthy organisms, uPARAP/Endo180 is primarily expressed by

mesenchymal cells such as fibroblasts and osteogenic cells and is present in sites showing active tissue remodelling. Since uPARAP/Endo180 is involved in events related to collagen remodelling, a uPARAP/ Endo180 deficiency aggravated renal fibrosis demonstrating increased collagen content and reduced collagen turnover, suggesting a protective role of the receptor during chronic kidney disease and fibrosis (López-Guisa 2012). Thus, we evaluated by WB, the levels of Endo180 and uPAR in kidney lysates, to investigate whether the abnormal increase of ECM accumulation could be explained by a defective collagen uptake and degradation. As shown by **Fig. 23**, no significant changes in Endo180 were observed between Ctrl and UUO kidneys. However, a clear increased was detected in UPAR after UUO but no changes between macrophage-CtsD sufficient and deficient obstructed kidneys were observed.
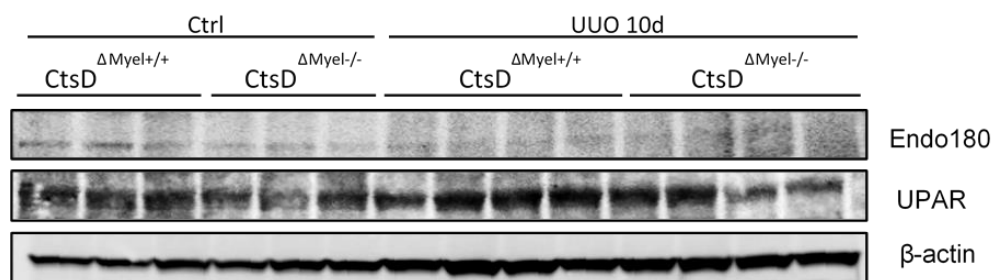
Figure 23. Collagen internalization receptors Endo180 and UPAR are not affected by a lack of CtsD in macrophages during renal fibrosis. Endo180 and UPAR WB on lysates from Ctrl kidneys and UUO 10d kidneys from macrophage-CtsD sufficient and deficient mice normalized versus β-actin.

4.5.9 Lack of CtsD in macrophages during renal fibrosis resulted in altered ECM remodelling enzyme gene expression

Next, we investigated whether proteolytic enzymes involved in ECM remodelling might be affected by the absence of CtsD in macrophages during renal fibrosis. Collagenolytic enzymes include secreted and membrane-associated proteases of the matrix metalloproteinase (MMP) family. Macrophages are the main sources of MMPs that facilitate ECM degradation during the remodelling phase in wound healing process; they also phagocytose apoptotic myofibroblasts and cellular debris preventing progress of the fibrotic process (Kryczka 2015). Therefore, we evaluated the expression of some metalloproteinases, uncovering a significant decrease in the expression of Matrilysin, also known as matrix metalloproteinase7 (MMP7) (**Fig. 24**) in macrophage-CtsD deficient mice versus sufficient ones after 10 days UUO but

no changes in MMP2 or MMP3. Thus, the absence of CtsD in macrophages resulted in defective MMP7 expression.
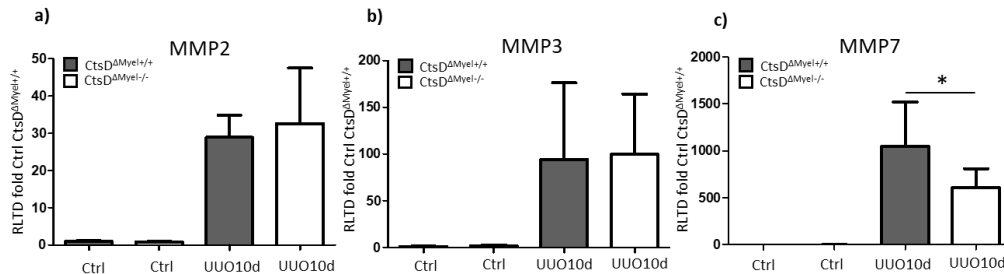
Figure 24. Lack of CtsD in macrophages during renal fibrosis results in decreased MMP7 gene expression. (a) MMP2, **(b)** MMP3, **(c)** MMP7 mRNA gene expression from Control and 10d UUO kidneys from macrophage-CtsD sufficient (grey) and deficient (white) mice (N=5). MMP7 gene expression in contralateral (ctrl) or obstructed (UUO) and kidneys 10 days after UUO from macrophage-CtsD sufficient (grey) and deficient (white) mice (N=5). Gene expression was normalized as relative fold versus 18S Ctrl CtsD$^{\Delta Myel+/+}$. Unpaired T-test, *P $\leq$ 0.05.

4.6 M1 polarized CtsD deficient PMT showed defective MMP profile

In order to investigate the effect of the absence of CtsD in M1 and M2 populations, peritoneal macrophages elicited with Thioglycolate were isolated and then stimulated to polarize toward M1 or M2 phenotype by treating them with LPS or a combination of IL4 and IL13 for 24 hours respectively.

Macrophages, both resident and circulating, may be activated by a wide range of stimuli. Notably, bacterial cell wall proteins such as lipopolysaccharide (LPS) activate macrophages by engagement of specific receptors collectively known as pattern recognition receptors (PRRs), including Toll-like receptors (TLRs) on macrophages membranes inducing a pro-inflammatory phenotype (Charles A. Janeway & Medzhitov 2003).

After stimulating PMT of LPS (10ng/mL or 50ng/mL) for 24h, RTPCR was performed (**Fig. 25**). As expected CtsD expression (**Fig. 25a**) was significantly decreased in PMT from macrophage-CtsD deficient (white) versus sufficient (grey) mice. Of note, stimulation with LPS did not increase CtsD levels in macrophage-CtsD sufficient PMT. To confirm a correct M1 polarization of the PMT, iNOS and CCL2 were investigated. Generally, macrophage polarization is measured by changes in expression of several surface markers which change in response to cytokines present in the microenvironment. Thus, we selected the inducible nitric oxide synthase (iNOS) as hallmark molecule of M1 macrophages, and CCL2, which expression is inducible, triggered upon exposure to inflammatory stimuli. iNOS expression is increased similarly after LPS stimulation at both doses (**Fig. 25b**), whereas CCL2 expression increased in a dose dependent manner after LPS stimulation (**Fig.**

25c). Moreover, to confirm the results obtained in the UUO 10d model, the expression of some metalloproteinases was examined. MMP2 (**Fig. 25d**), MMP3 (**Fig. 25e**), and MMP7 (**Fig. 25f**) gene expression was increased after LPS stimulation, but a significant decrease (only MMP2 and 7) was shown in PMT deficient in CtsD, suggesting a link between the depletion of CtsD in macrophages and a defective MMP profile.
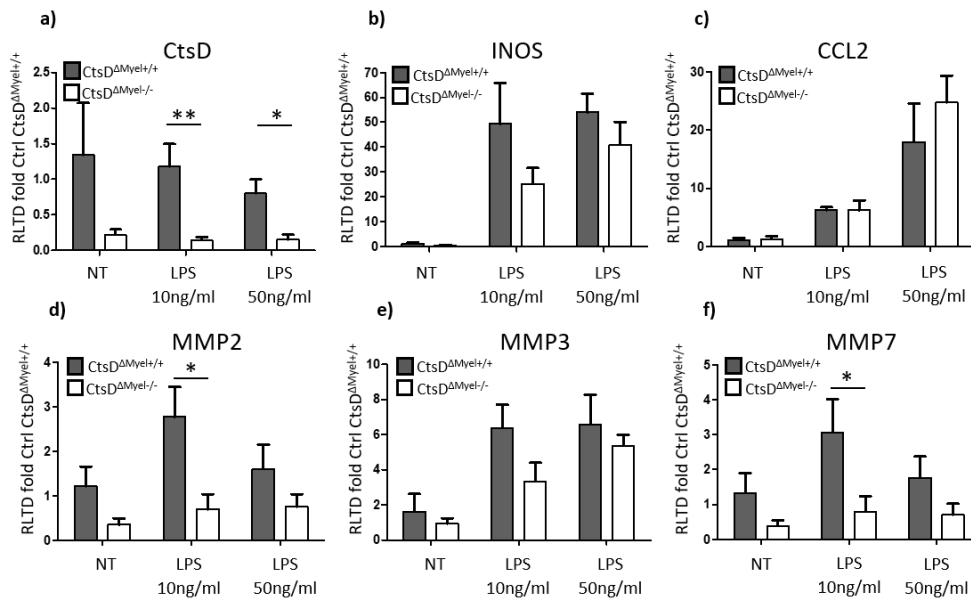
Figure 25. CtsD deficient macrophages stimulated with LPS (M1 polarization) showed defective MMP profile. (a) CtsD, **(b)** iNOS, **(c)** CCL2, (d) MMP2, **(e)** MMP3 and **(f)** MMP7 gene expression in PMT from macrophage-CtsD deficient (white) and sufficient (grey) mice after stimulation with LPS 10ng/mL or 50 ng/mL for 24h (N=3). Gene expression was normalised as relative fold versus 18S NT CtsD$^{\Delta Myel+/+}$. 1way ANOVA, *P ≤ 0.05, **P ≤ 0.01 or ***P ≤ 0.001.

4.7 M2 polarized CtsD deficient PMT showed defective MMP profile

Tissue remodelling and repair is believed to critically depend on a subpopulation of macrophages variably known as M2-polarized, alternatively activated or wound healing macrophages, which in tissues can be identified as they express elevated levels of mannose receptor (MRC1) and other markers (Madsen 2013). Indeed, although M2-polarized macrophages only constituted 15% of the cells, they accounted for 60% of all cellular collagen uptake. Hence, we stimulated PMT with a combination of IL4 and IL13 (20ng/mL or 50ng/mL) for 24h (**Fig. 26**), which is a widely recognized method to induce M2 polarization in isolated macrophages (Oishi 2016). In agreement with the previous experiment, CtsD expression (**Fig. 26a**) was significantly decreased in PMT from macrophage-CtsD deficient versus sufficient mice in all the conditions described and no significant increase in CtsD was detected after

IL4/IL13 stimulation. A dose-dependent increase in the expression of MRC1(**Fig. 26b**), which is a marker of M2 polarization was observed. Interestingly a decrease in IL10 expression (**Fig. 26c**), which is a well-characterized cytokine secreted by M2 macrophages was detected in CtsD deficient PMT indicating that M2 polarized CtsD deficient macrophages could show defective M2 inflammatory response. In addition, MMPs gene expression profiles of MMP2 (**Fig. 26d**), MMP3 (**Fig. 26e**) and MMP7 (**Fig. 26f**) was also defective in CtsD deficient PMT versus sufficient ones. These results added to the previous data in M1 polarized macrophages strongly support the hypothesis that deletion of CtsD in macrophages resulted in defective MMP profile (**Fig. 25d-f**). Dysregulation of the proteolytic profile of the MMPs due to the lack of CtsD in macrophages could be in part responsible for the accumulation of collagen and the increased renal fibrosis observed in macrophage-CtsD deficient mice.
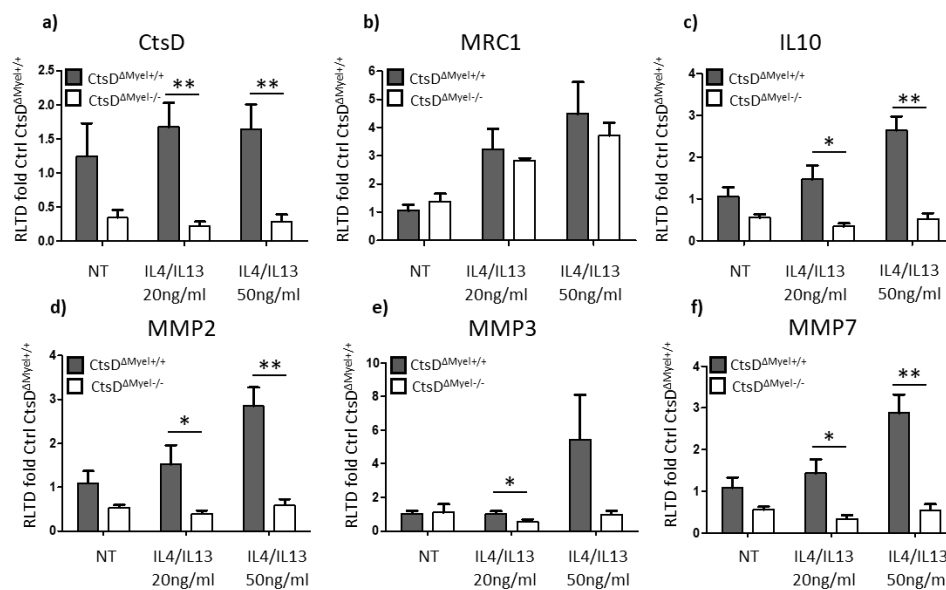
Figure 26. CtsD deficient macrophages stimulated with IL4/IL13 (M2 polarization) showed defective MMP profile. (**a**) CtsD, (**b**) MRC1, (**c**) IL10, (**d**) MMP2, (**e**) MMP3 and (**f**) MMP7 gene expression in PMT from macrophage-CtsD deficient (white) and sufficient (grey) mice after stimulation with IL4 and IL13 20ng/mL or 50 ng/mL for 24h (N=3). Gene expression was normalised as relative fold versus 18S NT CtsD$^{\Delta Myel+/+}$. 1way ANOVA, *P $\leq$ 0.05, **P $\leq$ 0.01 or ***P $\leq$ 0.001.

4.8 Macrophage deficient in CtsD showed defective collagen I degradation

Several studies support the hypothesis that M2 polarization dramatically enhances the capability to turnover extracellular matrix via intracellular internalization *in vivo* (Madsen & Bugge 2013). Given the important role of macrophages, in particular M2 phenotype, in repair and collagen recycling, we

decided to investigate the collagen internalization process in macrophage-CtsD deficient and sufficient PMT, to evaluate whether defective macrophages displayed an impaired collagen degradation, together with a dysregulation of the proteolytic profile of MMPs. The fluorogenic DQ™ collagen can be used to directly monitor its internalization and degradation in living cells. Fluorescein Conjugate DQ type I Collagen (DQ-collagen I) are analogues of the natural substrate that have an excessive number of fluorescent dyes attached so that the fluorescence signal is almost not-existent. This quenching of the signal is caused by the close proximity of the dyes on the intact substrate (Jedeszko 2008). Upon proteolytic cleavage, the fluorescence is released, directly reflecting the level of proteolysis by the cells (Bi 2014). Consistent with a function in collagen turnover, cultured M2-polarized macrophages display internalization of type I collagen at a 2.5-fold higher rate than M1-polarized macrophages (Madsen 2013). PMT from macrophage-CtsD deficient and sufficient mice were incubated with DQ-collagen I (1 μg/mL) for 3 hours at 4°C and 37°C to evaluate collagen degradation (Fig. 4.18a-c). As expected, collagen degradation was not occurring at 4°C as the proteolytic enzymes required for this processed remained inactive (**Fig. 27a**). A pronounced fluorescent intracellular vesicular pattern was observed after incubating the cells with DQ collagen I at 37°C. Co-stain of these PMT with LAMP2 (**Fig. 27d**), as a marker for lysosomes, demonstrated the partial colocalization of the DQ collagen probe with the lysosome. Analysis of the collagen degradative signature in the macrophage-CtsD deficient and sufficient PMT reveal decreased degradative profile of the macrophage-CtsD deficient versus the sufficient ones (**Fig. 27b-c**). Thus, less degradation of collagen in CtsD deficient macrophages could be responsible, at least in part, of the accumulation of collagen and the increased renal fibrosis detected in the macrophage-CtsD deficient mice after UUO 10d.
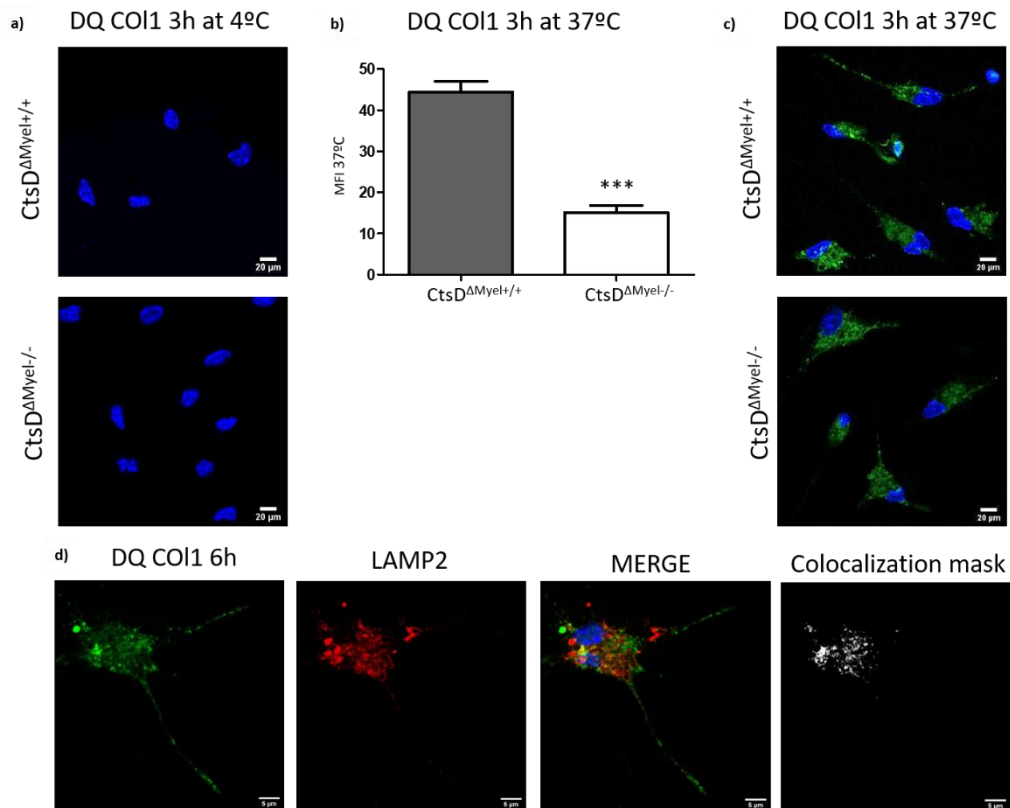
Figure 27. CtsD deficient macrophages present defective collagen I degradation (a) Representative images of PMT treated with 1ug/mL DQ collagen I for 3h at 4ºC. **(b)** Mean fluorescence intensity (MFI) of PMT from macrophage-CtsD deficient (white) and sufficient (grey) mice treated with1ug/mL DQcollagen I for 3h 37ºC (N=3). For each condition, 30–40 cells were examined. **(c)** Representative images of PMT treated with 1ug/mL DQ collagen I for 3h at 37ºC. **(d)** Representative images and colocalization mask of PMT treated with 1ug/mL DQcollagen I (green) for 6h at 37ºC and co-stained with LAMP2 (red), Merge of the two channels with DAPI (blue), and Colocalization mask of DQcollagen I and LAMP2. 1 way-ANOVA, *P ≤ 0.05, **P ≤ 0.01 or ***P ≤ 0.001.

5 Discussion

Kidney disease is a global public health issue which can be classified in two main groups of pathologies depending on the length of the disease. While acute kidney injury (AKI) is defined as an abrupt (within 48 hours) reduction in kidney function (Mehta 2007), chronic kidney disease (CKD) is a gradual, normally over years, loss of function (Gansevoort 2013). The estimated incidence of acute kidney injury is 3-18% for all hospitalized patients and is increasing over the years (Chawla 2011). The mortality rate for AKI in hospitalized patients is 10.8%, compared to 1.5% for cases without AKI (Wang 2012). In addition, patients that has suffer AKI are more likely to rapidly progress into CKD (Hsu & Hsu 2016). CKD has an indirect impact on global morbidity and mortality, being associated with age-related renal function decline accelerated in hypertension, diabetes, obesity and primary renal disorders. In Europe, CKD prevalence varied from 3,3% to 17,3% (Brück 2016). Globally, in 2017, there were 697,5 million cases and 1,2 million people died from CKD (Bikbov 2020). In addition, 19 million disability-adjusted life-years (DALYs), expressed as the number of years lost due to ill-health, disability or early death, from cardiovascular diseases were directly attributable to reduced glomerular filtration rates. Unfortunately, due to the lack of adequate specific treatments, many patients (>2 million worldwide) progress from CKD to end-stage renal disease (ESRD) (Hu and Coresh 2017) requiring renal replacement therapy.

The availability of renal replacement therapy (RRT) has grown from 1990 to 2017; global all-age incidence of dialysis and kidney transplantation increased by 43,1% and 34,4%, respectively, while global age-standardized incidence rose by 10,7% and 12,8%, respectively, with larger increases in all-age incidence of RRT resulting from population ageing (Bikbov 2020). Along with the cost in human lives, CKD is an economic burden for health systems around the world. The >1% of the population in need of renal replacement therapy consumes up to 5% of health care budgets (Ryan 2007). Treatment costs for CKD rose after the 1960s, with renal replacement therapy becoming a long-term lifesaving but costly treatment option for patients with end-stage renal disease (ESRD). The number of people receiving RRT exceeds 2,5 million and is projected to double to 5,4 million by 2030.

Targeted treatments for AKI or CKD are not available or with very limited efficacy and current treatments mainly focus on managing the underlying cause of the disease. Therefore, it is paramount to develop our understanding around the cellular and molecular mechanisms driving kidney disease in order to find new therapeutic candidates and reduce their clinical and economic burden.

Cathepsin D (CtsD) is a lysosomal protease endowed with several functions in physiological and pathological conditions. The role of CtsD in kidney disease has been previously reported in AKI and CKD, however, its cell specific role during kidney disease progression is still unknown. Previous reports revealed enhanced CtsD expression in murine models of AKI. In particular, its expression was highly increased in damaged tubular cells, suggesting a possible contribution of CtsD to cell death during AKI (Cocchiaro 2016). Indeed, CtsD inhibition using Pepstatin A resulted in improved renal function and reduced apoptotic cell death and tubular damaged in two independent models of AKI. In addition, Pepstatin A pre-treatment slow-down progression from AKI into CKD. In line with this work, Fox et al. demonstrated that CtsD inhibition by Pepstatin A resulted in a reduction of interstitial fibrosis in murine models of progressive CKD (Fox 2016). In this study, Pepstatin A administration resulted in increased extracellular urokinase and collagen degradation. *In vitro* and *in vivo* administration of chloroquine, an endo/lysosomal inhibitor, mimicked Pepstatin A effect on renal fibrosis. Therefore, the authors proposed a mechanism by which CtsD inhibition leads to increased collagenolytic activity due to an impairment in the lysosomal recycling. This results in enhanced extracellular activity of enzymes such as urokinase, triggering a proteolytic cascade, which culminates in more extracellular matrix (ECM) degradation. Thus, the authors suggest inhibition of CtsD as a new therapeutic approach to reduce renal fibrosis and slow progression of CKD. In agreement, a recent report showed that CtsD expression correlates with the worsening of kidney fibrosis, and that pharmacological modulation of CtsD activity further leads to a reduction in renal fibrosis (Singh 2021), supporting results obtained by Fox et al. with Pepstatin A (Fox 2016).

Opposite findings have been described depending on the cell type targeted for the inhibition of CtsD during CKD. While Fox et al. attribute most of the expression of CtsD in their models to distal tubular epithelial cells reporting CtsD inhibition as beneficial for AKI and CKD, Suzuki et al. employed a conditional knockout CtsD$^{flox/-}$; Spink3^{Cre} for deleting CtsD expression in the renal proximal tubular epithelial cells, demonstrating a cytoprotective role for CtsD against ischemia/reperfusion injury in the renal proximal tubular epithelial cells (Suzuki 2019). CtsD cell-specific deletion in podocytes reported by Yamamoto-Nonaka et al. demonstrated that the absence of CtsD in podocytes impairs autophagy through an accumulation of toxic subunit C–positive lipofuscins, causing podocyte apoptosis (Yamamoto-Nonaka 2016). Thus, podocyte-CtsD deficient mice developed an age-related glomerulosclerosis, supporting the hypothesis of a cytoprotective role of CtsD in podocytes.

As shown, controversial evidence has been reported by different authors about the effect of CtsD inhibition during chronic kidney disease, pointing towards a differential cell specific role of this peculiar endopeptidase. Thus, the aim of this thesis was to elucidate the role of CtsD in another cell type highly involved in the pathogenesis of kidney disease, the macrophages.

Macrophages have a pivotal role in kidney inflammation and fibrosis. Depending on the stage of kidney disease, macrophages exert a different role and polarize toward a pro-inflammatory or anti-inflammatory phenotype. During early phase of tissue damage, the kidney interstitial microenvironment is dominated by micro-organism-derived pathogen-associated molecular patterns (PAMPs) and pro-inflammatory cytokines, which promote full activation of the pro-inflammatory M1 macrophage. In contrast, the uptake of apoptotic cells and anti-inflammatory cytokines drive macrophage polarization toward an anti-inflammatory M2 phenotype, promoting renal repair and tissue remodelling (Cao 2015). Notably, the phenotypic switch is reversible depending on the tissue microenvironment, therefore macrophage function can vary according to the progression of the disease. Despite macrophage infiltration is one of the main events during tissue injury and inflammation, mounting evidence shows that macrophages also play a reparative role during the course of disease, by actively participating in clearance of apoptotic and necrotic cells to resolve injury and in remodelling of matrix to restore tissue homeostasis in acute and chronic kidney disease (Cao 2015). Thus, the depletion of M2 macrophages in an established model of AKI in mice was accountable for prolonged renal injury (Guzzi 2019).

As Antigen Presenting Cells (APC) macrophages express a large amount of cathepsins. Several studies describe CtsD function implicated in the degradation of proteins destined for the MHC class II (Nakagawa 1999). However, it can participate in the pathophysiological remodelling of the ECM in some specific condition, as in atherosclerotic lesions (Hakala 2003) or in cancer progression and metastasis (Kos 2000). The capability of macrophages of acidifying their environment by proton pumps and secretion of lactic acid (Tapper & Sundler 1992), ensures the macrophage pericellular environment to be sufficiently acidic for CtsD activation, otherwise with limited activity at neutral pH (Bidère 2003).

The main findings of this thesis are summarized in the diagram in **Fig. 28.**
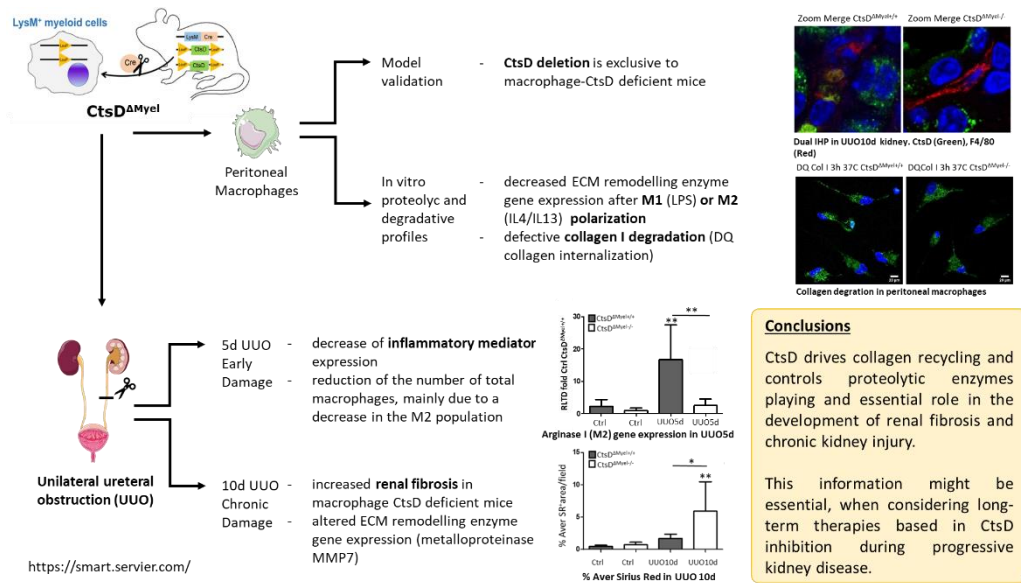
Figure 28. Schematic diagram summarizing the main results of this project.

In order to evaluate the effect of depleting CtsD in macrophages, we generated a macrophage-CtsD knock-out mouse by breeding CtsD floxed mice (Ketscher 2016) with LysM-Cre mice (Clausen 1999). LysM-Cre strain has been extensively applied to develop reporter mice for *in vivo* tracking or lineage tracing of macrophages and other myelomonocytic cells in normal and diseased conditions (Shi 2018). In spite of the high efficiency of LysM-Cre strain in manipulating endogenous macrophages, LysM is not a specific marker for macrophages. In addition to monocytes and mature macrophages, LysM is also expressed in most granulocytes and few CD11c+ dendritic cells (DCs), as well as a small percentage of non-hematopoietic cells such as type II lung alveolar cells in mice, as long as 60–80% neutrophils in spleen (Miyake 2007). Monocytes/macrophages represent a highly heterogeneous population which lacks common specific markers or transcriptional factors, compared to other relatively homogenous immune cell types such as neutrophils, mast cells and basophils. Therefore, there are no perfect Cre driver mice targeting macrophages currently available. Overall, the LysM-Cre mouse strain is a broadly used tool to investigate the macrophage population (Shi 2018).

This thesis work validates for the first time this novel cell-specific knock-out mice using peritoneal macrophages (**Fig. 10**). Our results demonstrate CtsD cell-specific deletion in macrophages. In addition, our data demonstrate that adult macrophage-CtsD deficient mice present normal renal function and morphology under physiological conditions (**Fig. 11**).

To describe the progression from an early damage to a chronic disease, we performed unilateral ureteral obstruction (UUO) at 5 (early) and 10 days

(chronic) in macrophage-CtsD sufficient and deficient mice. The UUO model is widely used to study the mechanisms underlying progression of kidney disease from acute to chronic stages (Ucero 2014) as the obstructed kidney suffers a decline in renal blood flow, glomerular filtration rate and rapid damage of the renal parenchyma. It is recommended that all UUO studies test an early time-point (less than 7 days) and a later time-point (more than 7 days) (Ucero 2014) to assess both early changes in inflammation but also parenchymal damage and interstitial fibrosis.

No changes in tubular damage were observed between macrophage-CtsD sufficient and deficient mice in the obstructed kidneys (**Fig. 13** and **Fig. 17**) in any of the time-points we studied.

We analyzed then the effect of the macrophage-CtsD deletion on inflammation, as cathepsins play an important role in the immune response. Remarkably, after 5 days of UUO, deletion of CtsD in macrophages caused decrease expression of inflammatory mediators (**Fig. 14**). Besides, it also resulted in the reduction in the number of total macrophages in the UUO diseased kidney, mainly and most likely due to a decrease in the M2 population (**Fig. 15**). In the kidney, resident macrophages, together with damaged epithelial and endothelial cells, are responsible for releasing chemoattractants and cytokines to recruit macrophages and neutrophils in the first phase of any inflammatory response (Black 2019). Both resident and infiltrating immune cells participate in the acute phase of kidney injury and contribute to the disease progression. Therefore, macrophages lacking CtsD seem to lead to a defective inflammatory response, as well as a defective recruitment and polarization of macrophages in response to early-stage kidney disease. A recent report shows that pharmacological cathepsin B, L and S inhibition in human primary M2-polarized macrophages leads to profound alterations in autophagy and fatty acid metabolism, promoting a polarization shift from M2 to M1 macrophages (Oelschlaegel 2020). However, they also detect an increase in CtsD levels upon inhibition of CtsB, L and S, most likely explained by a compensatory upregulation, not totally surprising as compensatory mechanisms in cathepsins are often described (Moles 2010). Therefore, CtsD expression has been already correlated with M2 phenotype polarization. In agreement with our results pharmacological inhibition of CtsD using Pepstatin A resulted in an amelioration of inflammation in inhibitor-treated mice with dextran–sulphate–sodium (DSS)-induced colitis, mouse model of inflammatory bowel disease (Menzel 2006).

To analyze the macrophage cell-specific role during chronic kidney disease we performed a second time-point at 10 days for the UUO model. This time-point is characterized by chronic inflammation, collagen deposition and

vascular rarefaction (Ferenbach & Bonventre 2015). Macrophage-CtsD deficient mice showed decreased CtsD activity in the kidney 10 days after UUO (**Fig. 16a**). This was confirmed by dual immunohistochemistry using F4/80, as a marker for macrophages, and CtsD demonstrating that CtsD was lacking only in renal macrophages from macrophage-CtsD deficient mice (**Fig. 16b**). Dual immunofluorescence corroborated the elevated CtsD expression in tubular epithelial cells previously described by Fox et al. (**Fig. 16b**). Thus, considering that most of the CtsD activity detected in whole kidney tissue will come from tubular epithelial cells, significant changes in CtsD activity in macrophage-deficient mice after 10 days UUO, due to the CtsD fraction expressed in macrophages, supports a highly relevant role for this fraction in whole kidney tissue. Indeed, we only observed a significant decrease in CtsD activity in whole kidney of macrophage-CtsD deficient mice after 10 days of UUO and not 5 days (**Fig. 16** and **Fig. 12**), indicating that the role of CtsD in macrophages is more relevant during chronic rather than early damage.

Contrarily to the UUO 5 days time-point, no alteration in the expression of inflammatory mediators was detected 10 days after UUO (**Fig. 21**). This is most likely due to a differential role of CtsD during early damage and inflammation, most likely driven by M1 macrophages, and another role during chronic disease driven by M2 macrophages (Guiteras 2016b). Despite in UUO 5 days time-point we found a significant impairment in the number and polarization of macrophages (**Fig. 15**), 10 days after UUO no differences in polarization markers were detected between macrophage-CtsD sufficient and deficient mice. This suggests a recovery in the M2 population, impaired during the more acute stage of the disease and supports the idea that this shift in macrophage population could be, at least, in part responsible for the shift in inflammatory markers detected between the 5 and 10 days time-points.

Interestingly, a significant decrease in the number of neutrophils was detected 10 days after UUO in macrophage-CtsD deficient mice (**Fig. 20**). Neutrophil recruitment is most likely not impaired as one of the main neutrophil-recruiting chemokine (CXCL-1) does not show changes in its expression in macrophage-CtsD deficient and sufficient mice after UUO (**Fig. 21**). Thus, another mechanism related to neutrophils survival might explain our result. It has already been described in the literature that some cathepsins trigger apoptotic cell death via various pathways, including the activation of caspases or the release of proapoptotic factors from the mitochondria, in particular CtsB and CtsD (Liaudet-Coopman 2006). Therefore, the depletion of CtsD in neutrophils, as a consequence of the lack of specificity of the LysMCre driver (Miyake 2007), could modulate other cathepsins, for instance CtsB, leading to an enhanced

apoptosis. However, investigating the role of CtsD in neutrophils in these models was not the aim of the thesis and further investigation needs to be done to clarify this observation.

Cathepsins are reported to play an important role in organ fibrosis and ECM homeostasis, such as CtsB in the liver (Moles 2009), CtsK in the lung (Srivastava 2008), CtsS in the heart (H. Chen 2013) and CtsD in kidney (Fox 2016). However, knowledge about the cellular mechanisms by which cathepsins contribute to fibrosis are still limited.

Remarkably, our results demonstrate that lack of CtsD in macrophages resulted in increased renal fibrosis after UUO-induced chronic renal injury (UUO 10d) (**Fig. 18**). Our results differ from those reported by Singh 2021 and Fox 2016 supporting that CtsD inhibition by Pepstatin A reduces renal fibrosis. This discrepancy can be explained by the different inhibition strategies used by us and the other authors. While Pepstatin A will partially inhibit CtsD and target the main reservoir of CtsD in the kidney, which we and Fox et al. have proved to be tubular epithelial cells (**Fig. 16**), our strategy genetically blunts CtsD expression exclusively in macrophages providing us with a high and specific inhibition of CtsD in this particular cell-type, explaining the different results obtained with the different approaches.

Next, we decided to investigate the mechanism by which absence of CtsD in macrophages resulted in increased renal fibrosis. Extracellular matrix homeostasis is a fine balance between synthesis and degradation that can be easily titled during pathology resulting in fibrosis amongst others. Thus, to study matrix synthesis we analyzed the gene expression of different fibrotic markers, including Col1A1 10 days after UUO. No significant differences were detected between macrophage-CtsD deficient and sufficient animals indicating that the increase in fibrosis observed in macrophage-CtsD deficient is not caused by an increase in the synthesis of extracellular matrix but most likely an alteration in matrix degradation or turnover. Indeed, the cells that are directly implicated in debris clearance are mononuclear phagocytes, meant as monocytes and macrophages.

Collagen is internalized after binding to the collagen receptor uPARAP/Endo180 (uPAR Associated Protein), product of the MRC2 gene. This recycling receptor drives basement membrane collagens as well as interstitial collagens to lysosomal degradation via endocytosis (Melander 2015). A previous report by López-Guisa suggested a protective role of this receptor during kidney fibrosis, as Mrc2-deficient mice presented increased collagen accumulation after UUO (López-Guisa 2012). Even though an alteration in this specific mechanism

could explain our findings, we did not observe any changes in this collagen receptor (**Fig. 23**).

CtsD could participate in proteolytic cascades and influence the expression or activation of other proteases, which ultimately could modulate collagen recycling as previously described in the case of UPA (Fox 2016).

Therefore, we investigated the expression of some matrix metalloproteinases, proteolytic enzymes involved in ECM remodelling, and found a significant decrease in the expression of Matrilysin (**Fig. 24**), also known as matrix metalloproteinase-7 (MMP7). Cells of the monocyte/macrophage lineage, including blood monocytes, dendritic cells, and tissue macrophages secrete diverse MMPs in large quantities. MMP2, 7, and 9 are considered to be particularly efficient in their ability to cleave type IV collagen, a major component of basement membranes, at least in vitro, although *in vivo*, MMP3 is the only one proven to cleave type IV collagen (Webster & Crowe 2006).

To better understand results obtained *in vivo*, we isolated peritoneal macrophages (PMT) and stimulated them with LPS or IL4/IL13 to induce macrophage polarization toward M1 and M2 phenotype respectively. Previous studies showed that monocyte stimulation with LPS and proinflammatory cytokines leads to induction of a number of MMPs, including MMP 1, 9, 2, and 3 (Welgus 1990).

Both M1 and M2 polarized CtsD deficient PMT showed defective MMP profile (**Fig. 25** and **Fig. 26**), supporting the results obtained in the UUO 10 days model. Therefore, the dysregulation of the proteolytic MMP profile in macrophage-CtsD deficient macrophages could contribute to an impairment in ECM recycling resulting in enhanced renal fibrosis in macrophage-CtsD deficient mice 10 days after UUO. Further investigation will need to be done to understand how CtsD contributes to the expression of MMP during activation of macrophages and their polarization.

Moreover, after M2 polarization a decrease in IL10 expression, cytokine secreted by M2 macrophages, was detected in CtsD deficient PMT indicating that M2 polarized CtsD deficient macrophages could display defective M2 inflammatory response.

Furthermore, PMT deficient in CtsD showed defective collagen I degradation, as shown by internalization and degradation of fluorogenic DQ™ collagen probe (**Fig. 27**). Thus, absence of CtsD in PMT contribute to impaired lysosomal activity resulting in defective degradation of internalized substrates, such as DQ™ collagen. In agreement, a previous report has demonstrated that CtsD deficiency leads to a strong impairment of the lysosomal-autophagy machinery. Indeed, enzyme replacement therapy (ERT) with recombinant pro-

CtsD corrects defective proteolysis and autophagy in neuronal ceroid lipofuscinosis (Marques 2020). Thus, less degradation of collagen in CtsD deficient macrophages could be responsible, at least in part, of the accumulation of collagen and the in increased renal fibrosis detected in the macrophage-CtsD deficient mice.

Whether CtsD could directly degrade ECM components within the lysosome is not so clear. A report from 1981 showed that CtsD purified from bovine thymus, has a limited proteolytic effect on types I and III bovine collagens (Scott & Pearson 1981), but no evidence from *in vivo* studies are available up to now. Further studies will need to be done to clarify whether CtsD in the macrophages directly or indirectly participates in the cleavage of collagens within the lysosomes during renal fibrosis.

Our study highlights the important role of CtsD in macrophages during kidney disease. During an early stage of kidney disease characterized by a strong inflammatory response, macrophage-specific deletion of CtsD alters chemokine expression, leading to an impaired downstream recruitment of circulating macrophages, as well as an altered polarization of macrophages toward a M2 phenotype. Besides, in a chronic stage of the disease, it is accountable for increased interstitial fibrosis, dysregulation of MMP expression profile and defective collagen recycling.

Our results present limitations and further work will need to be done in the future to fully understand the CtsD mechanism of action and partners during progressive kidney disease. Nevertheless, our results complement those from the previous literature and present relevant information about possible caveats related to CtsD expression in macrophages, when considering long-term therapies based in CtsD inhibition during progressive kidney disease.

6 Conclusions

This thesis work has demonstrated the important role of CtsD in macrophages during progressive kidney disease.

We validated for the first time a novel macrophage cell-specific CtsD knock-out mouse strain, confirming that CtsD is specifically deleted in macrophages from macrophage cell-specific CtsD deficient mice. In addition, we proved that macrophage-CtsD deficient adult mice displayed a preserved kidney function and normal kidney architecture.

During an early stage of kidney disease (UUO 5d), macrophage-CtsD deficient mice showed decreased expression of inflammatory markers, pointing towards a defective inflammatory response in macrophages lacking CtsD. Moreover, they showed an impaired downstream recruitment of circulating macrophages, as well as an altered polarization of macrophages toward an M2 phenotype.

In a chronic stage of the disease (UUO 10d), macrophage-CtsD deficient mice showed decreased CtsD activity in kidney after 10 days UUO, highlighting an important contribution of the CtsD fraction accountable to macrophages during renal fibrosis. Remarkably, in UUO 10d model, cell-specific deletion of CtsD in macrophages resulted in increased interstitial fibrosis without changes in renal damage or inflammation. In agreement, no changes in the total number of macrophages neither the M1 nor the M2 populations were detected indicating that the M2 population has recovered during the chronic-stage, compared to early-stage kidney disease (UUO 5d). Surprisingly, macrophage-CtsD deficient animals showed decreased neutrophil recruitment after 10d UUO, most likely not due to an impairment in chemokine expression however, further investigation will need to be done to clarify this observation.

Our results demonstrated that the increase in renal fibrosis was not a consequence of a differential increase in the expression of collagen in macrophage-CtsD deficient mice, or of an impairment in collagen endocytosis. The absence of CtsD in macrophages resulted in defective MMP7 expression pointing towards and effect of CtsD over proteolytic enzymes. In vitro experiments confirm that both M1 and M2 polarized peritoneal macrophages deficient in CtsD display defective MMP expression profile. Moreover, analysis of the collagen degradative signature in the macrophage-CtsD deficient and sufficient peritoneal macrophages revealed defective collagen recycling as a consequence of CtsD depletion. Together with the results obtained in the UUO 10d model, the dysregulation of the proteolytic profile of the MMPs and the impairment in collagen uptake due to the lack of CtsD in macrophages could be in part responsible for the defective collagen recycling and the increased

extracellular matrix accumulation and renal fibrosis observed in macrophage-CtsD deficient mice.

In summary this thesis provides novel experimental evidence of an important role for CtsD driving collagen recycling and controlling proteolytic enzymes during chronic renal injury. This information might be essential, when considering long-term therapies based in CtsD inhibition during progressive kidney disease.

List of Publications

1. De Pasquale V, Costanzo M, Siciliano RA, Mazzeo MF, **Pistorio V**, Bianchi L, Marchese E, Ruoppolo M, Pavone LM, Caterino M. *Proteomic Analysis of Mucopolysaccharidosis IIIB Mouse Brain.* Biomolecules. **2020** Feb 26;10(3):355. doi: 10.3390/biom10030355.

2. Costa R, Bellesso S, Lualdi S, Manzoli R, **Pistorio V**, Filocamo M, Moro E. *A transcriptional and post-transcriptional dysregulation of Dishevelled 1 and 2 underlies the Wnt signaling impairment in type I Gaucher disease experimental models.* Hum Mol Genet. **2020** Jan 15;29(2):274-285. doi: 10.1093/hmg/ddz293.

3. De Pasquale V, Sarogni P, **Pistorio V**, Cerulo G, Paladino S, Pavone LM. *Targeting Heparan Sulfate Proteoglycans as a Novel Therapeutic Strategy for Mucopolysaccharidoses.* Mol Ther Methods Clin Dev. **2018** Jun 18;10:8-16. doi:10.1016/j.omtm.2018.05.002.

References

Agarwal, A., Dong, Z., Harris, R., Murray, P., Parikh, S. M., Rosner, M. H., et al. (2016). Cellular and molecular mechanisms of AKI. *J. Am. Soc. Nephrol.* 27, 1288–1299. doi:10.1681/ASN.2015070740.

Akkari, L., Gocheva, V., Quick, M. L., Kester, J. C., Spencer, A. K., Garfall, A. L., et al. (2016). Combined deletion of cathepsin protease family members reveals compensatory mechanisms in cancer. *Genes Dev.* 30, 220–232. doi:10.1101/gad.270439.115.

Albina, J. E., Mills, C. D., Henry, W. L., Caldwell, M. D., Albina, J. E., Mills, C. D., et al. (1990). Temporal expression of different pathways of 1-arginine metabolism in healing wounds. *J. Immunol.*

Anders, H. J., and Ryu, M. (2011). Renal microenvironments and macrophage phenotypes determine progression or resolution of renal inflammation and fibrosis. *Kidney Int.* 80, 915–925. doi:10.1038/ki.2011.217.

Aregger, F., Uehlinger, D. E., Witowski, J., Brunisholz, R. A., Hunziker, P., Frey, F. J., et al. (2014). Identification of IGFBP-7 by urinary proteomics as a novel prognostic marker in early acute kidney injury. *Kidney Int.* 85, 909–919. doi:10.1038/ki.2013.363.

Baechle, D., Flad, T., Cansier, A., Steffen, H., Schittek, B., Tolson, J., et al. (2006). Cathepsin D is present in human eccrine sweat and involved in the postsecretory processing of the antimicrobial peptide DCD-1L. *J. Biol. Chem.* 281, 5406–5415. doi:10.1074/jbc.M504670200.

Bao, L., Wang, Y., Haas, M., and Quigg, R. J. (2011). Distinct roles for C3a and C5a in complement-induced tubulointerstitial injury. *Kidney Int.* 80, 524–534. doi:10.1038/ki.2011.158.

Baricos, W. H., Cortez, S. L., Le, Q. C., Wu, L. T., Shaw, E., Hanada, K., et al. (1991). Evidence suggesting a role for cathepsin L in an experimental model of glomerulonephritis. *Arch. Biochem. Biophys.* 288, 468–472. doi:10.1016/0003-9861(91)90222-5.

Bataller, R., and Brenner, D. a (2005). Liver fibrosis. *J. Clin. Invest.* 115, 209–218. doi:10.1172/JCI200524282.The.

Benes, P., Vetvicka, V., and Fusek, M. (2008). Cathepsin D-Many functions of one aspartic protease. *Crit. Rev. Oncol. Hematol.* 68, 12–28. doi:10.1016/j.critrevonc.2008.02.008.

Berchem, G., Glondu, M., Gleizes, M., Brouillet, J.-P., Vignon, F., Garcia, M., et al. (2002). Cathepsin D affects multiple tumor progression steps in vivo.pdf.

Bidère, N., Lorenzo, H. K., Carmona, S., Laforge, M., Harper, F., Dumont, C., et al. (2003). Cathepsin D triggers Bax activation, resulting in selective apoptosis-inducing factor (AIF) relocation in T lymphocytes entering the early commitment phase to apoptosis. *J. Biol. Chem.* 278, 31401–31411.

doi:10.1074/jbc.M301911200.

Biernacka, A., Dobaczewski, M., and Frangogiannis, N. G. (2011). TFG-b signaling in fibrosis. *Growth Factors* 29, 196–201. doi:10.3109/08977194.2011.595714.TGF-.

Bikbov, B., Purcell, C. A., Levey, A. S., Smith, M., Abdoli, A., Abebe, M., et al. (2020). Global, regional, and national burden of chronic kidney disease, 1990–2017: a systematic analysis for the Global Burden of Disease Study 2017. *Lancet* 395, 709–733. doi:10.1016/S0140-6736(20)30045-3.

Black, L. M., Lever, J. M., and Agarwal, A. (2019). Renal Inflammation and Fibrosis: A Double-edged Sword. *J. Histochem. Cytochem.* 67, 663–681. doi:10.1369/0022155419852932.

Bonventre, J. V., and Yang, L. (2011). Cellular pathophysiology of ischemic acute kidney injury. *J. Clin. Invest.* 121, 4210–4221. doi:10.1172/JCI45161.

Bowdish, D. M. E. (2016). Macrophage Activation and Polarization. *Encycl. Immunobiol.* 1, 289–292. doi:10.1016/B978-0-12-374279-7.03002-2.

Brück, K., Stel, V. S., Gambaro, G., Hallan, S., Völzke, H., Ärnlöv, J., et al. (2016). CKD prevalence varies across the European general population. *J. Am. Soc. Nephrol.* 27, 2135–2147. doi:10.1681/ASN.2015050542.

Cao, Q., Harris, D. C. H., and Wang, Y. (2015). Macrophages in kidney injury, inflammation, and fibrosis. *Physiology* 30, 183–194. doi:10.1152/physiol.00046.2014.

Cao, Y., Liu, X., Li, Y., Lu, Y., Zhong, H., Jiang, W., et al. (2017). Cathepsin L activity correlates with proteinuria in chronic kidney disease in humans. *Int. Urol. Nephrol.* 49, 1409–1417. doi:10.1007/s11255-017-1626-7.

Chalmers, C. (2019). Applied Anatomy and Physiology and the Renal Disease Process. *Ren. Nurs.*, 21–58. doi:10.1002/9781119413172.ch2.

Charles A. Janeway, J. and, and Medzhitov, R. (2003). Innate Immune Recognition: mechanisms and pathways. *Annurev.Immunol.20.083001.084359*, 197–216.

Chawla, L. S., Amdur, R. L., Amodeo, S., Kimmel, P. L., and Palant, C. E. (2011). The severity of acute kidney injury predicts progression to chronic kidney disease. *Kidney Int.* 79, 1361–1369. doi:10.1038/ki.2011.42.

Chawla, L. S., Eggers, P. W., Star, R. A., and Kimmel, P. L. (2014). Acute kidney injury and chronic kidney disease as interconnected syndromes. *N. Engl. J. Med.* 371, 58–66. doi:10.1056/NEJMra1214243.

Chen, C. J., Kono, H., Golenbock, D., Reed, G., Akira, S., and Rock, K. L. (2007). Identification of a key pathway required for the sterile inflammatory response triggered by dying cells. *Nat. Med.* 13, 851–856. doi:10.1038/nm1603.

Chen, H., Wang, J., Xiang, M. X., Lin, Y., He, A., Jin, C. N., et al. (2013).

Cathepsin S-mediated fibroblast trans-differentiation contributes to left ventricular remodelling after myocardial infarction. *Cardiovasc. Res.* 100, 84–94. doi:10.1093/cvr/cvt158.

Chertow, G. M., Burdick, E., Honour, M., Bonventre, J. V, and Bates, D. W. (2005). Clinical Science Articles Acute Kidney Injury, Mortality, Length of Stay, and Costs in Hospitalized Patients. *J Am Soc Nephrol* 16, 3365–3370. doi:10.1681/ASN.2004090740.

Chou, Y. H., Huang, T. M., and Chu, T. S. (2017). Novel insights into acute kidney injury–chronic kidney disease continuum and the role of renin–angiotensin system. *J. Formos. Med. Assoc.* 116, 652–659. doi:10.1016/j.jfma.2017.04.026.

Christ, C., and Dainton, M. (2015). "Chapter 5: Acute Kidney Injury," in *American Journal of Kidney Diseases*, S47–S56. doi:10.1053/j.ajkd.2015.04.022.

CKD Evaluation and Management – KDIGO (2012). Available at: https://kdigo.org/guidelines/ckd-evaluation-and-management/ [Accessed April 7, 2020].

Clausen, B. E., Burkhardt, C., Reith, W., Renkawitz, R., and Förster, I. (1999). Conditional gene targeting in macrophages and granulocytes using LysMcre mice. *Transgenic Res.* 8, 265–277. doi:10.1023/A:1008942828960.

Cocchiaro, P., De Pasquale, V., Morte, R. Della, Tafuri, S., Avallone, L., Pizard, A., et al. (2017). The multifaceted role of the lysosomal protease cathepsins in kidney disease. *Front. Cell Dev. Biol.* 5, 1–12. doi:10.3389/fcell.2017.00114.

Cocchiaro, P., Fox, C., Tregidgo, N. W., Howarth, R., Wood, K. M., Situmorang, G. R., et al. (2016). Lysosomal protease cathepsin D; A new driver of apoptosis during acute kidney injury. *Sci. Rep.* 6, 1–15. doi:10.1038/srep27112.

Conley, S. M., Abais, J. M., Boini, K. M., and Li, P.-L. (2016). Inflammasome Activation in Chronic Glomerular Diseases. *Curr. Drug Targets* 18. doi:10.2174/1389450117666160817103435.

Conus, S., Perozzo, R., Reinheckel, T., Peters, C., Scapozza, L., Yousefi, S., et al. (2008). Caspase-8 is activated by cathepsin D initiating neutrophil apoptosis during the resolution of inflammation. *J. Exp. Med.* 205, 685–698. doi:10.1084/jem.20072152.

Conus, S., and Simon, H. U. (2010). Cathepsins and their involvement in immune responses. *Swiss Med. Wkly.* 140, 1–8. doi:10.4414/smw.2010.13042.

Coresh, J., Astor, B. C., Greene, T., Eknoyan, G., and Levey, A. S. (2003). Prevalence of chronic kidney disease and decreased kidney function in the adult US population: Third National Health and Nutrition Examination Survey. *Am. J. Kidney Dis.* 41, 1–12. doi:10.1053/ajkd.2003.50007.

Davidson, A., Berthier, C., and Kretzler, M. (2013). "Pathogenetic Mechanisms

in Lupus Nephritis," in *Dubois' Lupus Erythematosus and Related Syndromes: Eighth Edition* (Elsevier Inc.), 237–255. doi:10.1016/B978-1-4377-1893-5.00018-2.

Eardley, K. S., Kubal, C., Zehnder, D., Quinkler, M., Lepenies, J., Savage, C. O., et al. (2008). The role of capillary density, macrophage infiltration and interstitial scarring in the pathogenesis of human chronic kidney disease. *Kidney Int.* 74, 495–504. doi:10.1038/ki.2008.183.

Falkson, S. R., and Bordoni, B. (2020). *Anatomy, Abdomen and Pelvis, Bowman Capsule*. StatPearls Publishing Available at: http://www.ncbi.nlm.nih.gov/pubmed/32119361 [Accessed March 27, 2020].

Ferenbach, D. A., and Bonventre, J. V (2015). Mechanisms of maladaptive repair after AKI leading to accelerated kidney ageing and CKD. doi:10.1038/nrneph.2015.3.

Fox, C., Cocchiaro, P., Oakley, F., Howarth, R., Callaghan, K., Leslie, J., et al. (2016). Inhibition of lysosomal protease cathepsin D reduces renal fibrosis in murine chronic kidney disease. *Sci. Rep.* 6, 1–15. doi:10.1038/srep20101.

Gabbiani, G. (2003). The myofibroblast in wound healing and fibrocontractive diseases. *J. Pathol.* 200, 500–503. doi:10.1002/path.1427.

Gansevoort, R. T., Correa-Rotter, R., Hemmelgarn, B. R., Jafar, T. H., Heerspink, H. J. L., Mann, J. F., et al. (2013). Chronic kidney disease and cardiovascular risk: Epidemiology, mechanisms, and prevention. *Lancet* 382, 339–352. doi:10.1016/S0140-6736(13)60595-4.

Garsen, M., Rops, A. L. W. M. M., Dijkman, H., Willemsen, B., van Kuppevelt, T. H., Russel, F. G., et al. (2016). Cathepsin L is crucial for the development of early experimental diabetic nephropathy. *Kidney Int.* 90, 1012–1022. doi:10.1016/j.kint.2016.06.035.

Geissmann, F., Manz, M. G., Jung, S., Sieweke, M. H., Merad, M., and Ley, K. (2010). Development of monocytes, macrophages and dendritic cells. doi:10.1126/science.1178331.

George, J. F., Lever, J. M., and Agarwal, A. (2017). Mononuclear phagocyte subpopulations in the mouse kidney. *Am. J. Physiol. - Ren. Physiol.* 312, F640–F646. doi:10.1152/ajprenal.00369.2016.

Guha, S., and Padh, H. (2008). Cathepsins: Fundamental Effectors of Endolysosomal Proteolysis.

Guiteras, R., Flaquer, M., and Cruzado, J. M. (2016a). Macrophage in chronic kidney disease. *Clin. Kidney J.* 9, 765–771. doi:10.1093/ckj/sfw096.

Guiteras, R., Flaquer, M., and Cruzado, J. M. (2016b). Macrophage in chronic kidney disease. doi:10.1093/ckj/sfw096.

Guzzi, F., Cirillo, L., Roperto, R. M., Romagnani, P., and Lazzeri, E. (2019).

Molecular mechanisms of the acute kidney injury to chronic kidney disease transition: An updated view. *Int. J. Mol. Sci.* 20. doi:10.3390/ijms20194941.

Haase, M., Bellomo, R., Albert, C., Vanpoucke, G., Thomas, G., Laroy, W., et al. (2014). The identification of three novel biomarkers of major adverse kidney events. *Biomark. Med.* 8, 1207–1217. doi:10.2217/bmm.14.90.

Hakala, J. K., Oksjoki, R., Laine, P., Du, H., Grabowski, G. A., Kovanen, P. T., et al. (2003). Lysosomal enzymes are released from cultured human macrophages, hydrolyze LDL in vitro, and are present extracellularly in human atherosclerotic lesions. *Arterioscler. Thromb. Vasc. Biol.* 23, 1430–1436. doi:10.1161/01.ATV.0000077207.49221.06.

Hsu, R. K., and Hsu, C. yuan (2016). The Role of Acute Kidney Injury in Chronic Kidney Disease. *Semin. Nephrol.* 36, 283–292. doi:10.1016/j.semnephrol.2016.05.005.

Hume, D. A., and Gordon, S. (1983). MONONUCLEAR PHAGOCYTE SYSTEM OF THE MOUSE DEFINED BY IMMUNOHISTOCHEMICAL LOCALIZATION OF ANTIGEN F4/80 Identification of Resident Macrophages in Renal Medullary and Cortical Interstitium and the Juxtaglomerular Complex*.

Jedeszko, C., Sameni, M., Olive, M. B., Moin, K., and Sloane, B. F. (2008). Visualizing protease activity in living cells: From two dimensions to four dimensions. *Curr. Protoc. Cell Biol.* doi:10.1002/0471143030.cb0420s39.

Johansson, A. C., Steen, H., Öllinger, K., and Roberg, K. (2003). Cathepsin D mediates cytochrome c release and caspase activation in human fibroblast apoptosis induced by staurosporine. *Cell Death Differ.* 10, 1253–1259. doi:10.1038/sj.cdd.4401290.

Joyce, J. A., Baruch, A., Chehade, K., Meyer-Morse, N., Giraudo, E., Tsai, F. Y., et al. (2004). Cathepsin cysteine proteases are effectors of invasive growth and angiogenesis during multistage tumorigenesis. *Cancer Cell* 5, 443–453. doi:10.1016/S1535-6108(04)00111-4.

Joyce, J. A., and Hanahan, D. (2004). Multiple roles for cysteine cathepsins in cancer. *Cell Cycle* 3, 1516–1519. doi:10.4161/cc.3.12.1289.

Kalluri, R., Neilson, E. G., Kalluri, R., and Neilson, E. G. (2003). Epithelial-mesenchymal transition and its implications for fibrosis Find the latest version : Epithelial-mesenchymal transition and its implications for fibrosis. *J Clin Invest* 112, 1776–1784. doi:10.1172/JCI200320530.For.

Kaneko, M., Tomita, T., Nakase, T., Ohsawa, Y., Seki, H., Takeuchi, E., et al. (2001). Expression of proteinases and inflammatory cytokines in subchondral bone regions in the destructive joint of rhematoid arthritis. *Rheumatology* 40, 247–255. doi:10.1093/rheumatology/40.3.247.

Katunuma, N., Matsunaga, Y., Himeno, K., and Hayashi, Y. (2003). Insights into the roles of cathepsins in antigen processing and presentation revealed by

specific inhibitors. *Biol. Chem.* 384, 883–890. doi:10.1515/BC.2003.099.

Ketscher, A., Ketterer, S., Dollwet-Mack, S., Reif, U., and Reinheckel, T. (2016). Neuroectoderm-specific deletion of cathepsin D in mice models human inherited neuronal ceroid lipofuscinosis type 10. *Biochimie* 122, 219–226. doi:10.1016/j.biochi.2015.07.020.

Kitamoto, K., Machida, Y., Uchida, J., Izumi, Y., Shiota, M., Nakao, T., et al. (2009). Effects of liposome clodronate on renal leukocyte populations and renal fibrosis in murine obstructive nephropathy. *J. Pharmacol. Sci.* 111, 285–292. doi:10.1254/jphs.09227FP.

Kolwijck, E., Kos, J., Obermajer, N., Span, P. N., Thomas, C. M. G., Massuger, L. F. A. G., et al. (2010). The balance between extracellular cathepsins and cystatin C is of importance for ovarian cancer. *Eur. J. Clin. Invest.* 40, 591–599. doi:10.1111/j.1365-2362.2010.02305.x.

Kos, J., Werle, B., Lah, T., and Brunner, N. (2000). Cysteine proteinases and their inhibitors in extracellular fluids: Markers for diagnosis and prognosis in cancer. *Int. J. Biol. Markers* 15, 84–89. doi:10.1177/172460080001500116.

Lech, M., and Anders, H. J. (2013). Macrophages and fibrosis: How resident and infiltrating mononuclear phagocytes orchestrate all phases of tissue injury and repair. *Biochim. Biophys. Acta - Mol. Basis Dis.* 1832, 989–997. doi:10.1016/j.bbadis.2012.12.001.

Levey, A. (1988). Serum Creatinine And Renal Function. *Annu. Rev. Med.* 39, 465–490. doi:10.1146/annurev.med.39.1.465.

Liaudet-Coopman, E., Beaujouin, M., Derocq, D., Garcia, M., Glondu-Lassis, M., Laurent-Matha, V., et al. (2006a). Cathepsin D: newly discovered functions of a long-standing aspartic protease in cancer and apoptosis. *Cancer Lett.* 237, 167–179. doi:10.1016/j.canlet.2005.06.007.

Liaudet-Coopman, E., Beaujouin, M., Derocq, D., Garcia, M., Glondu-Lassis, M., Laurent-Matha, V., et al. (2006b). Cathepsin D: newly discovered functions of a long-standing aspartic protease in cancer and apoptosis. *Cancer Lett.* 237, 167–179. doi:10.1016/j.canlet.2005.06.007.

Lichtnekert, J., Kawakami, T., Parks, W. C., and Duffield, J. S. (2013). Changes in macrophage phenotype as the immune response evolves. doi:10.1016/j.coph.2013.05.013.

Liu, W. J., Shen, T. T., Chen, R. H., Wu, H. L., Wang, Y. J., Deng, J. K., et al. (2015). Autophagy-lysosome pathway in renal tubular epithelial cells is disrupted by advanced glycation end products in diabetic nephropathy. *J. Biol. Chem.* 290, 20499–20510. doi:10.1074/jbc.M115.666354.

Liu, Y. (2011). Cellular and molecular mechanisms of renal fibrosis. *Nat. Rev. Nephrol.* 7, 684–696. doi:10.1038/nrneph.2011.149.

Livak, K. J., and Schmittgen, T. D. (2001). Analysis of relative gene expression

data using real-time quantitative PCR and the 2-ΔΔCT method. *Methods* 25, 402–408. doi:10.1006/meth.2001.1262.

López-Guisa, J. M., Cai, X., Collins, S. J., Yamaguchi, I., Okamura, D. M., Bugge, T. H., et al. (2012). Mannose Receptor 2 Attenuates Renal Fibrosis. *J Am Soc Nephrol* 23, 236–251. doi:10.1681/ASN.2011030310.

Madsen, D. H., and Bugge, T. H. (2013). Imaging collagen degradation in vivo highlights a key role for M2-polarized macrophages in extracellular matrix degradation. *Oncoimmunology* 2, 11–13. doi:10.4161/onci.27127.

Mantovani, A., Sica, A., Sozzani, S., Allavena, P., Vecchi, A., and Locati, M. (2004). The chemokine system in diverse forms of macrophage activation and polarization. doi:10.1016/j.it.2004.09.015.

Marques, A. R. A., Di Spiezio, A., Thießen, N., Schmidt, L., Grötzinger, J., Lüllmann-Rauch, R., et al. (2020). Enzyme replacement therapy with recombinant pro-CTSD (cathepsin D) corrects defective proteolysis and autophagy in neuronal ceroid lipofuscinosis. *Autophagy* 16, 811–825. doi:10.1080/15548627.2019.1637200.

Martinez, F. O., Sica, A., Mantovani, A., and Locati, M. (2008). Macrophage activation and polarization - Martinez. *Bioscience* 13, 453–461. doi:10.2741/2692.

Matovinović, M. S. (2009). M. Sabljar Matovinović Pathophysiology and classification of kidney disease 1. PATHOPHYSIOLOGY AND CLASSIFICATION OF KIDNEY DISEASES. *Ejifcc* 20, 2–11. Available at: http://www.ifcc.org.

McAdoo, M. H., Dannenberg, A. M., Hayes, C. J., James, S. P., and Sanner, J. H. (1973). Inhibition of cathepsin D-type proteinase of macrophages by pepstatin, a specific pepsin inhibitor, and other substances. *Infect. Immun.* 7, 655–665. doi:10.1128/IAI.7.4.655-665.1973.

Mehta, R. L., Kellum, J. A., Shah, S. V, Molitoris, B. A., Ronco, C., Warnock, D. G., et al. (2007). Acute Kidney Injury Network: report of an initiative to improve outcomes in acute kidney injury. doi:10.1186/cc5713.

Melander, M. C., Jürgensen, H. J., Madsen, D. H., Engelholm, L. H., and Behrendt, N. (2015). The collagen receptor uPARAP/Endo180 in tissue degradation and cancer (Review). *Int. J. Oncol.* 47, 1177–1188. doi:10.3892/ijo.2015.3120.

Menzel, K., Hausmann, M., Obermeier, F., Schreiter, K., Dunger, N., Bataille, F., et al. (2006). Cathepsins B, L and D in inflammatory bowel disease macrophages and potential therapeutic effects of cathepsin inhibition in vivo. *Clin. Exp. Immunol.* 146, 169–180. doi:10.1111/j.1365-2249.2006.03188.x.

Mills, C. D. (2012). M1 and M2 macrophages: Oracles of health and disease. *Crit. Rev. Immunol.* 32, 463–488. doi:10.1615/CritRevImmunol.v32.i6.10.

Miyake, Y., Kaise, H., Isono, K., Koseki, H., Kohno, K., and Tanaka, M. (2007). Protective Role of Macrophages in Noninflammatory Lung Injury Caused by Selective Ablation of Alveolar Epithelial Type II Cells. *J. Immunol.* 178, 5001–5009. doi:10.4049/jimmunol.178.8.5001.

Moles, A., Murphy, L., Wilson, C. L., Chakraborty, J. B., Fox, C., Park, E. J., et al. (2014). A TLR2/S100A9/CXCL-2 signaling network is necessary for neutrophil recruitment in acute and chronic liver injury in the mouse. *J. Hepatol.* 60, 782–791. doi:10.1016/j.jhep.2013.12.005.

Moles, A., Tarrats, N., Fernández-Checa, J. C., and Marí, M. (2009). Cathepsins B and D drive hepatic stellate cell proliferation and promote their fibrogenic potential. *Hepatology* 49, 1297–1307. doi:10.1002/hep.22753.

Moles, A., Tarrats, N., Morales, A., Domínguez, M., Bataller, R., Caballería, J., et al. (2010). Acidic sphingomyelinase controls hepatic stellate cell activation and in vivo liver fibrogenesis. *Am. J. Pathol.* 177, 1214–1224. doi:10.2353/ajpath.2010.091257.

Munro, D. A. D., and Hughes, J. (2017). The origins and functions of tissue-resident macrophages in kidney development. *Front. Physiol.* 8, 837. doi:10.3389/fphys.2017.00837.

Nakagawa, T. Y., Brissette, W. H., Lira, P. D., Griffiths, R. J., Petrushova, N., Stock, J., et al. (1999). Impaired invariant chain degradation and antigen presentation and diminished collagen-induced arthritis in cathepsin S null mice. *Immunity* 10, 207–217. doi:10.1016/S1074-7613(00)80021-7.

Nishida, M., Fujinaka, H., Matsusaka, T., Price, J., Kon, V., Fogo, A. B., et al. (2002). Absence of angiotensin II type 1 receptor in bone marrow-derived cells is detrimental in the evolution of renal fibrosis. *J. Clin. Invest.* 110, 1859–1868. doi:10.1172/JCI200215045.

Oelschlaegel, D., Sadan, T. W., Salpeter, S., Krug, S., Blum, G., Schmitz, W., et al. (2020). Cathepsin inhibition modulates metabolism and polarization of tumor-associated macrophages. *Cancers (Basel).* 12, 1–22. doi:10.3390/cancers12092579.

Ozkayar, N., Piskinpasa, S., Akyel, F., Turgut, D., Bulut, M., Turhan, T., et al. (2015). Relation between serum cathepsin D levels and endothelial dysfunction in patients with chronic kidney disease. *Nefrologia* 35, 72–79. doi:10.3265/Nefrologia.pre2014.Oct.12609.

Paraoan, L., Gray, D., Hiscott, P., Garcia-Finana, M., Lane, B., Damato, B., et al. (2009). Cathepsin S and its inhibitor cystatin C: Imbalance in uveal melanoma. *Front. Biosci.* 14, 2504–2513. doi:10.2741/3393.

Ramachandran, P., Pellicoro, A., Vernon, M. A., Boulter, L., Aucott, R. L., Ali, A., et al. (2012). Differential Ly-6C expression identifies the recruited macrophage phenotype, which orchestrates the regression of murine liver fibrosis. *Proc. Natl. Acad. Sci. U. S. A.* 109. doi:10.1073/pnas.1119964109.

Ray, J. M., and Stetler-Stevenson, W. G. (1995). Gelatinase A activity directly modulates melanoma cell adhesion and spreading. *EMBO J.* 14, 908–17.

Reddy, V. Y., Zhang, Q. Y., and Weiss, S. J. (1995). Pericellular mobilization of the tissue-destructive cysteine proteinases, cathepsins B, L, and S, by human monocyte-derived macrophages. *Proc. Natl. Acad. Sci. U. S. A.* 92, 3849–3853. doi:10.1073/pnas.92.9.3849.

Reiser, J., and Altintas, M. M. (2016). Podocytes. doi:10.12688/f1000research.7255.1.

Reiser, J., Oh, J., Shirato, I., Asanuma, K., Hug, A., Mundel, T. M., et al. (2004). Podocyte migration during nephrotic syndrome requires a coordinated interplay between cathepsin L and α3 integrin. *J. Biol. Chem.* 279, 34827–34832. doi:10.1074/jbc.M401973200.

Repnik, U., Stoka, V., Turk, V., and Turk, B. (2012). Lysosomes and lysosomal cathepsins in cell death. *Biochim. Biophys. Acta - Proteins Proteomics* 1824, 22–33. doi:10.1016/j.bbapap.2011.08.016.

Robert Steinfeld,1Konstanze Reinhardt,1Kathrin Schreiber,1Merle Hillebrand,1Ralph Kraetzner,2Wolfgang Bru̇ck,3Paul Saftig, 4and Jutta Gȧrtner CtsD deficiency is associated with a Human Neurodegenerative disorder.pdf.

Roberts, A. B., Russo, A., Felici, A., and Flanders, K. C. (2003). Smad3: A Key Player in Pathogenetic Mechanisms Dependent on TGF-β. *Ann. N. Y. Acad. Sci.* 995, 1–10. doi:10.1111/j.1749-6632.2003.tb03205.x.

Rosenkranz, S. (2004). TGF-b1 and angiotensin networking in cardiac remodeling. *Cardiovasc. Res.* 63. doi:10.1016/j.cardiores.2004.04.030.

Rünger, T. M., Quintanilla-Dieck, M. J., and Bhawan, J. (2007). Role of cathepsin K in the turnover of the dermal extracellular matrix during scar formation. *J. Invest. Dermatol.* 127, 293–297. doi:10.1038/sj.jid.5700535.

Ryan, T. P., Sloand, J. A., Winters, P. C., Corsetti, J. P., and Fisher, S. G. (2007). Chronic Kidney Disease Prevalence and Rate of Diagnosis. *Am. J. Med.* 120, 981–986. doi:10.1016/j.amjmed.2007.05.012.

Saftig, P., Hetman, M., Schmahl, W., Weber, K., Heine, L., Mossmann, H., et al. (1995). Mice deficient for the lysosomal proteinase cathepsin D exhibit progressive atrophy of the intestinal mucosa and profound destruction of lymphoid cells. *EMBO J.* 14, 3599–3608. doi:10.1002/j.1460-2075.1995.tb00029.x.

Sakacı, T., Ahbap, E., Koc, Y., Basturk, T., Ucar, Z. A., Sınangıl, A., et al. (2015). Clinical outcomes and mortality in elderly peritoneal dialysis patients. *Clinics* 70, 363–368. doi:10.6061/clinics/2015(05)10.

Sancho-Martínez, S. M., López-Novoa, J. M., and López-Hernández, F. J. (2015). A K I Pathophysiological role of different tubular epithelial cell death

modes in acute kidney injury. doi:10.1093/ckj/sfv069.

Schaefer, L., Han, X., Gretz, N., and Schaefer, R. M. (1996). Alterations of cathepsins B, H and L in proximal tubules from polycystic kidneys of the Han:SPRD rat. *Kidney Int.* 50, 424–431. doi:10.1038/ki.1996.332.

Schwagerl, A. L., Mohan, P. S., Cataldo, A. M., Vonsattel, J. P., Kowall, N. W., and Nixon, R. A. (1995). Elevated Levels of the Endosomal-Lysosomal Proteinase Cathepsin D in Cerebrospinal Fluid in Alzheimer Disease. *J. Neurochem.* 64, 443–446. doi:10.1046/j.1471-4159.1995.64010443.x.

SCOTT, P. G., and PEARSON, H. (1981). Cathepsin D: Specificity of Peptide-Bond Cleavage in Type-I Collagen and Effects on Type-III Collagen and Procollagen. *Eur. J. Biochem.* 114, 59–62. doi:10.1111/j.1432-1033.1981.tb06172.x.

Sever, S., Altintas, M. M., Nankoe, S. R., Möller, C. C., Ko, D., Wei, C., et al. (2007). Proteolytic processing of dynamin by cytoplasmic cathepsin L is a mechanism for proteinuric kidney disease. *J. Clin. Invest.* 117, 2095–2104. doi:10.1172/JCI32022.

Shi, J., Hua, L., Harmer, D., Li, P., and Ren, G. (2018). "Cre driver mice targeting macrophages," in *Methods in Molecular Biology* (Humana Press Inc.), 263–275. doi:10.1007/978-1-4939-7837-3_24.

Shimoda, N., Fukazawa, N., Nonomura, K., and Fairchild, R. L. (2007). Cathepsin G is required for sustained inflammation and tissue injury after reperfusion of ischemic kidneys. *Am. J. Pathol.* 170, 930–940. doi:10.2353/ajpath.2007.060486.

Singh, M. P., Sharma, C., and Kang, S. C. (2021). Morin hydrate attenuates adenine-induced renal fibrosis via targeting cathepsin D signaling. *Int. Immunopharmacol.* 90, 107234. doi:10.1016/j.intimp.2020.107234.

Smoyer, W. E., and Mundel, P. (1998). Regulation of podocyte structure during the development of nephrotic syndrome. *J. Mol. Med.* 76, 172–183. doi:10.1007/s001090050206.

Sparks, M. A., Crowley, S. D., Gurley, S. B., Mirotsou, M., and Coffman, T. M. (2014). Classical renin-angiotensin system in kidney physiology. *Compr. Physiol.* 4, 1201–1228. doi:10.1002/cphy.c130040.

Srivastava, M., Steinwede, K., Kiviranta, R., Morko, J., Hoymann, H. G., Länger, F., et al. (2008). Overexpression of cathepsin K in mice decreases collagen deposition and lung resistance in response to bleomycin-induced pulmonary fibrosis. *Respir. Res.* 9, 1–12. doi:10.1186/1465-9921-9-54.

Stamatiades, E. G., Tremblay, M.-E., Bohm, M., Crozet, L., Bisht, K., Kao, D., et al. (2016). Immune Monitoring Of Trans-Endothelial Transport By Kidney Resident Macrophages. *Cell* 166, 991–1003. doi:10.1016/j.cell.2016.06.058.

Steinfeld, R., Reinhardt, K., Schreiber, K., Hillebrand, M., Kraetzner, R., Brück,

W., et al. (2006). Cathepsin D deficiency is associated with a human neurodegenerative disorder. *Am. J. Hum. Genet.* 78, 988–998. doi:10.1086/504159.

Stoka, V., Turk, B., Schendel, S. L., Kim, T.-H., Cirman, T., Snipas, S. J., et al. (2001). Lysosomal Protease Pathways to Apoptosis CLEAVAGE OF Bid, NOT PRO-CASPASES, IS THE MOST LIKELY ROUTE*. doi:10.1074/jbc.M008944200.

Stoka, V., Turk, V., and Turk, B. (2016). Lysosomal cathepsins and their regulation in aging and neurodegeneration. *Ageing Res. Rev.* 32, 22–37. doi:10.1016/j.arr.2016.04.010.

Strieter, R. M., Kunkel, S. L., and Bone, R. C. (1993). Role of tumor necrosis factor-α in disease states and inflammation. *Crit. Care Med.* 21, S447. doi:10.1097/00003246-199310001-00006.

Suzuki, C., Tanida, I., Ohmuraya, M., Trejo, J. A. O., Kakuta, S., Sunabori, T., et al. (2019). Lack of cathepsin D in the renal proximal tubular cells resulted in increased sensitivity against renal ischemia/reperfusion injury. *Int. J. Mol. Sci.* 20. doi:10.3390/ijms20071711.

Švara, T., Pogačnik, M., and Juntes, P. (2010). Distribution and amount of cathepsin B in gentamicin-induced acute kidney injury in rats. *Pol. J. Vet. Sci.* 13, 75–82.

Tan, G.-J., Peng, Z.-K., Lu, J.-P., and Tang, F.-Q. (2013). Cathepsins mediate tumor metastasis. *World J. Biol. Chem.* 4, 91. doi:10.4331/wjbc.v4.i4.91.

Tapper, H., and Sundler, R. (1992). Cytosolic pH regulation in mouse macrophages. *Biochem. J.* 281, 245–250.

Thomas, R., Kanso, A., and Sedor, J. R. (2008). Chronic Kidney Disease and Its Complications. *Prim. Care - Clin. Off. Pract.* 35, 329–344. doi:10.1016/j.pop.2008.01.008.

Turk, V., Turk, B., Gunčar, G., Turk, D., and Kos, J. (2002). Lysosomal cathepsins: Structure, role in antigen processing and presentation, and cancer. *Adv. Enzyme Regul.* 42, 285–303. doi:10.1016/S0065-2571(01)00034-6.

Wallace, M. (1998). Anatomy and Physiology of the Kidney. *Pathophysiol. Kidney Dis. Hypertens.* 68, 1–15. doi:10.1016/B978-1-4160-4391-1.50007-2.

Wang, C., Jiang, Z., Yao, J., Wu, X., Sun, L., Liu, C., et al. (2008). Participation of cathepsin B in emodin-induced apoptosis in HK-2 Cells. *Toxicol. Lett.* 181, 196–204. doi:10.1016/j.toxlet.2008.05.013.

Wang, H. E., Muntner, P., Chertow, G. M., and Warnock, D. G. (2012). Acute kidney injury and mortality in hospitalized patients. *Am. J. Nephrol.* 35, 349–355. doi:10.1159/000337487.

Wang, N., Bai, X., Jin, B., Han, W., Sun, X., and Chen, X. (2016). The

association of serum cathepsin B concentration with age-related cardiovascular-renal subclinical state in a healthy Chinese population. *Arch. Gerontol. Geriatr.* 65, 146–155. doi:10.1016/j.archger.2016.03.015.

Webster, A. C., Nagler, E. V., Morton, R. L., and Masson, P. (2017). Chronic Kidney Disease. *Lancet* 389, 1238–1252. doi:10.1016/S0140-6736(16)32064-5.

Webster, N. L., and Crowe, S. M. (2006). Matrix metalloproteinases, their production by monocytes and macrophages and their potential role in HIV-related diseases. *J. Leukoc. Biol.* 80, 1052–1066. doi:10.1189/jlb.0306152.

Welgus, H. G., Campbell, E. J., Cury, J. D., Eisen, A. Z., Senior, R. M., Wilhelm, S. M., et al. (1990). Neutral metalloproteinases produced by human mononuclear phagocytes. Enzyme profile, regulation, and expression during cellular development. *J. Clin. Invest.* 86, 1496–1502. doi:10.1172/JCI114867.

White, W., and Cove-Smith, A. (2015). Kidney disease in the elderly. *Med. (United Kingdom)* 43, 489–492. doi:10.1016/j.mpmed.2015.05.002.

Wynn, T. A., and Ramalingam, T. R. (2012). Mechanisms of fibrosis: therapeutic translation for fibrotic disease. doi:10.1038/nm.2807.

Yamamoto-Nonaka, K., Koike, M., Asanuma, K., Takagi, M., Oliva Trejo, J. A., Seki, T., et al. (2016). Cathepsin D in podocytes is important in the pathogenesis of proteinuria and CKD. *J. Am. Soc. Nephrol.* 27, 2685–2700. doi:10.1681/ASN.2015040366.

Zeisberg, E. M., Potenta, S. E., Sugimoto, H., Zeisberg, M., and Kalluri, R. (2008). Fibroblasts in kidney fibrosis emerge via endothelial-to-mesenchymal transition. *J. Am. Soc. Nephrol.* 19, 2282–2287. doi:10.1681/ASN.2008050513.

Zhou, J., Zhang, Y. Y., Li, Q. Y., and Cai, Z. H. (2015). Evolutionary history of cathepsin L (L-like) family genes in vertebrates. *Int. J. Biol. Sci.* 11, 1016–1025. doi:10.7150/ijbs.11751.